BRNO UNIVERSITY OF TECHNOLOGY
VYSOKÉ UČENÍ TECHNICKÉ V BRNĚ

CENTRAL EUROPEAN INSTITUTE OF TECHNOLOGY BUT
STŘEDOEVROPSKÝ TECHNOLOGICKÝ INSTITUT VUT

STŘEDOEVROPSKÝ TECHNOLOGICKÝ INSTITUT

ATELOCOLLAGEN PROCESSING, GELATION AND CHARACTERIZATION
ZPRACOVÁNÍ, GELACE A CHARAKTERIZACE ATELOKOLAGENU

DOCTORAL THESIS
DIZERTAČNÍ PRÁCE

AUTHOR — **Ing. Lukáš Zubal**
AUTOR PRÁCE

SUPERVISOR — **doc. Ing. Lucy Vojtová, Ph.D.**
ŠKOLITEL

BRNO 2018

DECLARATION

I declare that this doctoral thesis has been composed solely by myself and that all the quotations from the used literary sources are accurate and complete.

Brno ....

(author's signature)

ABSTRACT

Proposed thesis deals with the characterization, processing and gelation of soluble collagen. A literature review summarizes position of collagen at the transplant market, explains its application and describes different types of collagen. Various methods of characterization of soluble collagen are analysed in detail and different ways of its gelation are thoroughly discussed. The experimental part is divided into two sections. The first section of experimental part deals with the dissolution and gelation of soluble collagen in pressurized CO_2 atmosphere. Compared to the other similar methods, our method operates in a relatively low pressure (up to 0.9MPa) and and low temperatures (close to 0°C) that does not denature soluble collagen (works at low temperatures). This method can be used for fast formation of transparent gels containing very thin fibers. Speed of gelation and transparency of gels give a new potential to the concept of ophthalmology and should bring significant benefits to injectable products, creating microspheres and 3D printing. The second section describes the unique characterization of soluble collagen in native state by Asymmetric Flow Field Flow Fractionation - Multi Angle Light Scattering (AF4-MALS) method. The obtained molar mass perfectly fits the expected molar mass. Native and denatured collagen can readily be identified on the conformational graph. This new method provides stable and consistent results in comparison with other established methods. AF4-MALS method can be used either to optimize yields and purification during the production of soluble collagen or for sensitive detection of collagen denaturation during processing.

KEYWORDS

Soluble collagen, atelocollagen, Field Flow Fractionation, Multi Angle Light Scattering, molar mass, radius of gyration, gelation, self-assembly

ABSTRAKT

Předkládaná disertační práce se zabývá charakterizací, zpracováním a gelací rozpustného kolagenu. Literární rešerše shrnuje postavení kolagenu na trhu s transplantáty, jeho aplikace a jednotlivé typy kolagenu. Detailně jsou rozebrány jednotlivé metody charakterizace rozpustného kolagenu a způsoby jeho gelace. Experimentální část je rozdělena na dvě podkapitoly. První podkapitola experimentální části se zabývá rozpouštěním a gelací rozpustného kolagenu v natlakované CO_2 atmosféře. Proti jiným podobným metodám, metoda pracuje při poměrně nízkém tlaku (do 0.9MPa) a je bezpečná z pohledu denaturace kolagenu neboť funguje za nízké teploty blízké 0°C. Tímto způsobem mohou být průhledné gely, obsahující velmi tenká vlákna kolagenu, vytvořeny mnohem rychleji než za použití konvenčních metod. Rychlost gelace a transparentnost dává konceptu potenciál v oblasti oftalmologie a měla by přinést podstatné výhody pro injektovatelné produkty, vytváření mikro kuliček a 3D tisk. Druhá část popisuje unikátní charakterizaci rozpustného kolagenu v nativním stavu pomocí metody průtokové frakcionace s víceúhlovým rozptylem světla (AF4-MALS). Získaná molekulová hmotnost (při nejvyšší detekované koncentraci) odpovídá předpovězené hmotnosti a nativní i denaturovaný kolagen lze snadno rozeznat v konformačním grafu. Tato nová metoda poskytuje konzistentní a stabilní výsledky ve srovnání s ostatními zavedenými metodami. Metoda může být použita pro optimalizaci kvality výtěžků během výroby rozpustného kolagenu, nebo pro citlivou detekci denaturace během zpracování kolagenu.

KLÍČOVÁ SLOVA

Rozpustný kolagen, atelocollagen, průtoková frakcionace, víceúhlový rozptyl světla, molarní hmontnost, gyrační poloměr, gelace, samouspořádávaní

ZUBAL, Lukas *Atelocollagen processsing, gelation and characterization*: doctoral thesis. Brno: Brno University of Technology, Central Europen Institute of Technology, Advanced Polymers and Composites, 2018. 111 p. Supervised by Assoc. Prof. Lucy Vojtova, PhD.

ACKNOWLEDGEMENT

I would like to thank all the people who helped me to carry out the work presented in this dissertation, especially to my supervisor Assoc. Prof. Lucy Vojtova for her professional guidance and to Prof. Josef Jancar for providing me with appropriate working conditions. I would like to express my gratitude to the Department of Industrial Engineering University of Trento (Italy) for great collaboration, especially to Prof. Claudio Migliaressi, Walter Bonnani, Ph.D. and Devid Maniglio, Ph.D.. I am thankful to Drahomira Klemova, Ing. Ladislav Ilkovics and Assoc. Prof. Ales Hampl from the Department of Histology and Embryology for their help with electron microscopy and to my family with long time support.

Acknowledgment to Projects

This research has been supported by the Ministry of Education, Youth and Sports of the Czech Republic under the project CEITEC 2020 (LQ1601), in part by the project CZ.1.05/2.1.00/03.0086 funded by European Regional Development Fund, project LO1411 (NPU I) funded by Ministry of Education Youth and Sports of Czech Republic.

Brno ....

(author's signature)

CONTENTS

1 INTRODUCTION

Collagens are family of triple helical proteins, which appear in many body tissues. They are important for many body functions, including tissue repair, tissue scaffolding, cell adhesion and morphogenesis. Therefore, they are widely used in Tissue Engineering [1, 2], because of their high biocompatibility. While the collagen is available in various forms as allogenic transplant, decellularized tissue [3], collagen fibers [4, 5], or as soluble collagen [6–8], the main emphasis of this thesis is on soluble collagen.

Due to the covalent intermolecular crosslinks, dissolution of collagen is difficult and production of soluble collagen requires the use of expensive, multistep process based on acids and enzymes, such as proteases [6–8]. Soluble collagens have similar properties as insoluble collagen [8] so they find many uses. Mainly as a gel in medicine and in cosmetics. Soluble collagen has also better processability and reproducibility than insoluble collagen, but its mechanical properties are generally lower than in native tissues. It is believed that this limitation comes generally from two sources: impurities and the way of solubilisation and gelation. Impurities (gelatin, aggregates, collagen III, elastin etc.) influences regularity of the networks because of the presence of various building blocks. The way of gelation influences gelation kinetics, fiber sizes and general interconnection of collagen networks [9].

One part of proposed thesis describes the fast formation of atelocollagen transparent gels by dissolving bovine type I atelocollagen in pressurized carbon dioxide water solutions (between 0.5 and 0.9 MPa) followed by neutralization due to the depressurizing the atelocollagen solution resulting in the decomposition of carbonic acid back to carbon dioxide. When the neutralized solution is heated up to 37°C the fast formation of the atelocollagen transparent gel has proceeded. We have already published that the atelocollagen solution remained stable in pressurized CO_2 atmosphere.and transparent gels contain thin banded fibrils with the diameter of 10 nm [10].

Second part of the thesis deals with the utilization of AF4-MALS technique for measurement of particle size distribution of soluble collagen samples. The technique provides new insight to quality and function (conformation) of soluble collagen, because it provides high quality separation and furthermore provides both size and mass information. Using the native technique entangled (aggregates) collapsed and denatured (debris, gelatin) collagens could be easily recognized. The method is potentially useful for soluble collagen producers since the AF4-MALS technique is FDA/GMP compliant.

2 LITERATURE REVIEW

2.1 General Physiological Requirements on Transplants

2.1.1 Morphology

Macroscopic

According to target tissue (skin, bone, cartilage, ligament, heart, liver, etc.), there are always macroscopic requirements of transplants for those tissues. For example, decellularized tissues perfectly fit all macroscopic requirements (Fig. 2.1). However, contemporary human engineered transplants usually come up with more trivial shapes.

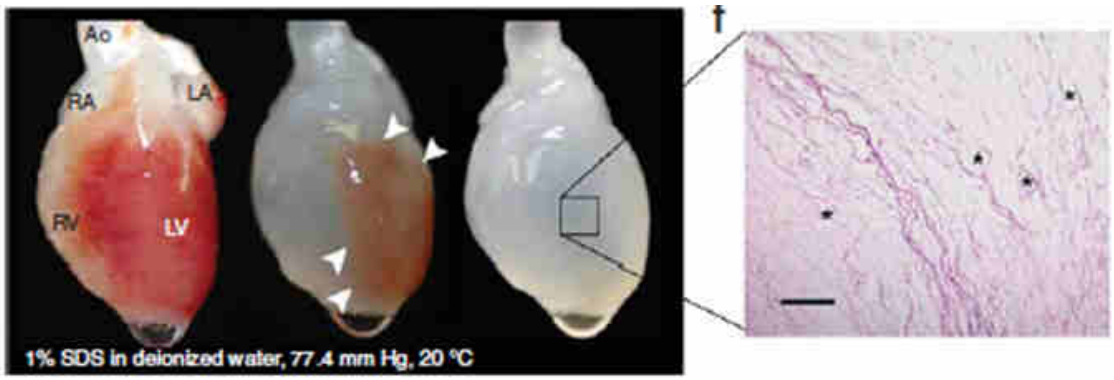

Fig. 2.1: Demonstration of tissue morphology - decellularized rat heart. Reprinted from [11]

.

Microscopic

Borders between macroscopic and microscopic morphology are not clear. For collagen gels, decellularized tissues and electrospun nanofibers are basic elements smaller than cells (Fig. 2.4C), so little changes in fiber diameters and pore sizes could be important in terms of nutrient and cell [12, 13] penetration, because of limits in cell plasticity (Fig. 2.2) [14]. Here chemistry (biomaterial composition, crosslinking density, the ability to swell, cytotoxicity, etc.) is very important, because of high cell-scaffold interaction area (Fig. 2.3) [15]. On the other hand, large pores (50 - 500 µm) of freeze-dried scaffolds allow rapid colonization of scaffolds. However, these scaffolds have low cell-scaffold interaction area (Fig. 2.4C), thus the scaffold material has low impact on cells. Collagen freeze-dried and electrospun scaffolds have already been compared in-vivo as skin substitutes [16].

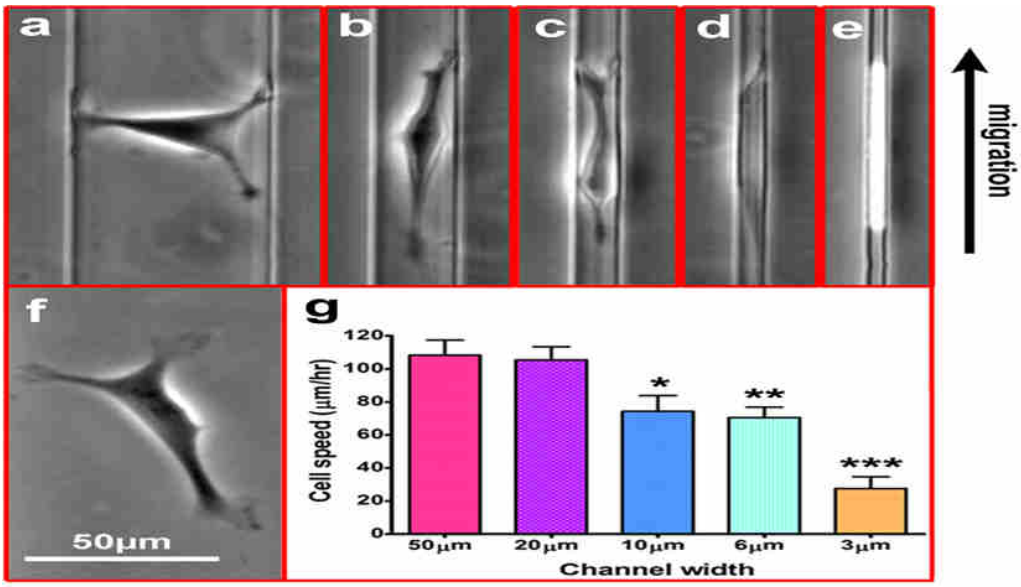

Fig. 2.2: The influence of channel width on cell morphology and migration speed. Reprinted from [14]

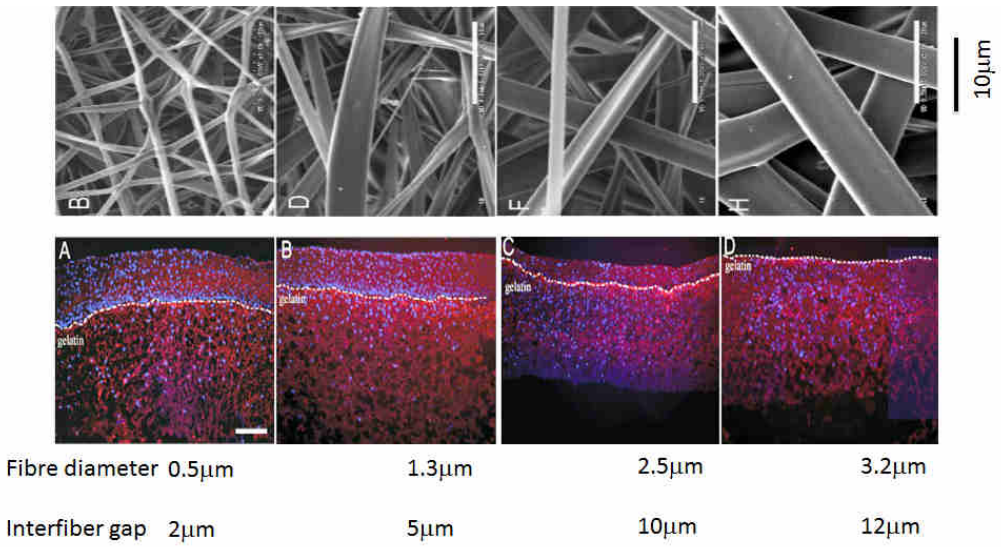

Fig. 2.3: Top: Gelatin electrospun fibers with different fibers diameters and pore sizes. Middle: In-vitro growth of human karatinocytes and fibroblast on electrospun materials. Bottom: Measured fibre diameters and pore sizes. Fiber diameter and pore size greatly influences cell growth. Reprinted from [15]

2.1.2 Biocompatibility

Important part of biocompatibility is the chemical composition of the material. Material should allow good attachment of cells, should be enough mechanically stable and its degradation products should be nontoxic.

Even if the choice of biomaterial is important, biocompatibility of whole transplant (or scaffold) cannot be simplified to biocompatibility of base material. Biocompat-

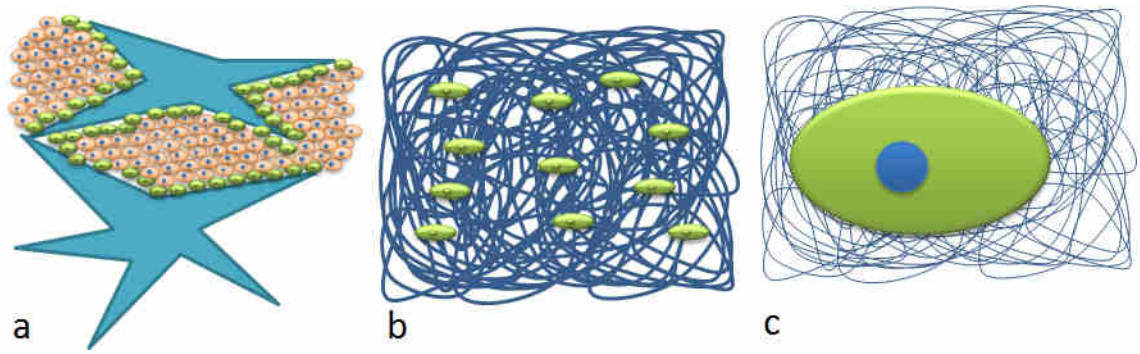

Fig. 2.4: Schematic view on interaction of cells and different transplants. Microporous scaffold(a), Microfiber scaffold(b), Nanofiber scaffold(c). The schematic demonstrates that morphology of transplant influences cell-scaffold surface area and biocompatibility.

ibility is also closely linked with microscopic morphology, resulting scaffold surface area, cell-scaffold interaction area and local micromechanics [18].

Schematic view on the Fig. 2.4 demonstrates that in case of **microporous scaffold** (Fig. 2.4a), only cells directly attached to scaffold are strongly influenced by the scaffold. Cells growing into the center of scaffold will be less influenced by the scaffold. In consequence, the phenotype, viability, apoptosis rate and other parameters will differ for cells with direct and indirect contact with scaffold. E.g. if scaffold contains growth factors, directly attached cells will get the biggest growth factor dosage. In other case, toxic products released from improper scaffold material, will increase apoptosis rate of cells attached directly to scaffold.

Using **microfiber scaffold (2.4)** (Fig. 2.4b), much more cells will be directly influenced by scaffold. Its sensitivity to scaffold will be higher. Good material biocompatibility or growth factors will influence the healing process more strongly. On the other hand, nutrition, waste, oxygen and carbon dioxide permeability are lower than in case of microporous scaffold. Poor material biocompatibility of the material will decrease the viability stronger than in case of microporous scaffold.

Nanofiber scaffold (Fig. 2.4) (Fig. 2.4c) includes native ECM (Extra Cellular Matrix), biopolymer fibrous gels (collagen, fibrin, elastin), electrospun scaffold. This type of scaffold influences cellular response much stronger than the others, because of large cell-scaffold surface area. Mechanism of cellular movement is also different, because cells are bigger than network pores. It was already demonstrated that cells are not able to penetrate in-vitro into many types of synthetic electrospun polymer materials [12], but they can grow into nanofibers, made from collagen with similar morphology (fiber size) [15]. Most probably it is because cells can manipulate with single natural fibers (with adequate mechanics) and dissolve them by metalloproteinases (Fig. 2.5) [17].

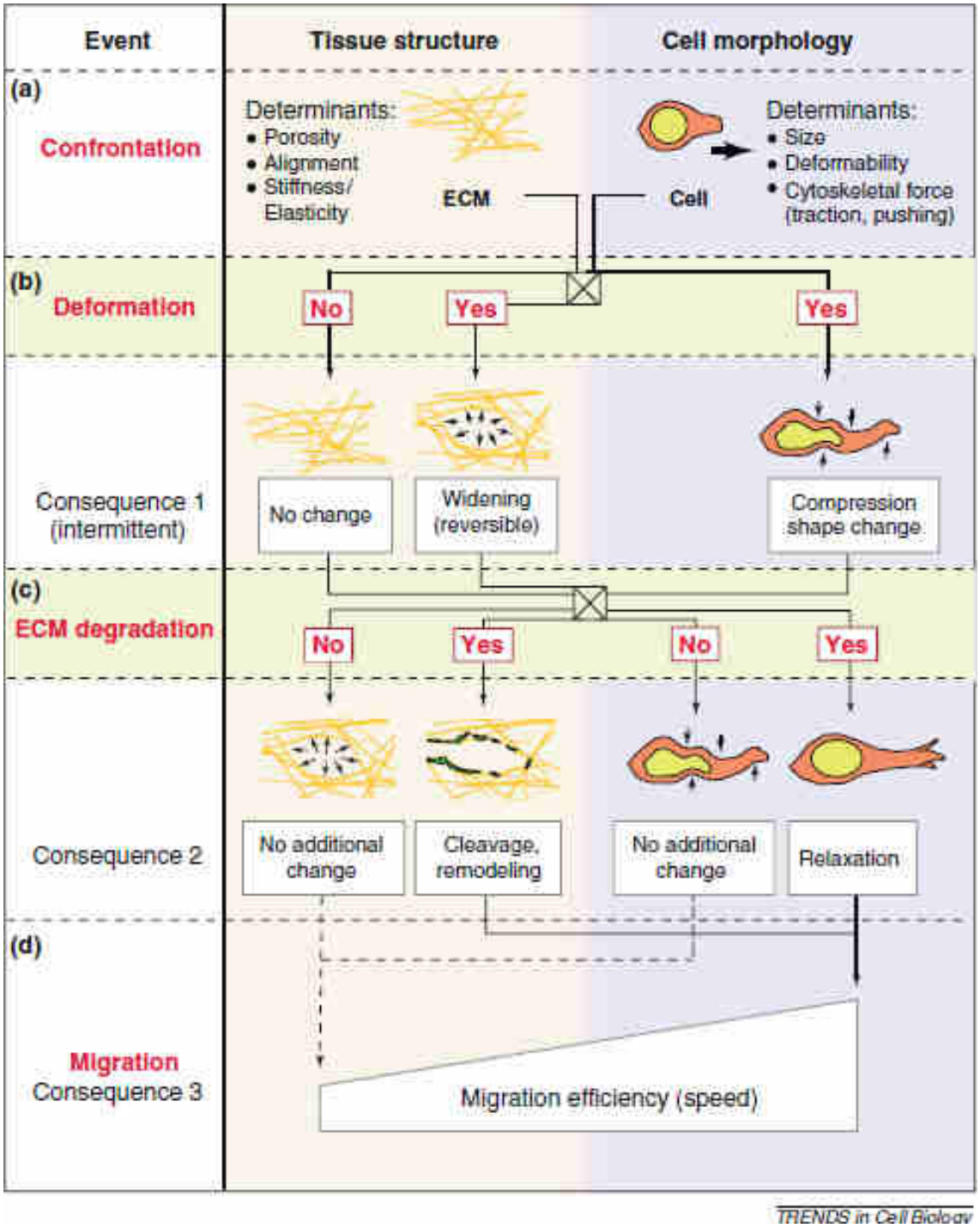

Fig. 2.5: ***Decision-making in cell invasion through 3D tissue(left).*** *Stepwise physicochemical events and decisions (the diagonally crossed square) during dynamic cell confrontation with 3D ECM depicting the perspectives of both the tissue structure and cell morphology, leading to either a proteolytic or non-proteolytic migration mode. The decision model and resulting migration efficiency assume a matching scenario between pore diameter smaller than the cell diameter, but large enough to allow protease-independent migration supported by combined ECM deformation, or by cell shape change alone. The rate-limiting spatial conditions leading to complete migration arrest in non-proteolytically moving cells remain to be determined. Reprinted from [17].*

2.1.2.0.1 Immune response

Immune response is the main allogenic and xenogeneic material limitation, but it can be also provoked by engineered materials. Researchers found that DNA content is strongly associated with immune response [19], but is expected that many other molecules/mechanisms could trigger imune response. Today the only efficient method to detect immune response is preclinical testing on higher mammalian animal models. However, cost and ethical problems connected with animal models motivates researchers to develop other predictors, which should be able to detect immune response in-vitro. Some researchers believed that macrophage phenotype could be good predictor [20, 21], but high quality evaluation of this method is still missing and should be also evaluated on another types of transplants than decellularized ECM.

2.1.3 Mechanical properties

It is natural that each transplant must be able to match mechanical properties of target tissue. Not just mechanical strength is important, but stiffness and elasticity are also important for many applications for example skin [22] or vascular applications [23].
Mechanical stability in-vivo could be problematic especially for natural polymers, because their degradation could be strongly modulated by immune response. On the other hand, mechanics and degradation of scaffolds made from synthetic polymers are normally well defined and not influenced by immune system. Unfortunately, their degradation products could directly induce later complications like inflammation, because of release of small particles or acidic products (low molecular weight polymers, oligomers). [24].

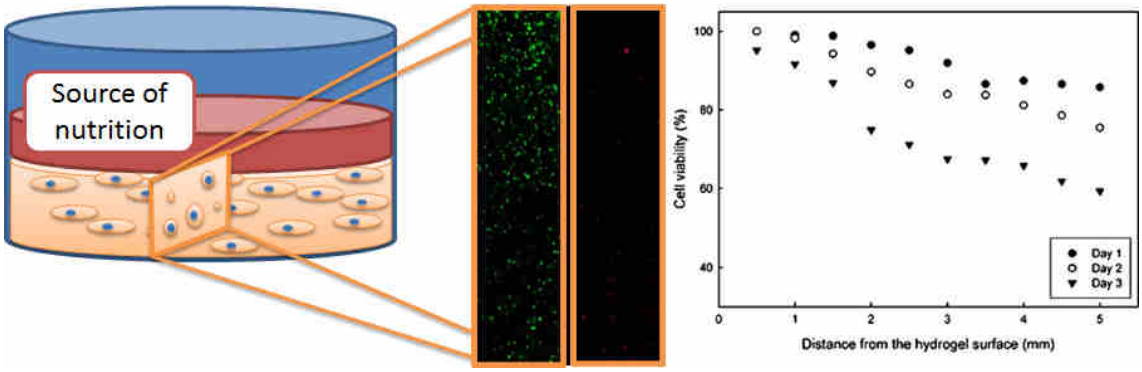

Fig. 2.6: Agarose gel diffusion model. Cells are less viable further from source of nutrition and oxygen. Reprinted from [25]

.

2.1.4 Vascularization - Nutrient delivery and waste removal

Physiological maximum distance between capillaries is 200 µm [26] (because of limited diffusion in tissues). Models of in-vitro diffusion have already been developed (Fig. 2.6) [25]. Decellularization protocols can preserve vascular system of donor tissues and allow vascularization in-vivo. Current Tissue Engineered Scaffolds are heavily limited by lack of vascularization of sufficient quality. Today's strategies for vascularization consist of in-vitro prevascularization (co-culture), in-vivo prevascularization, growth factors and adhesion peptides (Fig. 2.7) [25].

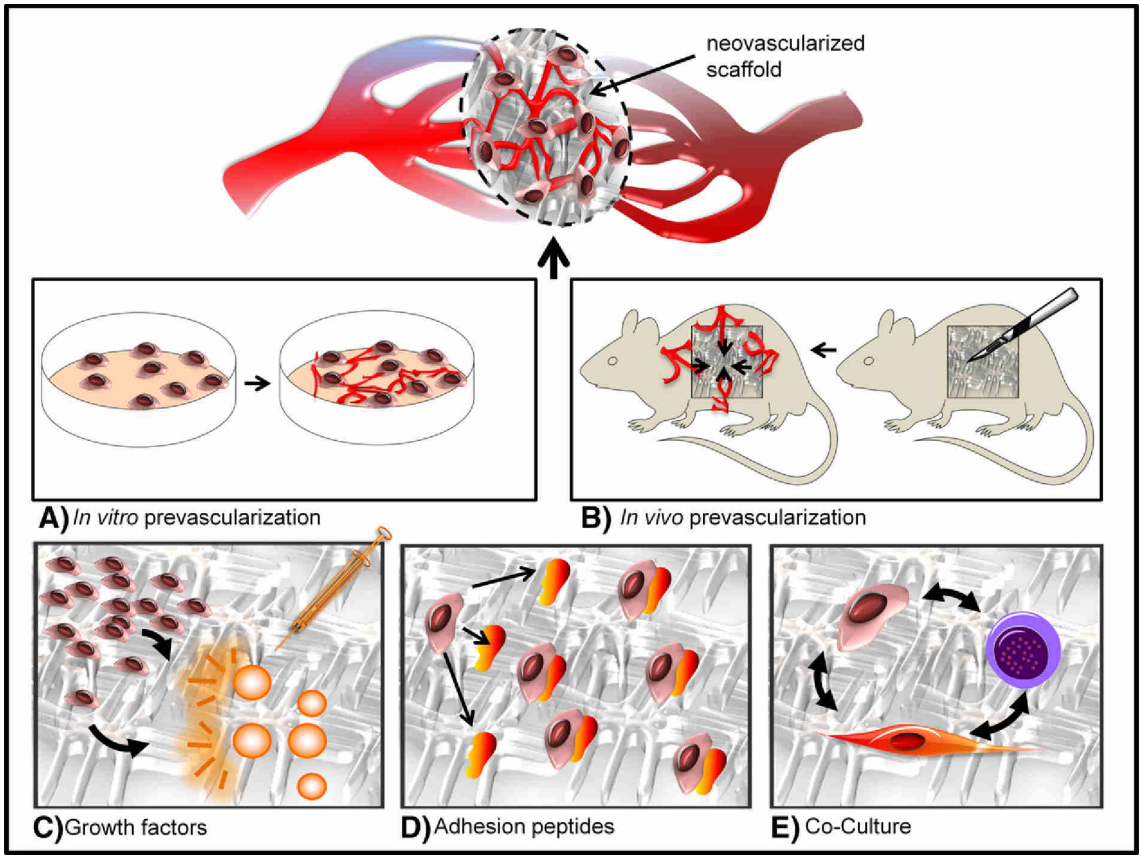

Fig. 2.7: Five different cell-based strategies to induce vascularization by stimulation of angiogenic processes. The strategies include the application of in vivo and in vitro prevascularization (A, B) as well as stimulation of vascularization by addition of growth factors (C), immobilization of adhesion peptides (D) and co-culture of different cell types (E). Reprinted from [25].

2.1.5 Reproducibility

Good reproducibility of manufactured products is always expected. Reproducibility of decellularized products will be always lower, because of natural variability between individuals. For the same reason, there are problems in production of naturally derived materials from tissues, but cell derived of recombinant produced materials

are possibly better purified and more reproducible. Synthetic materials generally offer great reproducibility.

2.2 Collagen in the Body

Collagen has several functions in the body. The most important is the mechanical function, but the other functions like morphogenesis and tissue repair are also important [1]. Collagen occurs in many tissues of the body - skin, ligament, bones, cartilage, muscles, blood vessels, cornea and others. Twenty-eight currently known collagen types form different macromolecular architectures are described in (Fig. 2.8). It is also well known, that collagen interacts with more than 50 ligands and proteoglycans [27].

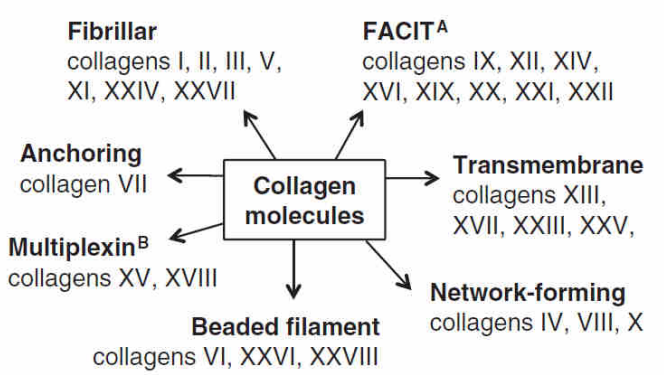

Fig. 2.8: Supramolecular assembly architectures of collagens I - XXVIII [27]

2.3 Insoluble Collagen

Insoluble collagen is made from chemically and physically processed tissue (animal skin, ligaments etc.). Fats, some proteins, proteoglycans, cells, DNA etc. should be removed during manufacturing process. Insoluble collagen contains highly cross-linked collagen fibril bundles mostly in micron scale and minor part of soluble collagen and gelatin. Other molecules, like elastin peptides, could also be found in insoluble collagen as impurities. Diameter of fibril bundles is mostly dependent on source of tissue. Length of fibers can be modified by physical processing (i.e. mixing/homogenizing). Insoluble collagen is not able to dissolve completely in acids or bases, but just swells into viscous suspension. Depending on processing, wide range of fiber sizes can be produced from sub-micrometer to few hundreds micrometers size (Fig. 2.10).

	Type	Molecular formula	Polymerized form	Tissue distribution
Fibril-Forming (fibrillar)	I	$[\alpha1(I)]_2\alpha2(I)$	fibril	bone, skin, tendons, ligaments, cornea (represent 90% of total collagen of the human body)
	II	$[\alpha1(II)]_3$	fibril	cartilage, intervertebrate disc, notochord, vitreous humor in the eye
	III	$[\alpha1(III)]_3$	fibril	skin, blood vessels
	V	$[\alpha1(V)]_2\alpha2(V)$ and $\alpha1(V)\alpha2(V)\alpha3(V)$	fibril (assemble with type I)	*idem* as type I
	XI	$\alpha1(XI)\alpha2(XI)\alpha3(XI)$	fibril (assemble with type II)	*idem* as type II
Fibril-associated	IX	$\alpha1(IX)\alpha2(IX)\alpha3(IX)$	lateral association with type II fibril	cartilage
	XII	$[\alpha1(XII)]_3$	lateral association with type I fibril	tendons, ligaments
Network-forming	IV	$[\alpha1(IV)]_2\alpha2(IV)$	Sheet-like network	basal lamina
	VII	$[\alpha1(VII)]_3$	anchoring fibrils	beneath stratified squamous epithelia

Fig. 2.9: Collagen types, forms and distribution in the body [28]

.

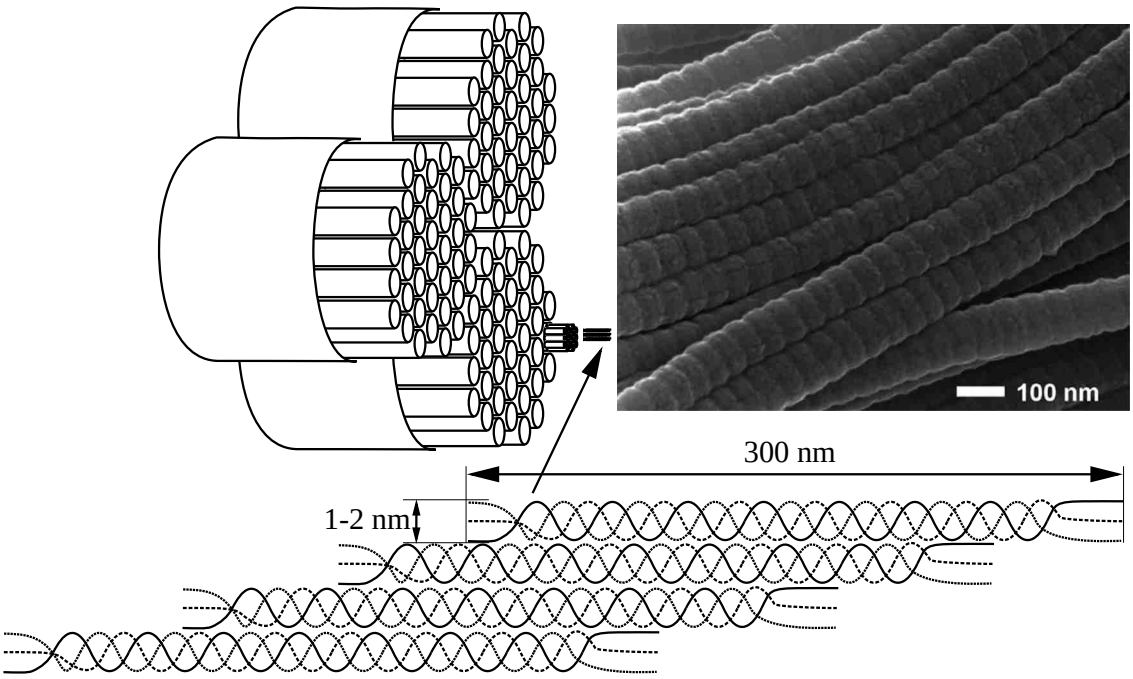

Fig. 2.10: Schematic view on collagen bundles. Upper right image showing collagen bundles visualized by Helium Ion Microscopy (Reprinted from [29]).

2.4 Soluble Collagen

Soluble collagen is manufactured by various processes from various tissues (see isolation section, 2.4.2). Unlike insoluble collagens (Chapter-2.3), soluble collagens are able to form solutions in acids, bases, or some organic solvents. Soluble collagen is able to form fibrous networks in-vivo and also in-vitro at neutral conditions [8] and mimics the native structure of various body tissues. Fiber formation capability, processability and purity of soluble collagens bring several advantages for TE. Limited mechanical properties are the main drawback of soluble collagens.

2.4.1 Soluble Collagen Types

2.4.1.1 Acid Soluble Collagen

Acid soluble collagen (ASC) is obtained from various tissues by prolonged acid exposures (> 3 days). Bovine skin, achiles tendom, rat tails [30, 31], cartilage [6], fish scales [32, 33], fish skin [33, 34], fish bone [33] etc. can be used to produce acid soluble collagen. Prolonged acid process could completely solubilize collagen, but yields are generally low. Resultant collagen molecules contain also telopeptides [8], which could provoke immune response. The self-assembly and stability of acid soluble collagen are very similar to pepsin processed atelocollagen [8]. Acid soluble collagen is soluble in weak acids at pH less than 4, in bases, urea or some organic solvents. Thermal stability of soluble collagens is much lower than of insoluble collagens and depends on animal origin. The denaturation temperature could be between 20-25 °C for some cold sea fish collagens [33] and 30 - 35 °C for most of mammalian collagens [35, 36].

2.4.1.2 Atelocollagen

Atelocollagen, also known as Pepsin Soluble Collagen (PSC), is obtained by processing of insoluble collagen in acid and pepsin. Here the pepsin cleaves the collagen at specific place of collagen telopeptide, resulting in faster, more effective and cheaper extraction process than in acid only. Various tissues are possible to use for atelocollagen extraction: skin [6, 7], aorta [6], muscle [6], human adipose tissue [35], fish scales [32] etc. The partly cleaved telopeptides by pepsin [8], Fig. 2.11 are just slightly different in comparison with acid soluble collagen. This resulted in almost identical electrophoresis, but still the thermal and self-assembly properties remain almost unchanged (Fig. 2.12). Atelocollagen is more attractive for use in medical application, because of shorter processing time, higher yields and lower immune response risk [8]. Usable solvents and thermal stability of atelocollagen are similar to

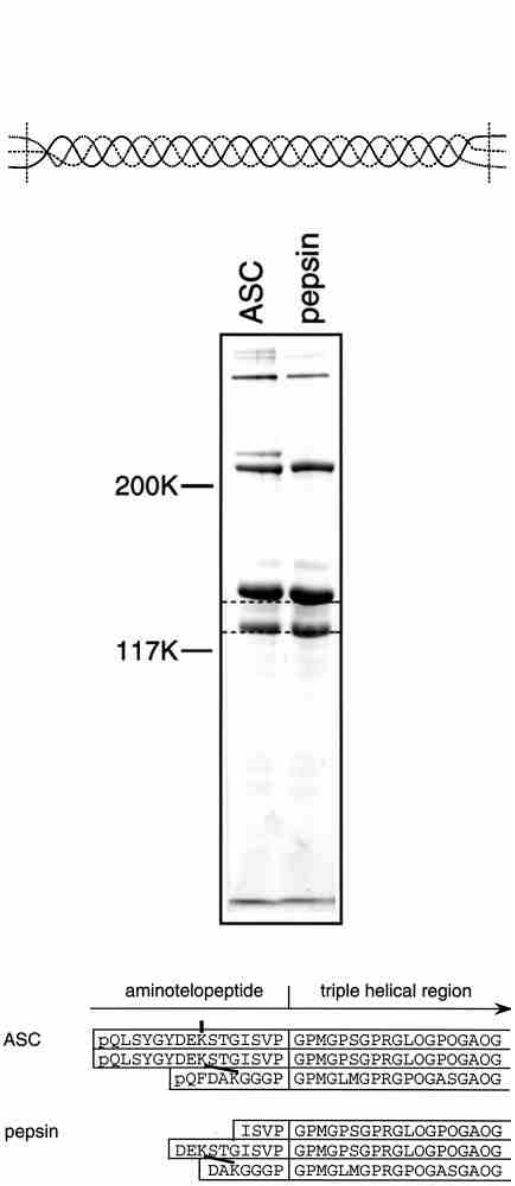

Fig. 2.11: Top - Schematic view of collagen molecule, Center - SDS-PAGE of Purified type I ASC (ASC), pepsin-treated ASC (PSC), Bottom - schematic view on ASC and PSC amino acid sequence cleavage sites. Reprinted from [8].

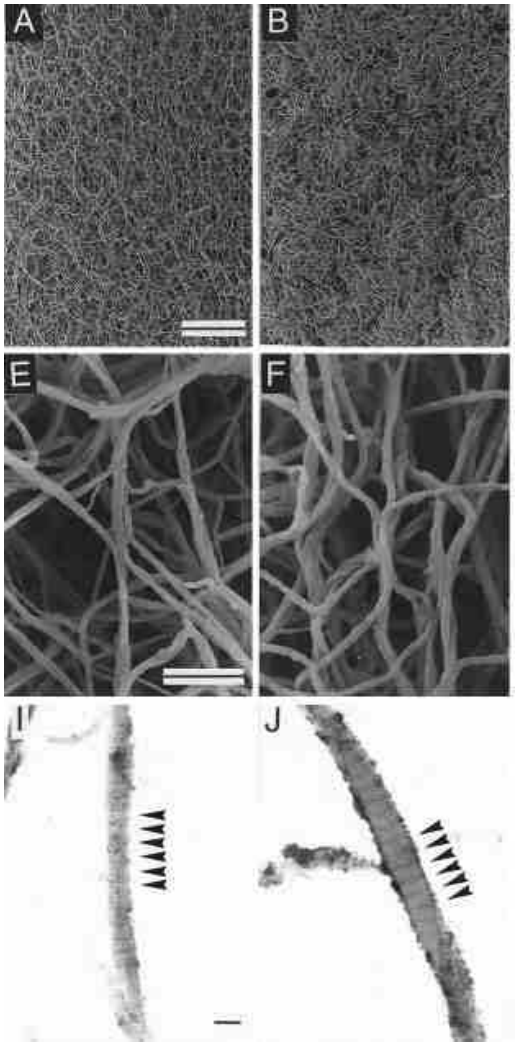

Fig. 2.12: Purified type I ASC (A, E, I), pepsin-treated ASC (B, F, J) gels. A, B (bar 20 μm), E, F (bar 1 μm) critical point dried gels visualized using SEM, I, J (bar 100 nm) fixed and negatively stained single collagen fibril visualized using TEM, reprinted from [8].

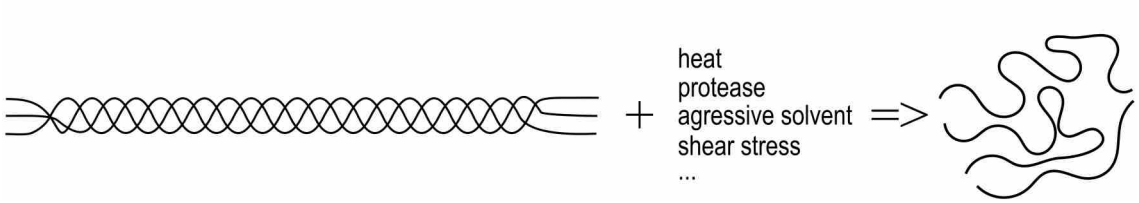

Fig. 2.13: Schematic conversion of collagen(left) to gelatine(right)

acid soluble collagen (Chapter 2.4.1.1).

2.4.1.3 Gelatin

Gelatin is made by denaturation of collagen (schematic view in Fig. 2.13) and contains collagen debris of various sizes. Denaturation can be done by heating, proteases, aggressive solvents and mechanical disruption. Gelatin is soluble at any pH and is not able to self-assemble into fibrous networks as collagen. Gelatin is able to form physical gel, but only at lower temperatures than physiological (less than 31 °C). Thus, chemical or physical crosslinking is necessary, otherwise gelatin melts into solution at physiological conditions. Electrophoresis, chromatographic techniques (2.4.4.1), circular dichroism (2.4.4.2), rheology (2.4.4.3), differential scanning calorimetry (2.4.4.8) and other techniques could be utilized to recognize collagen denaturation into gelatin.

2.4.2 Isolation

Production of soluble collagen could be split to four steps: pre-treatment, extraction, filtration and purification. Each step must be validated by Quality Control.

2.4.2.1 Quality Control

For development of collagen products, it is important to setup methods, which are able to recognize quality of freshly isolated material, and to do the comparison with commercial/clinical quality products.
Collagen I isolated for usage in tissue engineered medical products should be manufactured according to recommendation guide [37]. This document suggest the use of many characterization methods (concentration assays, amino acid analysis, SDS-PAGE, elastin assay, peptide mapping, Elisa, western blot, cytotoxicity, heavy metal content, microbial profile, carbohydrate analysis, Trypsin reaction analysis, DSC, TEM, endotoxin analysis, lipid analysis, etc.) in order to be absolutely sure in quality of collagen. Selected methods are described in detail in characterization section 2.4.4.

This list of methods seems to be too long for many researchers and unfortunately high number of articles use just a few methods [6–8, 30–32, 34–36] to describe atelocollagen quality. The quality of yielded material then is not clear, properties of collagen are variant and the collagens possibly contain significant part of insoluble content, aggregates and gelatin. Then mechanical and biological properties of yielded materials will differ.
It is very important to maintain good quality of filtration. Rheometer, together with light microscopy are robust tools for detection of micron scale material in the sample. Insufficient filtration leads to unexpected errors in many (nano scale) characterization methods. Only well filtrated material could be subjected to SDS-PAGE or CD spectroscopy, in order to detect collagen/gelatin content. Methods listed below (Fig. 2.14) [37] should be used in later stages of isolation, to ensure the quality of yielded material from many points of view.

2.4.2.2 Pre-treatment

First fresh tissue should be cut into the small pieces and then subjected to NaOH, ethanol, NaCl treatment in order to remove lipids and some other proteins [7, 33, 35, 38].

2.4.2.3 Extraction

Extraction is usually done in 0.5 M Acetic Acid (AA) [7, 8, 30, 31, 38] for more than three days in order to yield Acid Soluble Collagen. Second common option is to use 0.5 M AA together with pepsin [6–8, 32, 35] for 2-3, days in order to yield pepsin soluble collagen(atelocollagen). Before extraction, leastwise lipids must be removed from starting tissue. Tissue should be also well homogenized to sizes about few hundred micrometres or less, prior to extraction. Otherwise performance of used chemistry will be limited by insufficient diffusion.
Stirring is important variable influencing extraction kinetics. Because of possible shear stress denaturation of collagen triple helix, stirring speed should be limited from the top. Optimal stirring speed should be experimentally set.

2.4.2.4 Filtration

Various filters could be used for collagen filtration after extraction (clarification). The final filtration must be equivalent to at least 0.45 µm filter, otherwise the filtrate contains too many aggregates.
If higher volume of collagen needs to be filtrated, filters with descending pore sizes should be used prior to use of final 0.4 µm membrane. Direct filtration by submicrometer membrane will result in their block after few milliliters. The depth filters

Characterization Method	Applicable to
Chemical	
Appearance	Soluble or Insoluble
Concentration	Soluble or Insoluble
Purity	Soluble or Insoluble
Amino acid analysis	Soluble or Insoluble
Peptide mapping	Soluble or Insoluble
Impurities profile, includes Heavy Metal Analysis	Soluble or Insoluble
Carbohydrate analysis	Soluble or Insoluble
Trypsin resistance	Soluble or Insoluble, Mainly Insoluble
Collagenase resistance	Soluble or Insoluble, Mainly Insoluble
pH of implantable	Soluble or Insoluble
Additives (cross-linkers, lubricants, drugs, sterilents)	Soluble or Insoluble
Physical	
Shrink Temperature (DSC)	Insoluble
Viscosity	Mainly soluble
TEM	Insoluble
SDS-PAGE	Soluble or Insoluble
Moisture Content (5 to 20 %), dependent on storage environment	Insoluble
Electron Micrograph (native banded 640 Å structure for fibrils)	Insoluble
Biochemical	
Endotoxin level	Soluble or Insoluble
Bioburden	Soluble or Insoluble
% Type I collagen/Total Protein	Soluble or Insoluble
% Other Types Collagen and List of which Types present	Soluble or Insoluble
Total DNA (ppm or %)	Soluble or Insoluble
Total Lipid	Soluble or Insoluble
% native collagen (by trypsin resistance, circular Dichroism)	Soluble or Insoluble

Abbreviation in Table:
DSC = Differential Scanning Calorimetry
TEM = Transmission Electron Microscopy
SDS-PAGE = Sodium Dodecyl Sulfate Polyacrylamide Gel Electrophoresis

Fig. 2.14: Characterization methods for Collagen type I, reprinted from [37].

could be used directly.
Researchers often use centrifuge, because of their availability in most of the labs. General use centrifuges (reaching 15 000 - 20 000 g) were mentioned in many articles [7, 33, 35], but this kind of clarification does not lead to perfect nanoscale filtration. High speed centrifuge (40 000 g and higher) should be used [6, 38] in order to reach sufficient filtration efficiency. Moreover, in order to improve clarification (filtration to whiteness free solution), precipitation of aggregates by 0.3 M sodium chloride [38] could be used.

2.4.2.5 Purification

Final purification step consists of selective removal of molecules smaller than collagen (gelatine, elastin peptides, etc.). Sodium chloride is normally used for this purpose. Researchers use various concentrations of sodium chloride 2.5 M [7], 0.9 M [35], 0.6 M [38] in order to precipitate soluble collagen. Then, precipitated collagen is normally collected by low speed centrifuge (3 000 - 5000 g), the supernatant is removed, and the precipitate is redissolved (mostly in 0.5 M AA). Subsequent dialysis (cut off 15 - 30 kDa) for 3 days with change of water each day, removes sodium chloride and the smallest molecules. Many researchers use lyophilisation (freeze-drying) for preservation of soluble collagen for extended time periods. For that purpose, samples should be frozen at least at -45 °C to ensure complete freezing of soluble collagen (including bounded water [39]). Adequate pressure (0.1 - 0.3 of vapour pressure and temperature of -45 °C) should be used to ensure safe (eliminate shear stress denaturation) and fast lyophilisation [40].

2.4.3 Fibrilogenesis

Collagen is formed from tropocollagen (collagen precursor) molecules bundled together into fibrils and fibers by covalent crosslinks. Detailed view of production and deposition of collagen fibrils by cells is described by Hulmes et al. [44]. On the smallest level of organization, tropocollagen molecules form parallel fibrils, which are shifted to each other a bit less than one quarter. A bit less means that there is a gap of 67 nm between each fifth tropocollagen molecule as shown on Fig. 2.15 top-right. The gap in collagen bundles results in transversal direction bands of the collagen fibril. This structure is well observable by TEM (2.21), AFM (2.15) and recently by Helium Ion Electron microscopy (2.10). It is believed that the length of 67 nm gap is related to maximum interaction between charged chains of hydrophobic amino acids of adjacent triple helices [45]. This phenomenon is commonly called "Quarter staggered stacking model", because of the approximate quarter shift of the

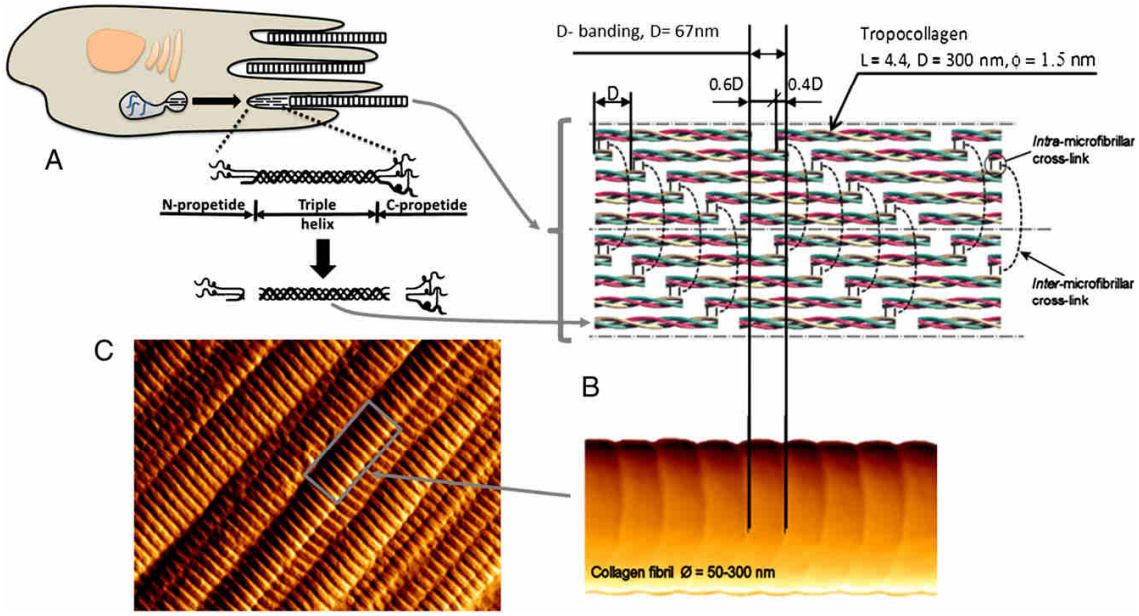

Fig. 2.15: Micro and ultra-structure of collagen. (A) Secretion of "procollagen" from osteoblast into extracellular matrix. "Procollagen" is then converted into "tropocollagen" by specific proteases that cleave the N- and C-propeptides; "tropocollagen" has the ability to spontaneously assemble into fibrils. (B) Collagen triple helix (right-handed coil of three left-handed polypeptide helices). Immature, intra-microfibrillar cross-links bond two collagen molecules head-to-tail; mature, inter-microfibrillar cross-links however bond two immature cross-links from adjacent microfibrils. "Quarter staggered stacking model" of a collagen fibril where five "tropocollagen" molecules are staggered side-by-side with an offset of D=67 nm with gap of 0.6D and overlap of 0.4D regions appear. (C) AFM image of aligned collagen fibrils in-situ of a tendon, displaying the very characteristic D-banding fibrillar annular periodicity. Reprinted from [5].

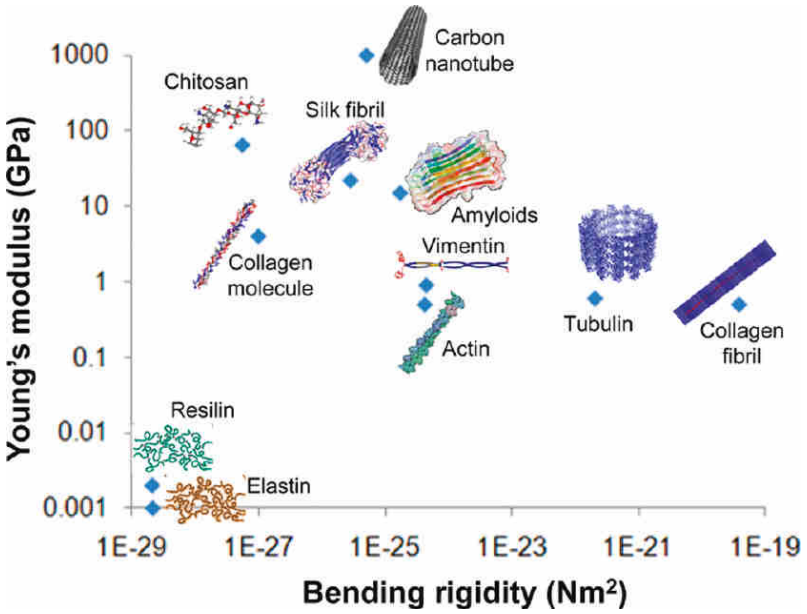

Fig. 2.16: Mechanical properties of various materials at nanoscale. Thanks to well packing collagen fibril present much higher bending rigidity than single collagen molecule with small drop of young moduli [41].

molecules.

The fibrils ranging from 10 to 300 nm could be interconnected with other fibrils forming larger fibers of diameters between 0.5 µm and 3 µm [28].

During experiments on single collagen molecule, researchers found [42], that there are four regimes of longitudinal molecule deformation: decoiling up to 17% of deformation, stretching of covalent bonds up to 33%, molecular fracture due to breaking peptide bonds up to 50%, flowed by rapid decay of the force [42] (Fig. 2.17).

Since collagen fibrils are well packed together, they have much higher bending rigidity while keeping the young moduli almost unchanged [41] (Fig. 2.16).

Fibrillogenesis could be induced also in-vitro [43, 46], at conditions similar to physiological (pH 7.4, 37 °C). There are usually two phases of collagen gelation in-vitro. Lag (nucleation) phase and growth(exponential) phase [47, 48]. Fibrilogenesis can also occur at non physiological pH and ionic strength collagen solutions [45, 49] (Fig. 2.20, Fig. 2.27). Christiansen et al. [50] demonstrated fibril formation at pH range between 5.5 - 8.5 and temperatures 25 - 37 °C. They found that extruded fibers formed at lower pH than 7.4 have much better mechanical properties the ones formed at pH 7.4 (2.19). This effect seems to be connected with prolonged lag phase, consequent creation of larger nucleation sites resulting in larger fibrils [48]. Interestingly, extremely slow gelation at pH = 3.5 of highly concentrated (up to 90 mg.ml^{-1}) collagen solutions, resulted in corneal like organization of the network [51].

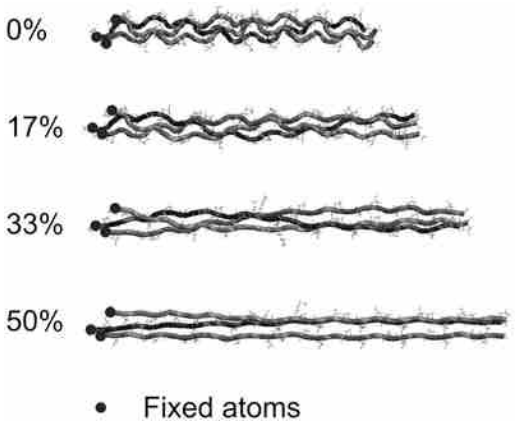

Fig. 2.17: Longitual deformation of single collagen molecule [42]

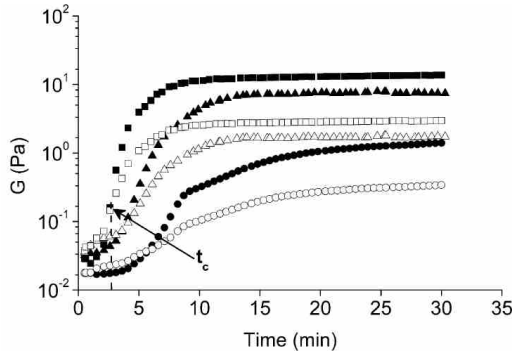

Fig. 2.18: Collagen gel formation at 37 °C evaluated by oscilatory rheology at 1Hz. Solid symbols indicate storage modulus G', and open symbols indicate loss modulus G". Collagen concentrations are 0.5 (circles), 1.0 (triangles), and 1.5 mg/mL (squares) [43].

2.4.3.1 Carbon dioxide collagen processing

Carbon dioxide forms carbonic acid in water. As a consequence of the Henry's Law, the lower the temperature and the higher the pressure, the larger is the dissolution of carbon dioxide in water (carbonic acid formation), that results in a corresponding decrease of the water solution pH (Fig. 5.1A right [52]).

By using CO_2 pressure and low temperature (Fig. 5.1B – region A) it is possible to get sufficient carbonic acid concentrations (low pH) necessary to dissolve acid soluble collagen, while low temperature also ensures stability of soluble collagen at storage temperatures below 10°C [53–56]. Grey rectangle on Region A (Fig. 5.1B, 0.3 – 0.9 MPa) points example of experimental conditions, providing relatively high carbonic acid concentrations. **As our best knowledge up to now, no-one utilized this principle to soluble collagens**. Previous studies on atelocollagen processing in carbonic acid at atmospheric pressure (Region B, Fig. 5.1B) [57], lacked of sufficient carbonic acid concentration (<0.07 M, Fig. 5.1A left [52]), that caused soluble collagen just swelling. Previous attempts to extract soluble collagen (Fig. 5.1B, stars) at higher temperatures (20 - 37°C) and pressures (1 - 5 MPa) [58, 59] yielded in pure gelatin, according to presented CD spectroscopy (missing peak at 221 nm) and SDS-PAGE (missing of typical collagen fingerprint, intensive band below 37kDa and broad range of molar mass). According to this result, it was concluded that the entire region C (Fig. 5.1B) is unsafe for soluble collagen processing. However, region C should still be useful for insoluble collagen processing in pressurized [60, 61] or supercritical conditions [62–64].

2.4.4 Characterization

2.4.4.1 Molar mass distribution analysis

Quantification of collagen monomer, its aggregates and debris (gelatin) is one of the most important tasks of soluble collagen characterization. Procollagen I is synthetized in cells by genes consisting of two $\alpha 1$ chains (139 kg.mol^{-1} [65]) and a single $\alpha 2$ chain (129 kg.mol^{-1} [66]), which form triple helix of approximately 407 kg.mol^{-1} (2x$\alpha 1$ + $\alpha 2$). It is believed that the procollagen molecule is more rigid (worm-like) than linear polymer chains (random coil), due to its helical secondary structure [67, 68].

Unfortunatelly, the molar mass distribution of soluble collagens (both acid soluble collagen and pepsin soluble atelocollagen) is usually accessed under denaturing conditions, [30, 35, 69–71, 71–73] giving limited information about the native state of molar mass distribution and aggregation. Therefore, development of new methods capable to access molar mass distribution in native state is important task for research in the collagen field.

Most frequently used method is sodium dodecyl sulphate-polyacrylamide gel electrophoresis (SDS-PAGE) [35, 69–71], due to its simplicity and low cost. However, a disadvantage of this method is the application of thermal denaturation and detergent to collagen in order to linearize and charge chains (to insure fractionation just by size). Using molar mass protein standards, SDS-PAGE usually provides a molar mass of soluble collagen I of about 300 kg.mol^{-1}, which is significantly lower than the expected molar mass of procollagen I (407 kg.mol^{-1}). Similarly, capillary electrophoresis [71, 72] characterizes only the denatured soluble collagens [71]. High-performace liquid chromatography (HPLC) is usually used for peptide mapping of collagen fragments [72]. Analytical Ultracentrifugation (AUC) is an important method for detection of protein aggregates [74], and it was applied to native soluble collagen a few decades ago [30, 75]. Native-PAGE has been successfully used for characterization of soluble collagens [76, 77] in native states, however it provides mixed information of atelocollagen molar mass, size, charge and shape. Size-exclusion chromatography (SEC) is the dominant method for characterization of molar mass distribution, but its application to proteins suffers from limited size range of molecules, limited buffer conditions (pH, high salt content) and aggregate formation, due to interaction with the large surface area of particles packed in columns [74, 78]. To the best of our knowledge, SEC has never been used for characterization of soluble collagens in native states. However, it has been applied to gelatin characterization (heat denatured collagen) [6, 30, 73, 79].

Asymetric Flow Field-Flow Fractionation with Multi-Angle Light Scattering (FFF-MALS) has been chosen for atelocollagen molar mass distribution charac-

Tab. 2.1: Soluble collagen molar mass distribution analysis methods overview

Method	Native (not denaturative)	Shear stress	Molar Mass Marker	Absolute Molar Mass	Handling	Repro-ducibility	Instrument cost	Widely used
SDS-PAGE	No	Low	Yes	No	Hard	Low	Low	Yes
Native-PAGE	Yes	Low	No	No	Hard	Low	Low	No
HPLC	No	Low	Yes	No	Easy	High	High	No
AUC	Yes	Low	No	No	Easy	High	Very high	No
SEC (MALS)	No	High	Yes	Yes	Easy	High	Very high	No
FFF (MALS)	Yes	Low	Yes	Yes	Easy	High	Very high	No

terization, because it allows separation without a stationary phase [78, 80, 81]. The method is unique in producing much smaller sample interaction area than SEC and lower tendency to aggregate [75, 78]. Therefore, it is generally more usable than SEC for characterization of various biomolecules [82–85]. Field-Flow Fractionation (FFF) is also usable with a wider range of buffers of various concentrations of salts and different pH. This allows operating at low pH, where positively charged soluble collagen dissolves (due to isoelectric point at neutral pH [86, 87]). Moreover, the FFF process could be applied to wide range of particle sizes, from a few nm to several μm. MALS and refractive index (RI) detectors could be combined with FFF in order to measure molar mass and root mean square (RMS) radius according to the Zimm's equation [88].

$$\frac{R_\theta}{K*c} = MP(\theta) - 2A_2cM^2P^2(\theta) + ...$$

Here R_θ is the Rayleigh ratio, c is the concentration (mg.ml^{-1}), M is the molar mass, A_2 is the second viral coefficient, K is the optical constant of the instrument and $P(\theta)$ is the particle scattering function (different for random coil, sphere, rod, etc.). Furthermore RMS radius and molar mass could be plotted into a conformation plot, which provides information about molecular conformation. Spheres should have a conformation plot slope of about 0.33, with random coils between 0.5 - 0.6 and rods equal to 1.0 [89]. Similarly to SEC, FFF was used in the past only for the characterization of gelatin [90, 91], but never for characterization of native collagen.

To the best of our knowledge, MALS together with the Zimm's equation have been used just once (in 1956) for the characterization of acid soluble fish carp bladder collagen (molar mass of about 345 kg.mol^{-1}, RMS radius of 52 nm) and gelatin (125 - 138 kg.mol^{-1}) solutions in batch (unfractionated) mode [92]. Advantages and disadvantages of the methods discussed above are summarized in table Tab. 2.1.

2.4.4.2 Circular Dichroism

Circular dichroism (CD) is able to detect properties of secondary structure of proteins because of its chirality. CD is often used in analysis of soluble collagen, thanks to its triple-helical secondary structure [8, 35, 93]. Because gelatin loses chirality, CD is able to sensitively detect difference between collagen and gelatin. It is known that CD signal at 221.5 nm is linearly proportional to collagen content, while gelatin signal at the same wavelength in any concentration is always very close to zero. Measured sample must be pure solution, without micron scale content, otherwise researcher is risking significant errors. Proper characterization of proteins by CD spectrophotometer was described in detail by Kelly et al. [94]. Today's common CD spectrophotometers measure also UV absorbance and many accessories could be involved in the measurement (Peltier temperature control, fluorescence detector, titration equipment, stopped flow equipment, etc.).

2.4.4.3 Rheology

Flow rheology measurements are often used for determination of denaturation temperature and filtration quality of isolated collagen [32, 33]. Also detailed analysis of the collagen solution is possible [38]. Other researchers use oscillatory rheology measurements to describe gel formation kinetics and mechanical properties of collagen gels [43] (Fig. 2.18).

2.4.4.4 Stress-strain mechanical testing

Stress strain mechanical testing is useful tool for characterizing fibres made by extrusion of collagen into bath [50] (Fig. 2.19), lyophilized collagen sponges [95] or composites with other biopolymer [96]. Collagen gels are usually tested by rheometers (as mentioned above).

2.4.4.5 Scanning Electron Microscopy

Scanning Electron Microscopy (SEM) is powerful imaging tool often used by material engineers. Its main advantage is the resolution (less than 10 nm), thanks to shorter wavelength used for imaging (of high voltage accelerated electrons). Unfortunatelly samples for SEM must be dried, because of the necessary vacuum inside the instruments. Thus, most of biological samples must be dried by adequate method before they are observed in microscope:

- **Freeze drying** is the simplest way to dry biological samples. Samples are fast frozen in liquid nitrogen and then dried in freeze dryer. Method suffers of several artefacts which are connected with crystallization of water during

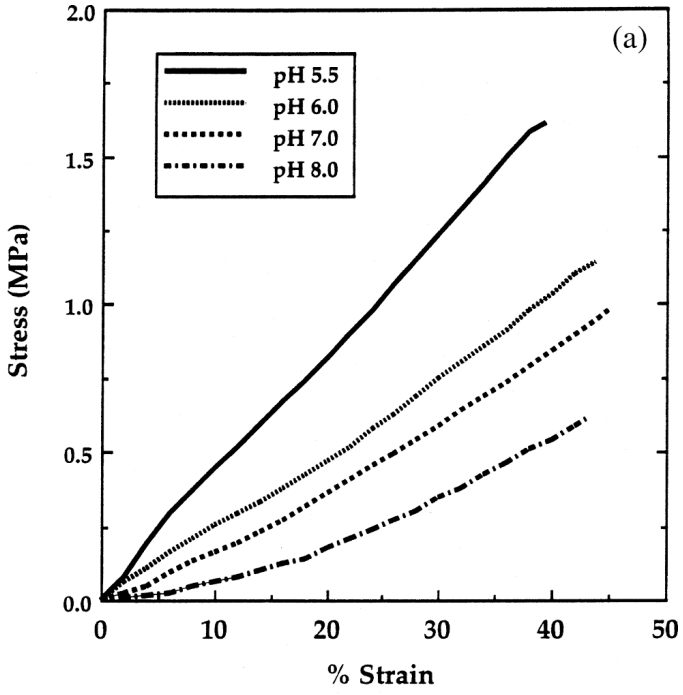

Fig. 2.19: Extruded collagen fibers shown different mechanical properties when formed at different pH [50].

freezing (instead of vitrification) [93, 97], so only very thin samples are recommended for this method. Some collagen products are directly produced by freeze drying method (collagen sponges), so they are ready to be observed by SEM.

- **Critical Point Drying (CPD)** is the most common way to dry biological samples for SEM. Thanks to negligible surface tensions of supercritical CO_2 liquid, drying of biological samples is possible with minor changes at the nano scale level (still shrinks up to 25%). Glutaraldehyde is basically used for (pre) fixation, but another fixatives (like osmium tetroxide) have to be used to obtain better (post) fixation [8, 43, 45]. Fig. 2.12 and Fig 2.20 show typical micrographs of in-vitro formed gels.
- **Cryo SEM** is rare method for observing biological samples due its expensiveness.

Biological samples are usually sputter coated by metal (gold, palladium, platinum) in order to make samples conductive, otherwise charging artefacts will occur.

2.4.4.6 Transmission Electron Microscopy

Transmission electron microscopy allows to visualize single collagen fibril or fibril bundles and observe its quarter staggered structure (Fig. 2.12 bottom, Fig. 2.21, Fig. 2.22) [8, 93]. This is unexceptionally useful to confirm soluble collagen ability

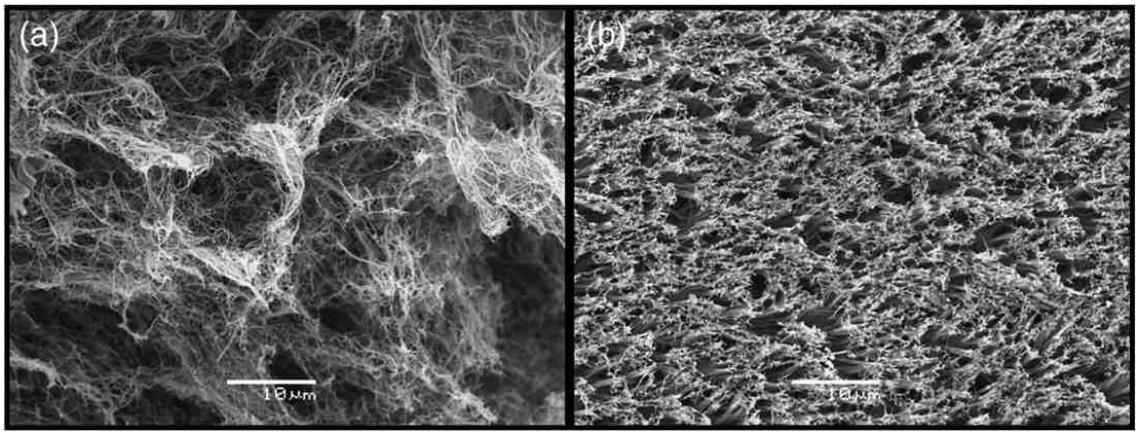

Fig. 2.20: Scanning electron micrographs of soluble collagen fibrillar gels: (a) 30 mg/ml, (b) 80 mg/ml.(Reprinted from [45])

.

to self-assemble into collagen fibres under various chemical, physical and processing conditions. Scientists use TEM for observing collagen fibrils of gels [8], gels with cells [98] and also for verifying recombinant collagen self-assembly ability [99].

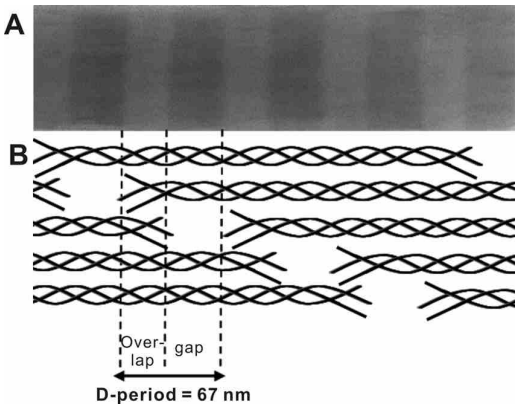

Fig. 2.21: Negativly stained single collagen fibril observed in TEM (reprinted from [93])

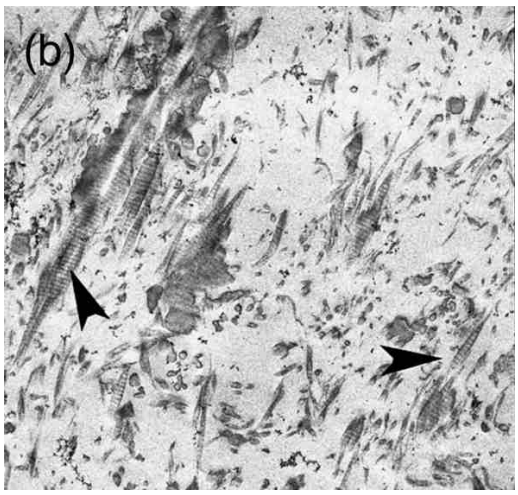

Fig. 2.22: Self-assembled collagen gels observed by TEM (negatively stained)

2.4.4.7 Atomic Force Microscopy

Atomic force microscopy is used to observe collagen at almost angstrom resolution with ability to see quarter staggered structure [5, 93, 97] (Fig 2.15). Collagen samples are normally observed in dry state. Wet state imaging is also possible, but difficult with limited resolution and many possible artefacts. AFM can be also used for mechanical testing of single collagen fibril [93, 100].

2.4.4.8 Differential Scanning Calorimetry

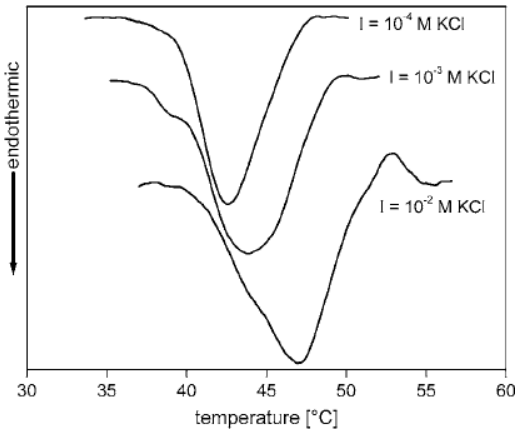

Fig. 2.23: DSC measuremnt shows increased stability of collagen solution in presence of KCl [86].

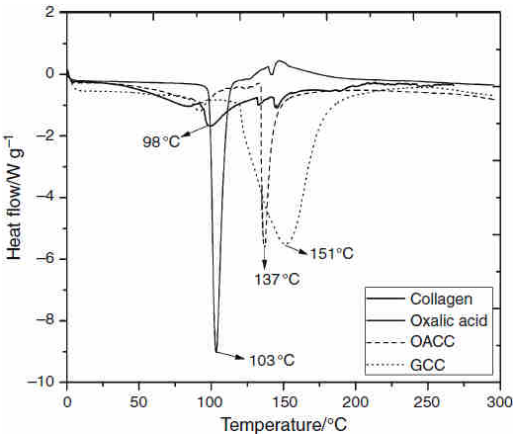

Fig. 2.24: Increased thermal stability of collagen membranes in presence of crosslinkers. Oxalic acid cross-linked collagen (OACC), and glutaraldehyde (GCC) [101].

Differential Scanning Calorimetry (DSC) is useful tool to evaluate stability of collagen solutions and solids. DSC could be applied to evaluate quality of collagen when isolated from tissues [32], observe denaturation temperature change in presence of additives in the collagen solution [86] (Fig. 2.23), or observe effect of crosslinkers to thermal stability of collagen products [101].

2.4.4.9 Confocal Reflectance Microscopy

In recent years Confocal Reflectance Microscopy(CRM) was used to visualize collagen gels in-vitro [43, 46]. Advantage of this method is simplicity of usage, no need of complicated sample preparation and possibility to measure in wet state. For example fibrilogenesis could be observed continuously (Fig. 2.25). The resolution is limited by Rayleigh resolution limit of visible light (300 - 500 nm). In consequence collagen fibers of sizes between 50 - 500 nm will be imagined in nonlinear contrast. This means 500 nm fibers will be visible with high contrast, 300 nm fibers with much lower contrast and 50 nm fibers will be invisible in confocal laser microscope.

2.4.4.10 SAXS

Small Angle X-ray Scattering (SAXS) could be used to quantify total amount of quarter staggered structure within the sample [45]. This method measures the scattering pattern within whole sample volume, thus it has high contrast. This brings big advantage against microscopy methods like SEM (2.4.4.5), TEM (2.4.4.6) and

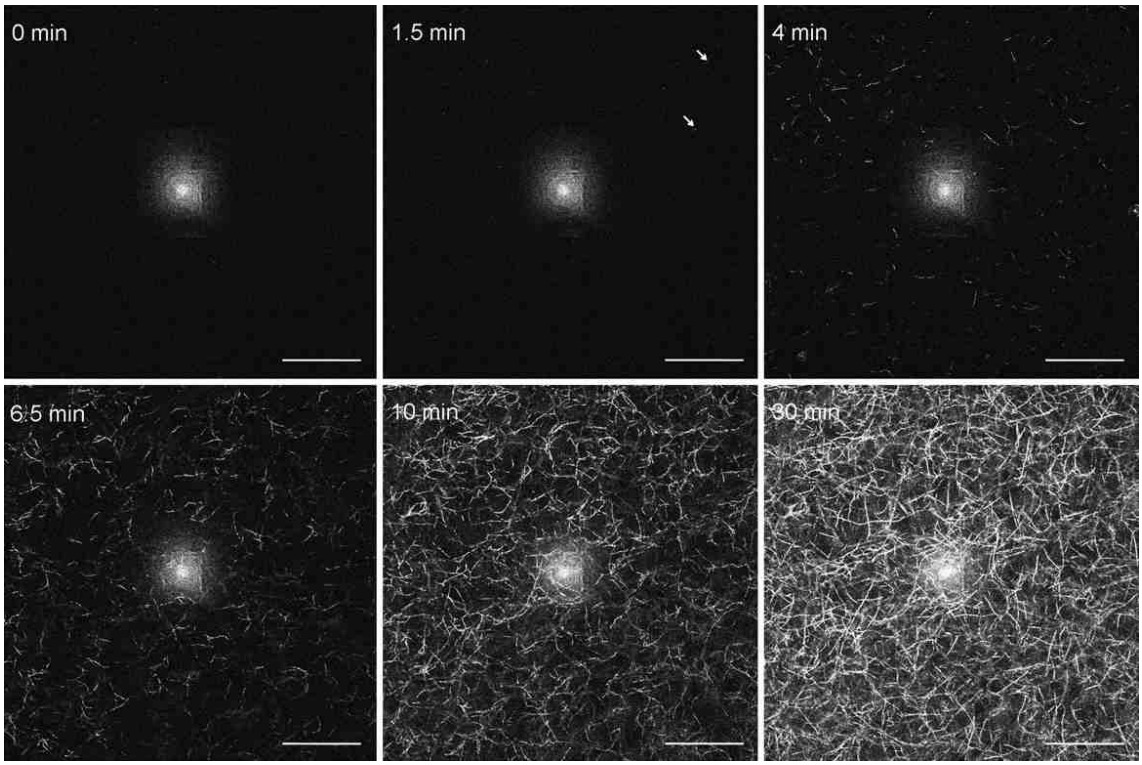

Fig. 2.25: Collagen 1 mg/ml during gelation at 37 °C, observed by confocal reflectance microscopyReprinted from [46].

CRM (2.4.4.9). Possibly fiber orientation [102] or another parameters could be also calculated from the SAXS spectra.

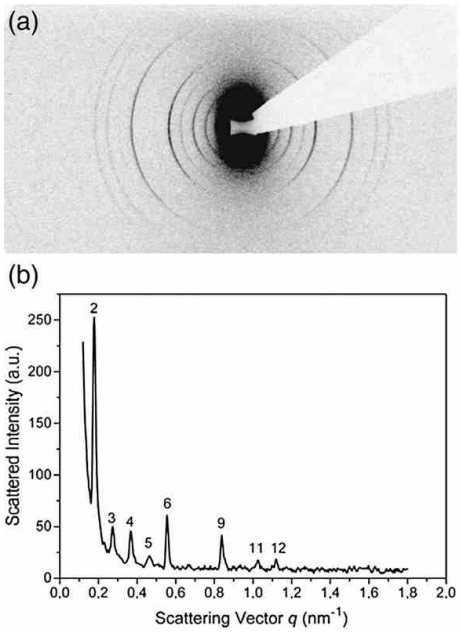

Fig. 2.26: (a) SAXS pattern of a 145-mg/ml fibrillar gel and (b) the corresponding linear plot of the scattered intensity I as a function of the scattering vector modulus q along the axial (equatorial) direction. The peaks labeled 2– 12 correspond to the reflections arising from the staggered stacking of the collagen molecules in the fibrils (67-nm period). Reprinted from [45].

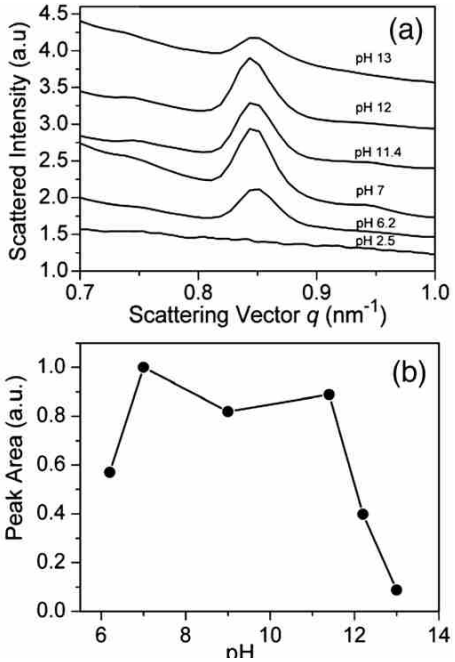

Fig. 2.27: SAXS detected quarter staggered structure(67 nm periodicity) of collagen samples at different pH. Reprinted from [45].

3 MAIN AIMS OF DISSERTATION WORK

The purpose of this work is to improve characterization and processing of soluble collagens. The main aims of this dissertation thesis are based on the structure properties, relationship and evaluation and are divided into two parts summarized in following highlights:

1. Soluble collagen dissolution and assembling in pressurized carbon dioxide water solutions
   - Dissolve atelocollagen in pressurized CO_2-water solution
   - Verify stability of atelocollagen under these conditions
   - Cast gels from atelocollagen CO_2-water solutions
   - Compare the results with conventional techniques
2. Molar Mass Characterization of soluble collagen in native state by Asymetric Flow Field Flow Fractionation-Multi Angle Light Scattering Technique (AF4-MALS)
   - Utilize and optimize the AF4-MALS technique for atelocollagen separation
   - Get information about collagen conformation
   - Compare the results with conventional techniques

4 EXPERIMENTAL PART

4.1 Materials

4.1.1 CO_2 experiments specific

Type I Bovine Atelocollagen solution PureCol® (0.01 M hydrochloric acid solution 3 mg.ml^{-1}, pH 2.0) was purchased from Advanced BioMatrix, (San Diego, CA, USA) and used either as it is or as a powder after freeze-drying (Lyophilizer Martin Christ Alpha 2-10 for 2 days at -80°C). The isoelectric point of PureCol® is reported following the producer datasheet in a range from pH 7 to 8.

Prior to drying, the PureCol® solution was dialyzed against deionized water (DI) water (Helix, Millipore, Temecula, CA, USA) for three days using Spectra/Por® dialysis tubing (MWCO 15 KDa, Spectrum Labs, CA, USA). Liquefied carbon dioxide, with a gas purity greater than 99.5 vol%, was acquired from Air Liquide (Milan, Italy). NaOH, acetic acid (AA) and PBS were purchased from Lachner (Neratovice, Czech Republic) and Sigma Aldrich (St. Louis, Missouri, USA), respectively. For the preparation of collagen solutions in CO_2/water, 10 ml polypropylene (PP) bottles with a perforated PP cup, connected to the CO_2 reservoir via Fizz giz valves (Jamestown, NC, USA) were used (Fig. 5.5A).

4.1.2 FFF experiments specific

Commercial atelocollagen (Nutragen®, Advanced BioMatrix, San Diego, CA), commercial gelatin type A (St. Louis, MO, USA), acetic acid (AA, 99.9%, Penta, Czech Republic) and sodium chloride (NaCl, Lachner, Germany) were used for all experiments.

4.1.2.1 Sample preparation

0.1 M NaCl in 0.5 M AA (pH 2.4) was used as the solvent (or mobile phase) for FFF, DLS and CD experiments. The commercial atelocollagen (Nutragen) was dialyzed for 3 days against the solvent (daily solvent change, 15 kDa cut off) in order to equilibrate the solvent with the atelocollagen samples. Samples were diluted in solvent to a concentration of 0.5 mg.ml^{-1} and filtrated using a 0.2 μm syringe filter. The electrophoresis of samples was characterized as supplied, without solvent exchange and without filtration. For thermal denaturation experiments bulk atelocollagen sample was divided into aliquots and subjected to thermal treatment at either 37°C or 50°C for 0, 15, 30, 60 and 120 min. Then, the denatured and non-denatured samples were characterized by FFF, CD and DLS and electrophoresis.

4.2 Experimental Protocols

4.2.1 Control atelocollagen self-assembly

Dissolution of freeze-dried atelocollagen powders in different solvents (AA - 0.1 and 0.5 M, H_20 and carbon dioxide CO_2 water solutions in equilibrium with CO_2 atmospheres at 0.5 and 0.9 MPa pressure) was determined by measuring the concentration of solubilized atelocollagen at fixed time intervals during the dissolution process (every time the sample was pressurized and depressurized for sampling and measurement). The concentration of solubilized atelocollagen was determined with MicroBCA® Protein Assay Kit (Thermo Scientific) following the manufacturer's instructions. Absorbance values from a microplate reader (Infinite 200, TECAN) at 562 nm were correlated to the dissolved atelocollagen concentration. Concentration of 0.5M AA at final time point was taken as reference (100%) as the 0.5 M AA is the most common solvent used in literature.

4.2.2 Dissolution kinetics of atelocollagen powder at different conditions

The dissolution of freeze-dried atelocollagen powders in different solvents (Acetic acid, -AA- 0.1 and 0.5 M, H_20 and Carbon dioxide -CO_2- water solutions in equilibrium with CO_2 atmospheres at 0.5 and 0.9 MPa pressure) was determined by measuring the concentration of solubilized atelocollagen at fixed time intervals during the dissolution process. In all cases, the final concentration of atelocollagen was 3 $mg.ml^{-1}$. The different atelocollagen suspensions were held at 4°C under constant agitation by using an orbital shaker. At fixed time points (5 - 120 min), the batches were shortly removed from the shaker and 10 μl of solution was collected.

The concentration of solubilized atelocollagen was determined with MicroBCA Protein Assay Kit (Thermo Scientific) following manufacturer's instructions. All samples were diluted 12 times till a concentration of 0.25 $mg.ml^{-1}$ (to insure micro BCA linearity). Samples were mixed with the assay at 1:1 ratio and heated for 1 h at 60°C. Absorbance values from microplate reader (Infinite 200, TECAN) at 562 nm were correlated with the dissolved atelocollagen concentration.

4.3 Characterization Methods

4.3.1 Atelocollagen denaturation detection by Electrophoresis

4.3.1.1 SDS-PAGE

0.3 $mg.ml^{-1}$ diluted solutions were mixed with assay buffer (Novex® Tris-Glycine SDS Sample Buffer 2X) following the manufacturer's instructions. Samples were analysed by 1D, sodium dodecylsulfate polyacrylamide gel electrophoresis (SDS-PAGE, with an XCell4 SureLockTM Midi-Cell (Carlsband, CA, USA), at a constant voltage of 100 V. Acrylamide gel SDS-PAGE NuPAGE® (Invitrogen, Carlsbad, CA, USA) Novex Tris-Acetate Gels (3%, 8%) was used. Novex® Sharp Pre-Standard (Lifetechnologies, Carlsband, CA, USA) presented the MW reference. The acrylamide gels were stained using a Comassie stain (Imperial Protein Stain, Thermo Scientific, Rockford, IL, USA). Gels were digitalized using a GEL LOGIC 200 (Kodak Scientific Imaging Systems, Rochester, NY, USA) imaging system.

4.3.1.2 Native-PAGE

Native-PAGE was performed under acidic conditions (pH 2.4) using 0.1 M glycine/HCL running buffer (glycine 11.1 $g.l^{-1}$, HCL 8.6 $g.l^{-1}$). Loading buffer was prepared by adding 20% sucrose into running buffer. Nutragen atelocollagen was diluted with 0.01 M HCl to 3 $mg.ml^{-1}$. Half of the samples were heated for 15 min at 37°C in order to denature the atelocollagen. A 5% separating gel was prepared by mixing 5.6 ml of acrylamide:bisacrylamide (29:1), 39 ml of water, 0.08 g of calcium acetate and 90 μl of acetic acid (final pH 3.4). Gelation of the separating gel was initialized by adding 315 μl of TEMED (Tetramethylethylenediamine) and 3.15 ml of 10% APS (Ammonium persulfate). The samples were then mixed with loading buffer in a 1:1 ratio, loaded into gel wells and separated for 15h at 50 V and 15°C using a temperature-controlled submersible apparatus (SE600, Hoefer Scientific) containing circulating buffer. The acrylamide gels were stained for 15 min using a comassie stain (G-250, 50% methanol, 10% acetic acid). Samples were unstained in 30% methanol and 10% AA for 1h.

4.3.2 Atelocollagen denaturation detection by circular dichroism

4.3.2.1 CO_2 experiment specification

CD spectroscopy was used in order to quantify atelocollagen denaturation during the experimental procedures using a dedicated analysis protocol modified from [35]. The above defined CO_2 and AA atelocollagen solutions (two samples for each experimental conditions) were diluted with 0.1M AA 10 times to 0.3 mg.ml^{-1}. Then, the diluted solutions were transferred into quartz cells (2 mm path length) and measured by Jasco J-710 (Jasco, Tokyo, Japan) at a wavelength range between 190 and 350 nm at room temperature.

4.3.2.2 FFF experiments specific

CD spectroscopy (Jasco J-1500, wavelength range between 216 - 260 nm, bandwidth 1 nm, path length 2 mm, temperature 21°C) was used as the reference method for the detection of atelocollagen denaturation [35]. A selection of samples used in the FFF experiments were diluted in solvent to 300 μg.ml^{-1} in order to obtain adequate absorbance within scanning range. Measurement of CD spectra at wavelengths shorter than 216 nm was not possible due to the high absorbance of the solvent at these wavelengths (0.5M AA, 0.1 M NaCl). Native atelocollagen was used as the fully folded (triple helix) reference and commercial gelatin was used as the unfolded (random coil) reference.

4.3.3 Scanning Electron Microscopy

Atelocollagen powder in water (3 mg.ml^{-1}) was dissolved in CO_2 atmosphere (0.5 MPa) for two days, depressurized, transferred into petri dishes and covered by 1 mM of NaOH (pH 9.0) overnight. The formed gel was fixed in 1-Ethyl-3-(3-dimethylaminopropyl) carbodiimide/ N-Hydroxysuccinimide (EDC/NHS), dehydrated in graded ethanol solutions and critical-point dried (CPD 030, Bal-Tec). Finally, dried gels were gold coated (6nm) and observed with a scanning electron microscope at 7 kV (Tescan Mira3, Czech Republic). The mean fiber and pore diameters were calculated from 100 manual measurements using Fiji software [103].

4.3.4 Transmission Electron Microscopy

CO_2 samples for TEM were cast as for SEM. The control sample was cast according to section 2.2. For the sectioned method [9], atelocollagen solutions were pipetted

into 1mM NaOH solutions to form stable gels, and left overnight at room temperature. Gels were fixed by glutaraldehyde, then by osmium tetroxide, dehydrated in graded ethanol solutions, converted to acetone and fixed in Durcupan® (Sigma-Aldrich, St. Louis, Missouri, USA). Fixed samples were sectioned by ultramicrotome (Leica EM UC6, Wetzlar, Germany) to 50 nm slices and negatively stained by lead nitrate. TEM samples were observed by FEI Morgagni 268D (Brno, Czech Republic) at 70 kV.

4.3.5 Rheology

Continuous flow experiments were performed in cone-plate geometry on both CO_2 and AA dissolved atelocollagen solutions by using an Anton Paar Physica MCR 301 Rheometer, connected to a Lauda RE 204 cooling thermostat (4 °C) and to a Peltier HPTD200 cell for heating. Methodology was adopted from Gobeaux et al.[38]. Measurements were done at shear rates between 0.001 s^{-1} and 400 s^{-1} at 4 °C without pre-shearing. Oscillatory experiments to observe gel formation kinetics[29] were performed using a TA Ares G2 Rheometer, with a Peltier cooling cell and cone-plate geometry. Samples were prepared according to Table 4.1.

The control atelocollagen sample was prepared according to section 2.2 at 1.5 mg ml^{-1} [9]. Pre shear at 2 rad s^{-1} for 10 s was performed prior to oscillation. Time sweep oscillation was performed at 1 Hz, 0.8 % strain.

Tab. 4.1: CO_2 samples used in the rheological oscillatory experiments

	dissolution conditions					**rheometer conditions**		
sample	concentration [mg.ml^{-1}]	pressure [MPa]	temperature [°C]	duration [days]	depressurized overnight	dilution 1:1 by 1 mM NaOH on rheometer	final concentration [mg.ml^{-1}]	heated on rheometer geometry [°C]
CO_2 0.5 MPa 37 °C	1.5	0.5	4	2	Yes	-	1.5	37
CO_2 0.5 MPa 37 °C NaOH	3.0	0.5	4	2	-	Yes	1.5	37
CO_2 0.1 MPa 4°C	1.5	0.1	4	2	Yes	-	1.5	4
CO_2 0.5 MPa 4°C	1.5	0.5	4	2	Yes	-	1.5	37
control	Purecol as supplied (in 0.01M HCL, 4°C) neutralized by PBS and NaOH					-	1.5	37

4.3.6 Light transmittance

Samples prepared according to Tab. 1 (0.5 MPa CO_2 37°C and control sample), before heating, were pipetted into a 2 mm cuvette and heated to 37°C by a Peltier cell in a Jasco-J1500 CD spectrophotometer (Jasco, Tokyo, Japan). The transmittance values were read one hour after heating, at 310 and 550 nm [49].

4.3.7 AF4-MALS

The atelocollagen separation was performed in an asymmetric-flow FFF system (Eclipse AF4, Wyatt Technology) using Long Channel (LC, 275 mm), wide 350 μm spacer and a 30 kg.mol^{-1} RC (Regenerated Cellulose) semipermeable membrane. The elution profile was run according to Fig. 5.13A.

Online concentration was detected by RI detector (Optiplab T-rEX,Wyatt Technology). Angular dependent Light scattering was detected by MALS instrument (Fig. 4.1, Dawn Heleos II, Wyatt Technology). Molar mass, RMS radius (R_g) and other operations were calculated from scattering and concentration data using Astra software (version 6.1, Wyatt Technology). Berry formalism was used for molar mass and RMS radius calculations. If not mentioned otherwise, 50 μg of injection solution was used for FFF experiments. 50 μg of protein was injected (100 μl) per single AF4 run. Dn/dc = 0.164 was use according to [90, 91] (this constant was also experimentally confirmed for collagen, data not presented).

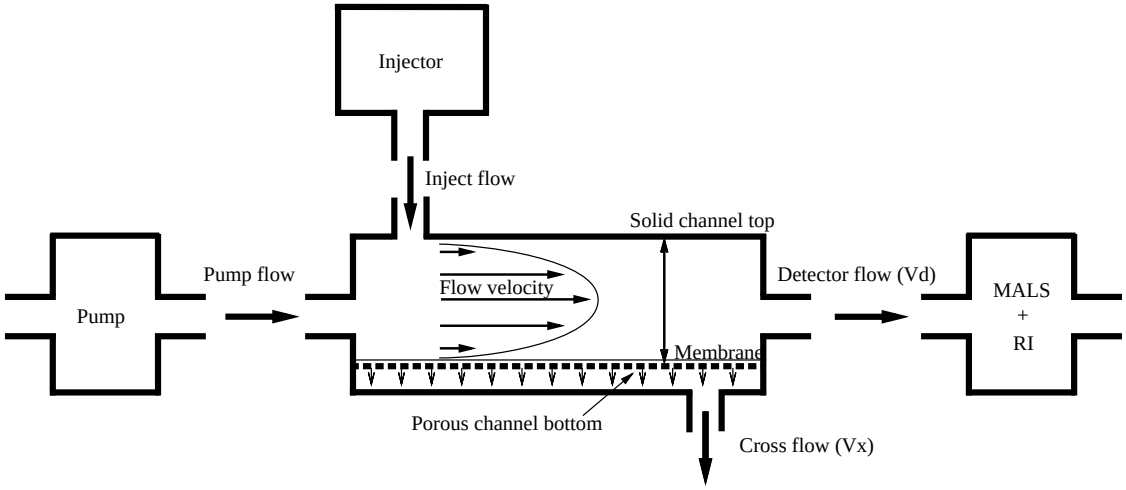

Fig. 4.1: Pump-FFF-detectors instrumentation setup

4.3.8 DLS

Batch mode DLS (unfractionated) was used as the reference method in the denaturation experiment. A portion of the samples used in FFF experiments were further diluted by mobile phase to 50 μg.ml^{-1} in order to prevent aggregation and keep good signal to noise ratio. The measurements were performed on a DLS Wyatt NanoStar instrument (disposable cuvette, acquisition time 2 s, 20 acquisitions at 21°C). The lowest resolution was used for calculation of distributions.

4.3.9 Data processing

Measured (Light scattering and RI) signals and calculated (molar mass, RMS radius) datasets from FFF (Astra) and from other facilities (CD, DLS, electrophoresis) were loaded using the Python programing language (Python Software, Python Language Foundation Reference, version 3.5. Available at http://www.python.org) and processed (select, join tables etc.) with additional libraries [104–108] and visualized by seaborn [109].

4.3.9.1 Modeling

WLC Monte Carlo simulation (100 chains, each 500 000 random moves) was processed using [110] library. Contour length of atelocollagen molecule was assumed to be constant at 300 nm [68], with Kuhn length optimized in order to get the same RMS radius as measured by MALS. Straight rod RMS radius was calculated according to Rubinstein et al.[111].

5 RESULTS AND DISCUSSION

5.1 Soluble collagen dissolution and assembling in pressurized carbon dioxide water solutions

5.1.1 Results and discussion

This study evaluated the solubility, gelation and gel structural properties of bovine type I atelocollagen processed by pressurized carbon dioxide in water. Atelocollagen processed in standard conditions in acetic acid solution was used for comparison. An increase of CO_2 solubilized in water results in an increased carbonic acid content and with increased pressure and temperature and decrease in solution pH (Fig. 5.1A). This principle was previously investigated to process various proteins including soy [112] insulin [113], silk fibroin [114] and others.

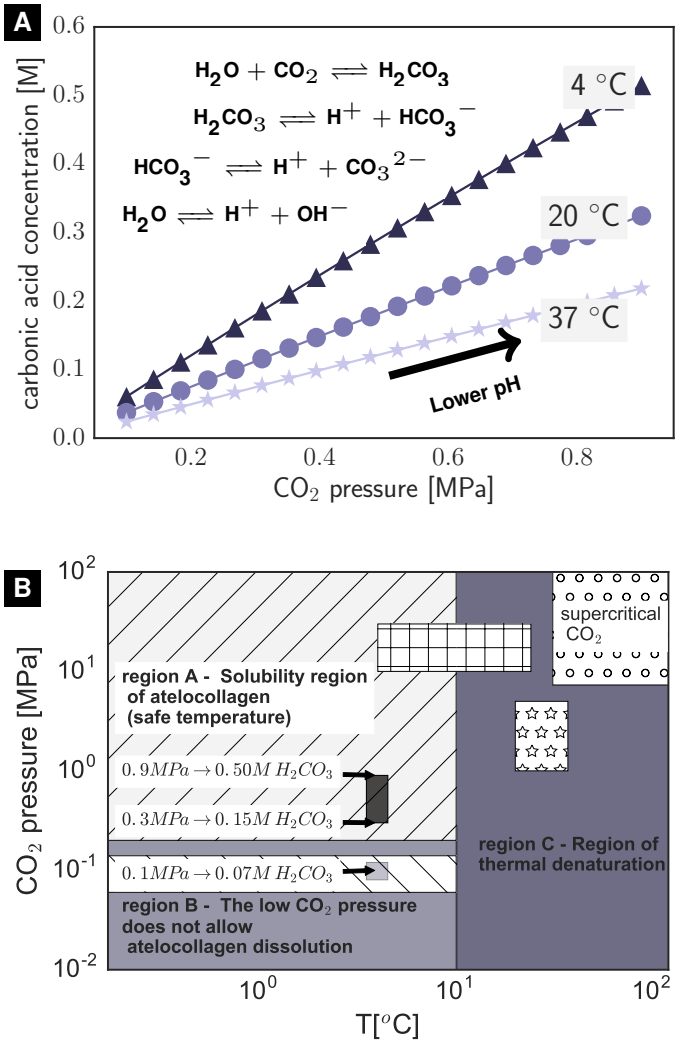

Fig. 5.1: ***A*** *Solubility of carbonic acid in water as of function of pressure and temperature, the curves were calculated according to Duan et al. measurements/model [33].* ***A*** *CO_2 pressures and temperatures used for soluble collagen processing in present work (region A) and overview of similar previous works.*

Previous attempts to extract soluble collagen (Fig. 5.1B, stars) at higher temperatures (20 - 37°C) and CO_2 pressures 1 - 5 MPa [58, 59] yielded into pure gelatin, according to the presented Circular Dichroism (CD) spectroscopy (missing peak at 221 nm) and sodium dodecyl sulfate polyacrylamide gel electrophoresis (SDS-PAGE, missing the typical collagen fingerprint of an intensive band below 37kDa) and broad range of molar mass. From this results, it was concluded that the entire region C (Fig. 5.1B, Fig. 5.2 right) is unsafe for soluble collagen processing. However region C should be still useful for insoluble collagen processing in pressurized [60, 61] or supercritical conditions [62, 63, 115]. Other previous studies on atelocollagen processing in carbonic acid at atmospheric pressure (Region B, Fig. 5.1B,Fig. 5.2 left)[57], lacked sufficient carbonic acid concentration (< 0.07 M, Fig. 5.1A left[33]) causing soluble collagen just to swell.

From these results we can assert that the combination of both high pressure (0.3 - 0.9 MPa) and low temperature (4°C) (Fig. 5.1B region A, Fig. 5.2 center) should represent optimal conditions for solubilisation [33]. The low temperature also ensures stability of soluble collagen at storage temperatures below 10°C [54–56, 116]. The grey rectangle on Region A (Fig. 5.1B, 0.3 - 0.9 MPa) points to experimental conditions used in presented work.

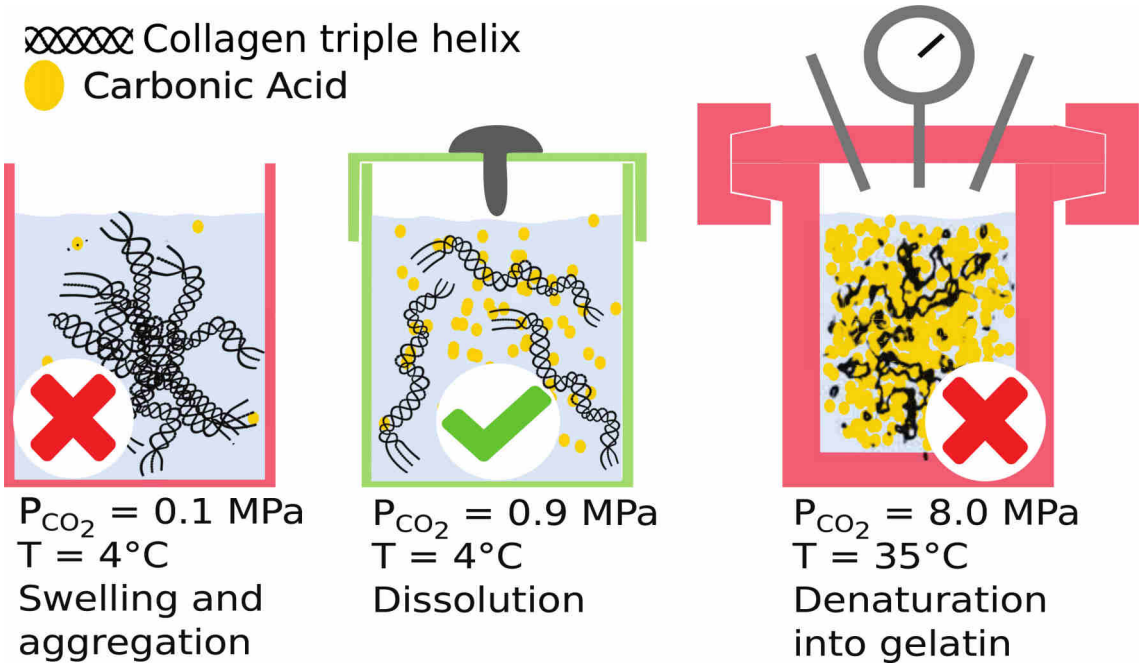

Fig. 5.2: Solubility and stability of soluble collagen at different CO_2 pressure and temperature.

5.1.1.1 Effect of CO_2 pressure and pH on atelocollagen self-assembly

The gelation degree of atelocollagen solutions was measured by varying the pH of AA (pH = 3) by step-by-step neutralization with NaOH. Summarizing the results in a plot (Fig. 5.3A) has shown that collagen precipitation and gelation started when pH was higher than 4. Similar pH conditions were obtained applying 0.9 MPa of CO_2 pressurized atmosphere for two days to an atelocollagen solution (3mg.ml^{-1}). In this case, immediately after depressurization, the measured pH was equal to 3.2, thus compatible with the condition of dissolved collagen. The increase of pH necessary to obtain solution gelation is simply a function of time (up to 5.7 after 70 min), and is due to the gas evolution from the solution (Fig. 5.3B). The dissolution effect seems to be correlated with the CO_2 pressure-induced drop of pH, since the use of an inert gas pressurization like N_2 does not allow solubilisation.

5.1.1.2 Atelocollagen dissolution kinetics

Swelling and dissolution behaviours of atelocollagen powders were first qualitatively recorded in different solvents (AA 0.5 M, H_2O and 0.9 MPa CO_2) by using a camera. Digital images were collected immediately after mixing the atelocollagen powder with solvents at predetermined time intervals. For the 0.9 MPa CO_2 sample, images one minute before pressurization were also acquired.

The higher the CO_2 pressure, the faster the dissolution of atelocollagen in the solutions was observed. In the H_2O and AA 0.5 M samples, bubbles remained attached to atelocollagen powder (Fig. 5.4 upper and center line, time 0 - 60 min), reducing the atelocollagen-solvent contact. Pressurization by CO_2 allow bubbles compression, improving the solvent-atelocollagen contact and contributing to the atelocollagen dissolution (fig. 4 bottom, time 0 - 10 min).

The dissolved atelocollagen in AA 0.1M, AA 0.5M, 0.5 MPa CO_2, and 0.9 MPa CO_2 at defined time points was quantified by microBCA® assays (Fig. 5.5B). Taking the dissolution in AA 0.5M after 2 hours, as a reference of 100% dissolution, about 140% of atelocollagen was dissolved in 0.5 or 0.9 MPa CO_2 and only 75% in 0.1M AA.

Even if the pH equilibrium of CO_2 samples under pressure was not measurable, by the way, right after depressurization the pH was equal to 3.2 acquired at atmospheric pressure (Fig. 5.3B). Therefore the effect of pH on the dissolution cannot be directly discussed. However, it seems the improved solvent-atelocollagen contact (due compression of bubbles surrounding atelocollagen powder, Fig. 5.4) is the major effect improving the speed of dissolution of CO_2 samples. The effect was even improved by the fact, that the samples were repeatedly pressurized and depressurized during the experiment, causing the reduction of bubbles number and size and,

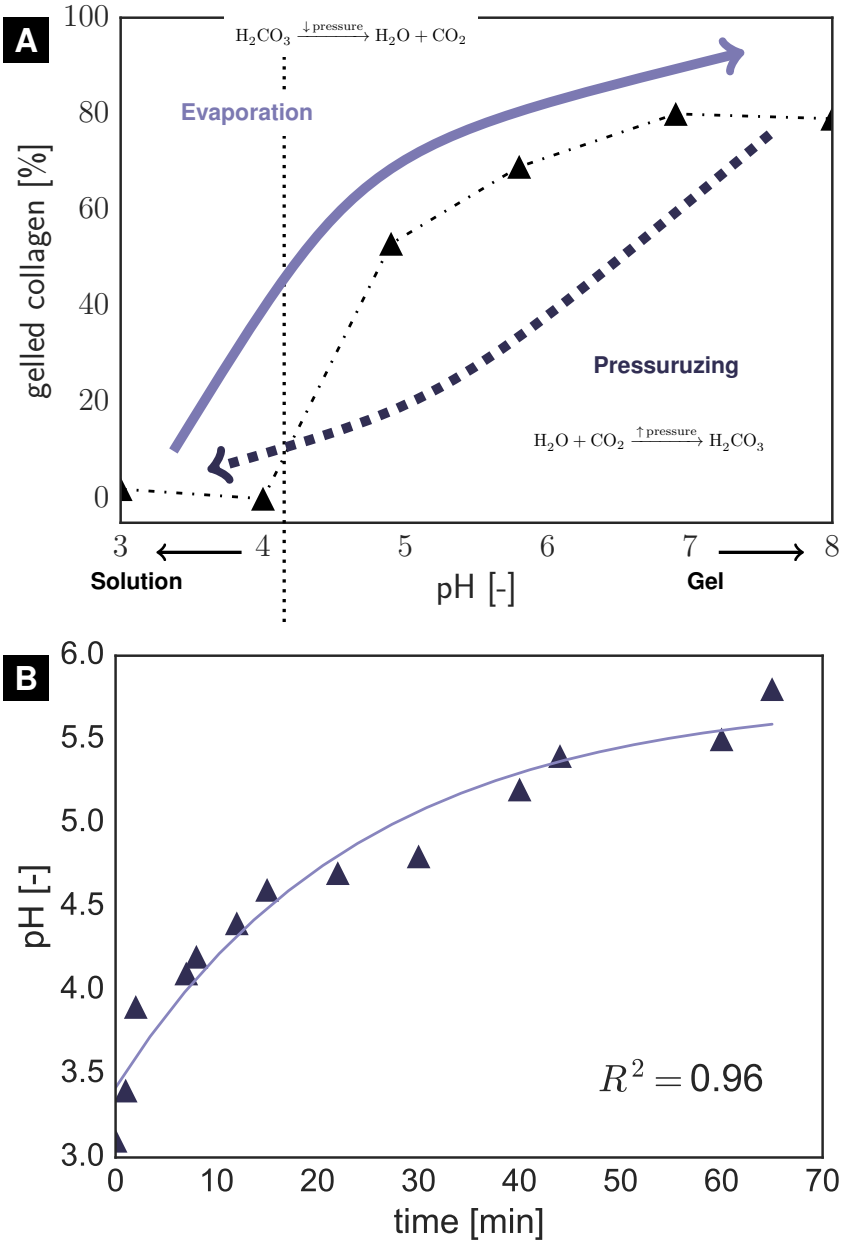

Fig. 5.3: ***A*** *Self-assembly of atelocollagen dissolved in 0.1 M AA and neutralized by NaOH (triangle), arrows and equations demonstrate the principle of CO_2 processing. Dashed arrow represents CO_2 pressurizing and full arrow CO_2 removal.* ***B*** *Time development of pH in the CO_2 0.9 MPa sample immediately after opening the pressurized bottle.*

thus enabling better solvent-atelocollagen interaction, as can be seen in the time sequence of Fig. 5.4

5.1.1.3 Stability of atelocollagen within AA and CO_2 dissolution

Atelocollagen stability in samples AA 0.1M, AA 0.5M, 0.5 MPa CO_2, and 0.9 MPa CO_2 was evaluated by both SDS-PAGE (Fig. 5.6) and CD spectroscopy (Fig. 5.7)

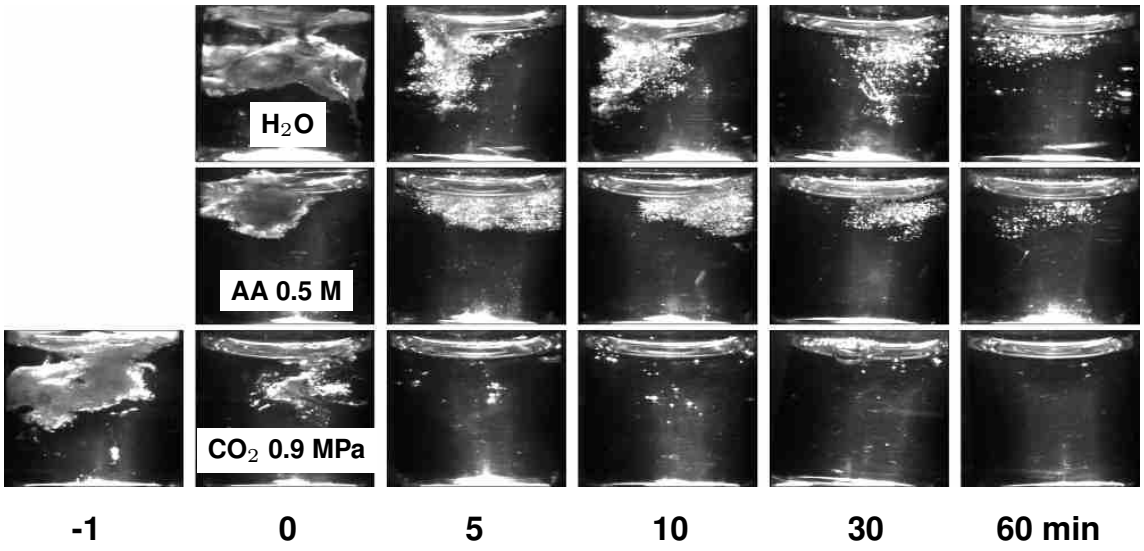

Fig. 5.4: Dissolution of atelocollagen in water, AA 0.5 M solution and CO_2 athmosphere at 0.9 MPa observed by camera.

after 2, 4, and 6 days. CD signals at 221.5 nm were normalized and converted to percentage where the maximum at 2, 4 and 6 days for each solvent was set as 100 %. Small variation in signals is probably induced by pipetting error rather than denaturation. We did not find any significant differences between individual samples, both with SDS-PAGE and CD spectroscopy. These results indicate that denaturation has not occured in any of the tested samples.

5.1.1.4 Rheological behaviour of atelocollagen in both AA and CO_2 water solutions

The viscosity of AA 0.1M and CO_2 0.5 MPa samples was determined by continuous flow rheological analysis. The atelocollagen sample prepared in 0.1 M AA has not show any pH changes during the measurement (pH = 3.0), while the pH of sample in 0.5 MPa CO_2 increased during the measurement from 3.8 to 4.3, due to CO_2 gas evolution from the solution. This inconvenience cannot be avoided, since it is impossible to perform the viscosity measurements under constant pressurized conditions. Much more intensive gas evolution of CO_2 0.9 MPa samples resulted in escaping part of the sample out of the rheometer geometry, so the measurements were excluded from the results. CO_2 0.1 MPa samples were not measurable because of evidence of incomplete dissolution, containing few millimeter sized atelocollagen aggregates.

Results showed (Fig. 5.8B) clear differences between viscosities of AA 0.1 M (triangles) and 0.5 MPa CO_2 (circles) samples. Intrinsic viscosity was calculated [38] using regression of reduced viscosity to the zero concentration (Fig. 5.8B). The

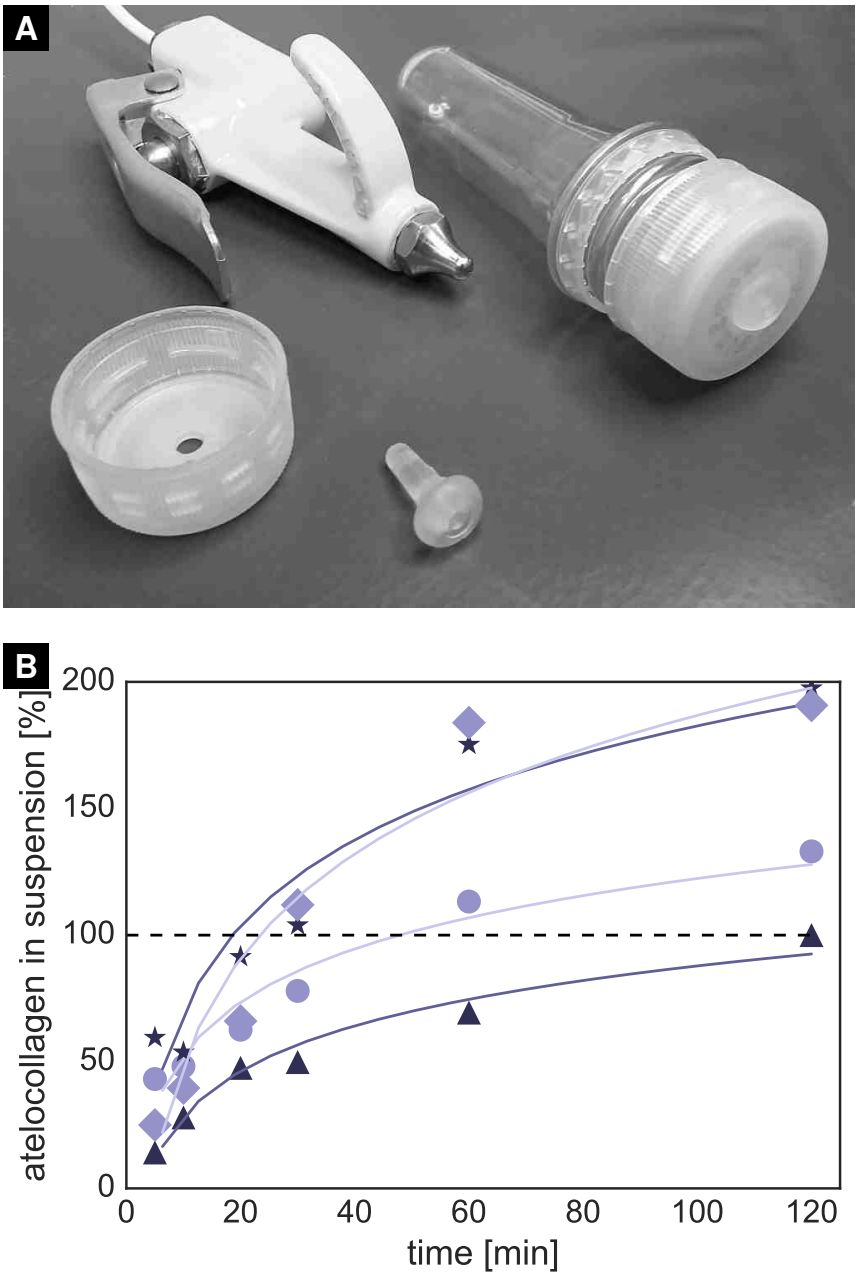

Fig. 5.5: ***A*** *Pressurizable polypropylene bottles, cups, valves and dispenser used in the experiments.* ***B*** *Dissolution kinetics of atelocollagen dry powder in different solvents determined by microBCA assay: Sample AA 0.1M (triangles), AA 0.5M (circles), CO_2 0.5 MPa (stars), CO_2 0.9 MPa (diamonds)*

obtained intrinsic viscosity value for 0.1 M AA ($[\eta] = 602$) is lower than previously reported, while $[\eta] = 764$ for the CO_2 sample is in good agreements with the value found in literature ($[\eta] = 765$) [38]. The difference also correlates well with the atelocollagen self-assembly curve obtained in Fig. 5.3A. Prolonged (16h) continuous flow measurements (Fig. 5.8 B) of a depressurized 0.5 MPa CO_2 sample showed increased viscosity from 14 to 110 Pa.s as a consequence of carbon dioxide loss from the solution at atmospheric pressure initiating gelation.

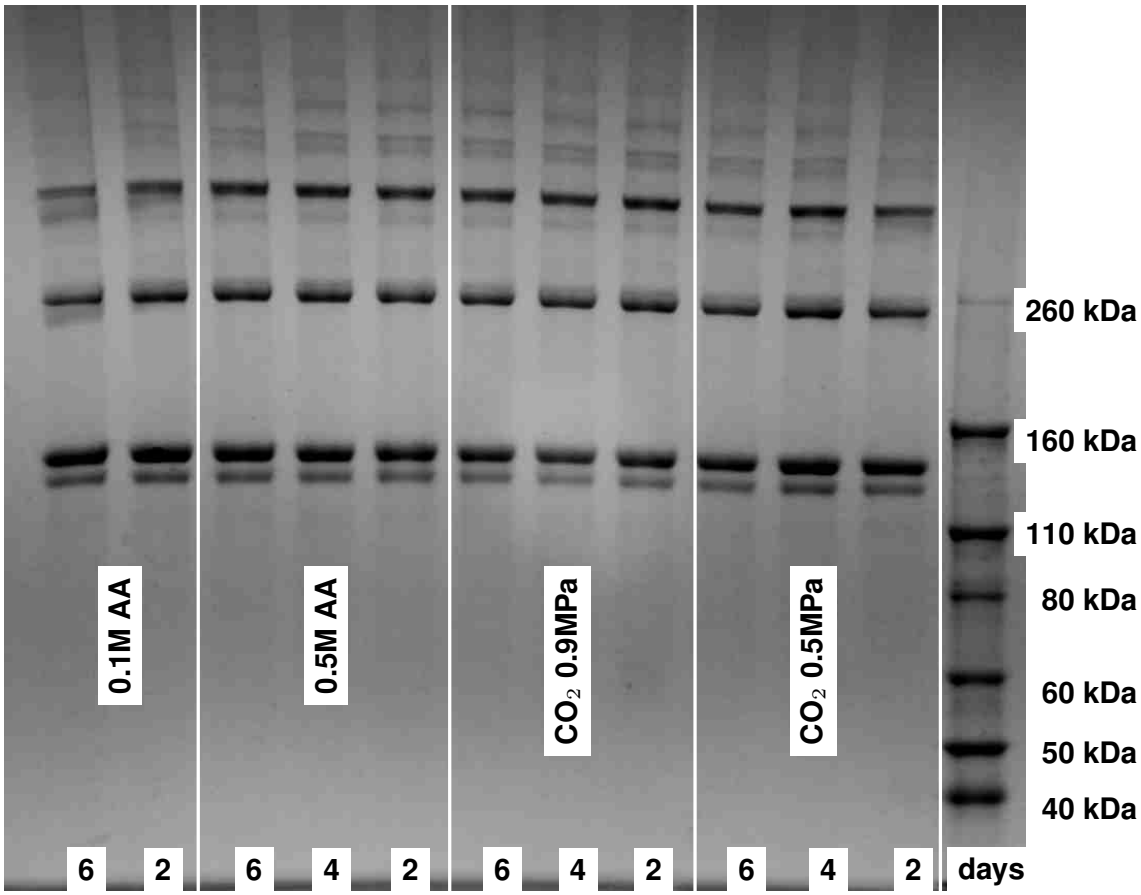

Fig. 5.6: SDS-PAGE of samples incubated for 2, 4, and 6 days in different solvents.

Gelation kinetics of samples prepared according to table 4.1 was evaluated by using oscillatory rheological analysis, on samples prepared according to Table 4.1. G" and G' (storage and loss modulus respectively) are representative of the viscous and elastic behaviour of a material. A larger value of G' in comparison to G" indicates that a material displays predominantly elastic properties, while G" > G' indicates that viscous properties prevail.

The experimental curves are reported in Fig. 5.9A and B, while the synthesis of the solutions properties at different times (the beginning, the first gelation plateau, and at the end) are provided inTable 5.1.

The samples depressurized overnight (0.5 MPa CO_2 4°C and 0.5 MPa CO_2 37°C) were prepared identically (Table 4.1). The cooled 0.5 MPa CO_2 4°C samples were liquid at the beginning of the experiment (Table 5.1, $\tan\delta = 1.5$), however they became weak gels ($\tan\delta = 0.9$) by the end of the experiment, probably due to manipulation, pre-shear, and rheometer vibrations, which induced the release of CO_2. The 0.5 MPa CO_2 37°C sample became a gel very fast within 0.6 min ($\tan\delta = 0.4$). Similarly, 0.5 MPa CO_2 37°C NaOH, formed a gel very quickly ($\tan\delta = 0.2$ at 1.3 min), despite the lack of overnight depressurization (Table 4.1). CO_2 0.9 MPa sam-

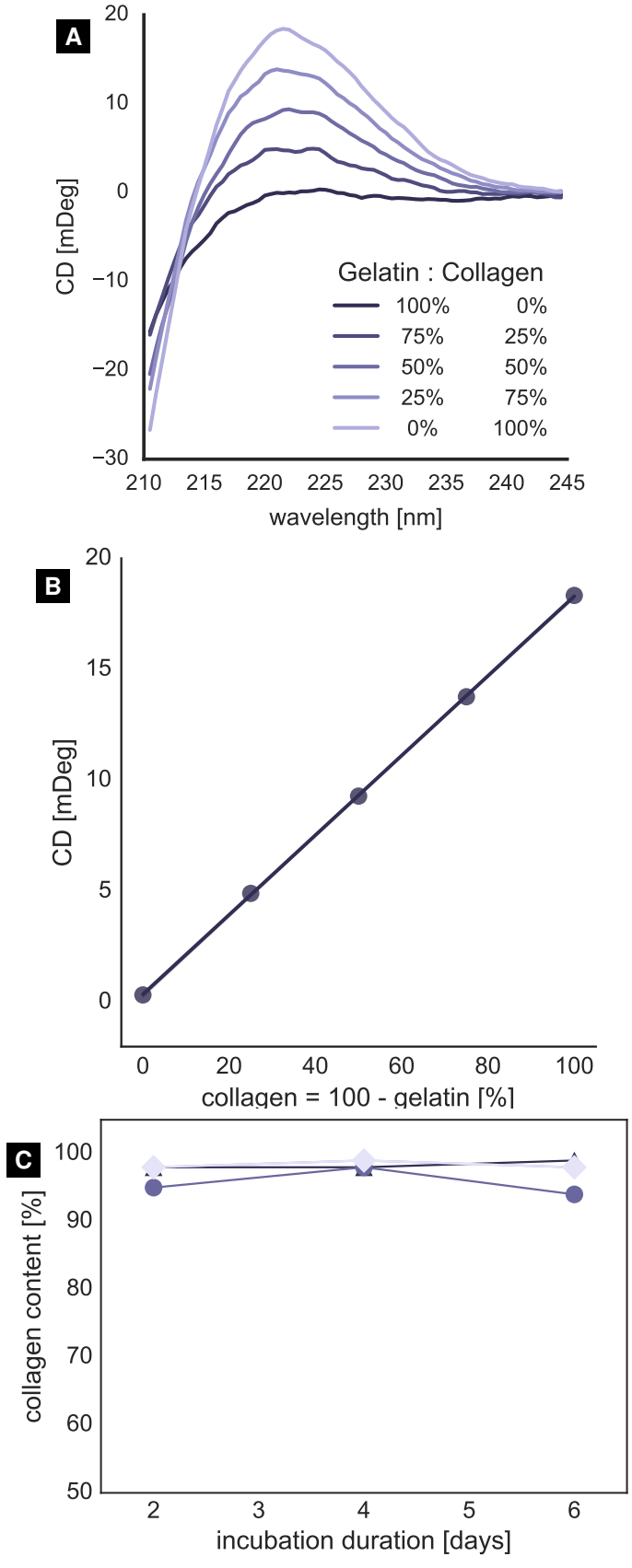

Fig. 5.7: Ability of CD spectrophotometer to recognize collagen and gelatin mixtures. ***A*** *CD spectras,* ***B*** *CD signal at 221.5 nm dependence on collagen concentration [%].* ***C*** *CD signal at 221.5 nm of CO_2 0.5 MPa (triangles), CO_2 0.9 MPa (circles), 0.1M AA (stars), 0.5M AA (diamonds) samples incubated for 2, 4 and 6 days is dropping down = no denaturation.*

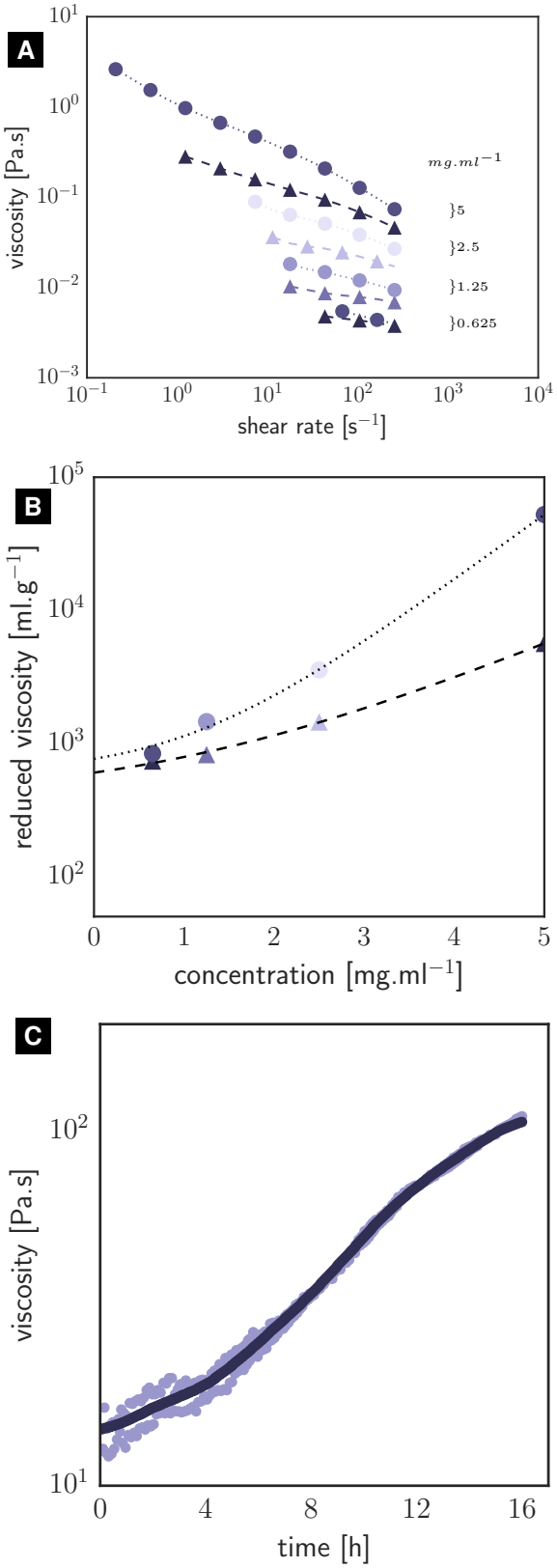

Fig. 5.8: A Flow curve of atelocollagen dissolved in 0.1M AA (triangles) and in 0.5 MPa CO_2 (circles) at concentrations 0.625, 1.25, 2.5 and 5 mg.ml^{-1}, B Reduced viscosity against atelocollagen concentration., C Increase of viscosity of CO_2 sample as consequence of 16h evaporation of carbon dioxide at 4 °C. All samples measured at atmospheric pressure (0.1 MPa).

ples showed similar results as CO_2 0.5 MPa (Table 4.1), so they were not shown in the graphs.

CO_2 0.1 MPa sample was used as a demonstration of insufficient dissolution pressure conditions. This result is in contrast with those similar by Tanaka et al.[57] experiment, who reported good dissolution and processing of fish-derived soluble collagen at atmospheric pressure (0.1 MPa) of carbon dioxide. Probably different collagen source material is responsible for this inconsistency.

All samples displayed large increase of G' going along with a decrease of tanδ, for the atelocollagen dissolved in 0.5 MPa CO_2 and heated at 37°C. G' for both 0.5 MPa CO_2 and 0.5 MPa CO_2 NaOH treated and kept at 37 °C reached plateau level equal to about 6200 Pa.s and 15000 Pa.s, respectively, by the end of the test indicating further and progressive assembling of the gel.

Attempts to heat up CO_2 samples to 37°C immediately after depressurization failed. While G' raised to higher values for a short time, after few minutes it dropped down to low values, indicating denaturation of the collagen. This can be explained by the fact that pH was not enough close to neutrality (7.4). To prevent denaturation after heating as well as keep the samples solubilized prior rheometer experiment depressurization procedure has to be applied over night (slow down).

The gelation kinetics are much faster for CO_2 than AA samples. The faster kinetics of CO_2 samples seems to be connected with the fact that the solutions cooled and depressurized of CO_2 overnight (Fig. 5.8A, B 0.5 MPa CO_2 4°C, 0.5 MPa CO_2 37°C) have a pH of 4.0 - 4.5 (Table 5.1), which is already at the border of the atelocollagen gelling region (Fig. 5.3A) and relatively close to its isoelectric point (assumed to be 7.4, but generally between 5 - 9 depending on type and amount of salts) [86]. Thus, part of the atelocollagen molecules interact, have a lower tanδ (Fig. 5.9, Table 5.1). These molecules act as nucleation sites, consequently greatly reducing gelation times[9].

The gelation kinetics of the sample produced as control (Fig. 5.9, Table 5.1)[43, 48] is most probably down-regulated by the presence of ions (salts), which hinder functional groups of the atelocollagen monomers, thus lowering the probability of monomer-monomer interaction. CO_2 gels showed two fold higher modulus (Table 5.1, right) than gels produced as control [43, 117], which is most probably connected to the presence of smaller diameter fibers size (8.6±4 nm for CO_2 samples versus 76±30 nm for control samples) and consequently higher number of network links (Fig. 5.11, Table 5.2).

The depressurization overnight helped us to work completely without additives during gelation, however, with the time the solution viscosity tend to increase about one fold (Fig. 5.8C). If this fact by one side could influence negatively the processability of the material, not using additives could represent a clear advantage.

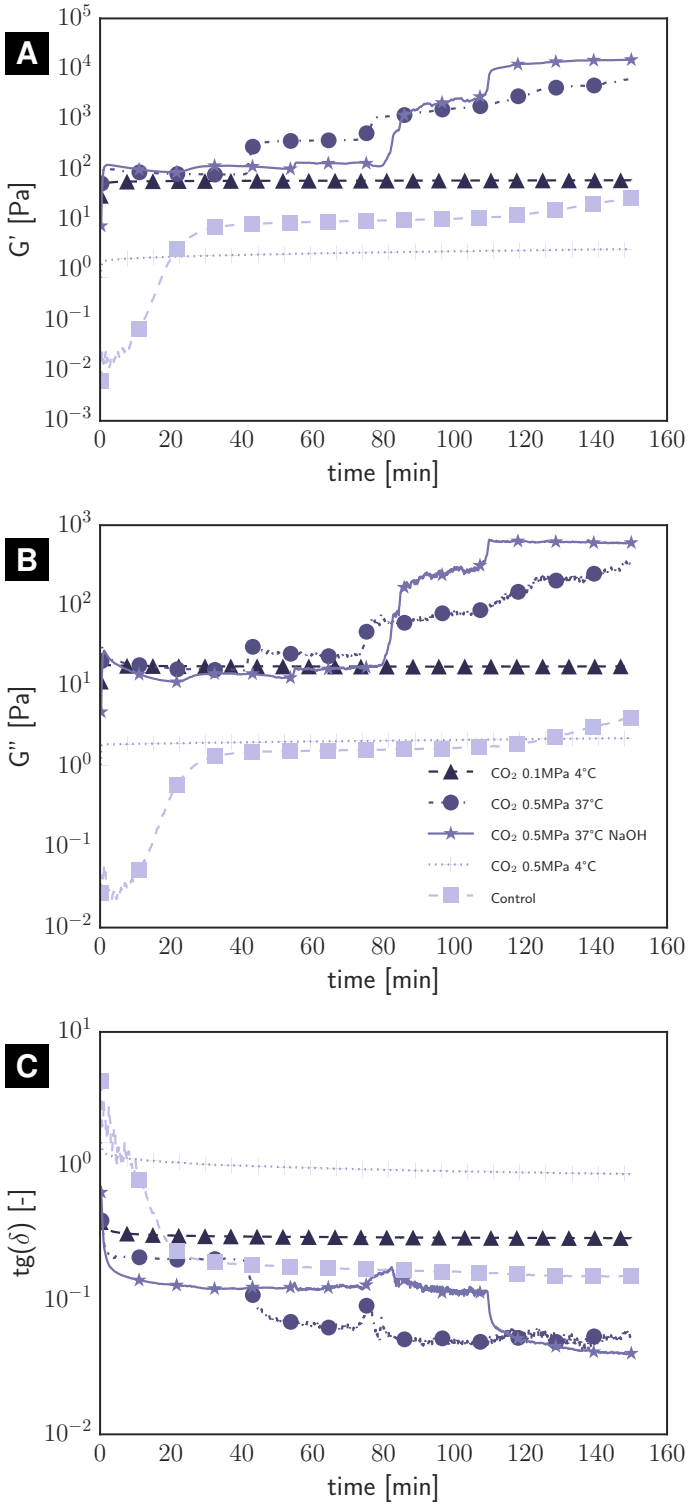

Fig. 5.9: Viscoelastic properties development during atelocollagen self-assembly. The samples were prepared according to Table 4.1. ***A*** *Storage modulus,* ***B*** *Loss modulus of sample,* ***C*** *tg(δ) = ratio of loss modulus to storage modulus. Higher than 1 means solution, lower than 1 means gel.*

Tab. 5.1: Viscoelastic properties development during atelocollagen self-assembly. The samples were prepared according to Table 4.1.

sample	**Initial solution properties**					**First gelation plateau**				**Final gel properties**			
	pH	time [min]	G' [Pa.s]	G" [Pa.s]	tanδ [-]	time [min]	G' [Pa.s]	G" [Pa.s]	tanδ [-]	time [min]	G' [Pa.s]	G" [Pa.s]	tanδ [-]
CO_2 0.5 MPa 37 °C	4.4	0.3	52.1	20.5	0.4	0.6	90.6	32.9	0.4	150	6189.6	341.2	0.05
CO_2 0.5 MPa 37 °C NaOH	4.0	0.3	11.2	6.7	0.6	1.2	113.1	26.6	0.2	150	15094.0	605.5	0.04
CO_2 0.1 MPa 4°C	5.3	0.3	39.5	15.2	0.4	25.0	58.5	17.6	0.3	150	60.6	17.6	0.30
CO_2 0.5 MPa 4°C	4.5	0.3	1.0	1.4	1.5	-	-	-	-	150	2.6	2.3	0.90
control	7.4	0.3	0.013	0.041	3.1	35.0	7.5	1.4	0.2	150	26.7	4.0	0.15

5.1.1.5 Structural analysis of gels

Structure of self-assembled gels prepared by both the control AA and the CO_2 protocol was characterized using camera (Fig. 5.10A), SEM (Fig. 5.10B,C,D,E), TEM (Fig. 5.11) and AFM (Fig. 5.12). The camera pictures (Fig. 5.10A) showed clear differences in transparency between gels casted from the control solutions (top, Table 4.1) and from the CO_2 0.5 MPa solutions (bottom, Table 4.1). Resulting fiber diameters and banding lengths (D-banding in case of control) are summarized in Table 5.2.

Overall, the AFM approach produced numbers corresponding to higher thickness of the fibers compared to other methods due to differences in the preparation of samples. The banding length was almost the same for TEM and AFM. Shorter banding of CO_2 fibers cannot be simply explained by TEM and AFM (Figs. 5.11 and 5.12) images and the structure should be carefully investigated by more accurate techniques like SAXS (Small Angle X-Ray Scattering) [118]. Previous work of Na [9] reported atelocollagen gels formed by control way (acidic solution neutralized by buffer and base). Na and colleagues described formation of fibrils having diameter between 3 - 15 nm in early stage of atelocollagen gel formation (up to 10 min from start of experiment). In later phases ($>$ 20 min) of gel formation, the initial fibers regrow/aggregate to larger D-banded fibers. It seems, that CO_2 gels form similar thin fibers (mean of methods 10.1$\pm$2 nm), but these fibers do not regrow to thicker ones. We assumed, fibers made by CO_2 protocol can not regrow to thicker ones due to a very fast nucleation phase (tan (δ) = 0.2-0.4 in one minute). The same tg(δ) in control samples was obtained after 30 minutes. Therefore the control gel had about 20x longer time for fiber growth. By other words, faster gelation (CO_2 protocol) resulted in formation of fibers that were thinner that those produced by slower gelation (control protocol). This is in agreement with the fact that faster crystallization produces smaller crystals than slower crystallization [119].

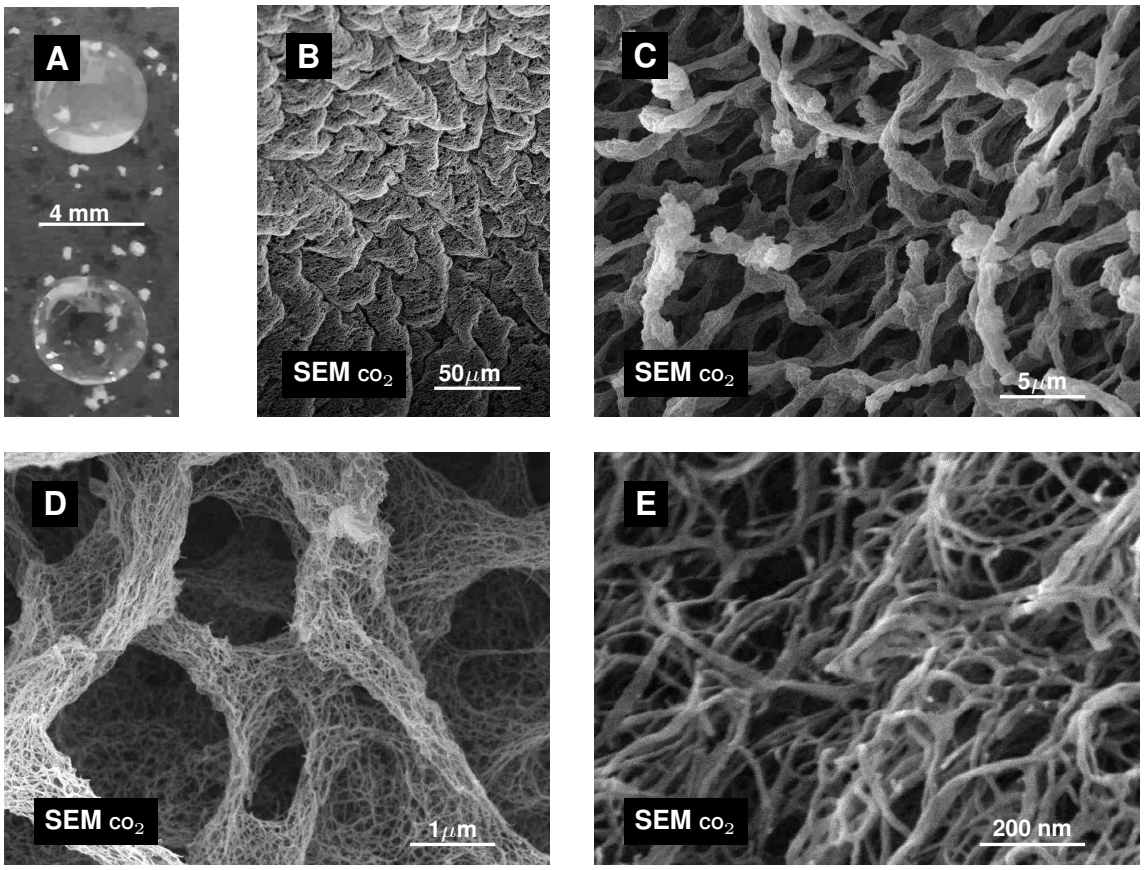

Fig. 5.10: Camera and SEM structural analysis of atelocollagen gels. CO_2 indicator in the left bottom corner of each image indicating CO_2 casted gel, Ctrl. indicating control gel casting procedure. A macroscopic gel view – top control, bottom CO_2 casting protocol, bar 4 mm, B gel crossesction, C-E gel surface

5.1.1.6 Gel transparency

Using camera (Fig. 5.9A) and UV/Vis spectroscopy (Table 5.3) we found that the CO_2 casted gels transmit light much better than gels casted by the control way. The transparency difference could be correlated with the collagen fiber sizes.

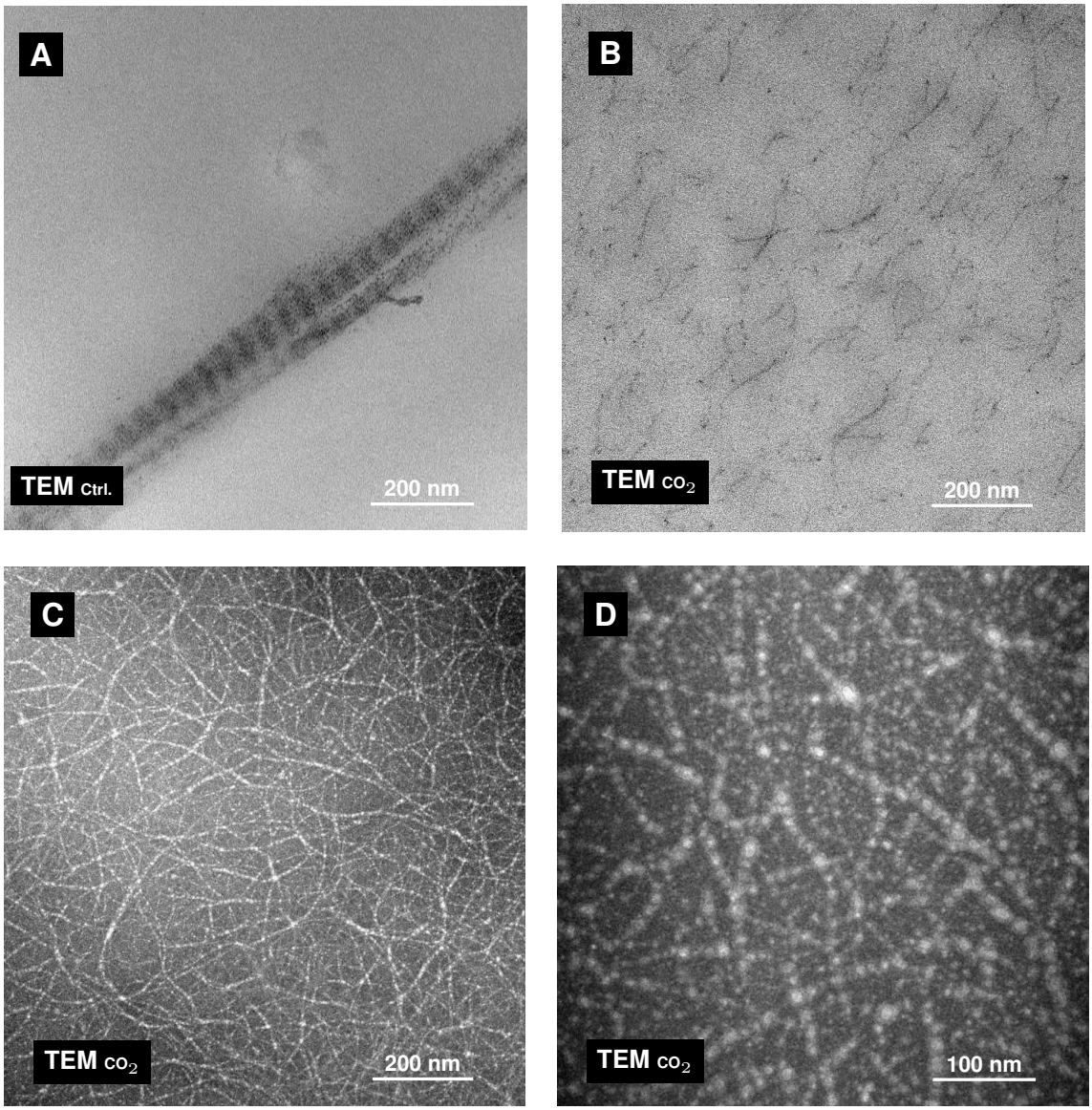

Fig. 5.11: TEM structural analysis of atelocollagen gels. A 50 nm section TEM micrograph of atelocollagen fiber formed by control protocol, B 50 nm section TEM micrograph of atelocollagen gel formed by CO_2 protocol, C and D CO_2 sample visualized by TEM droplet method.

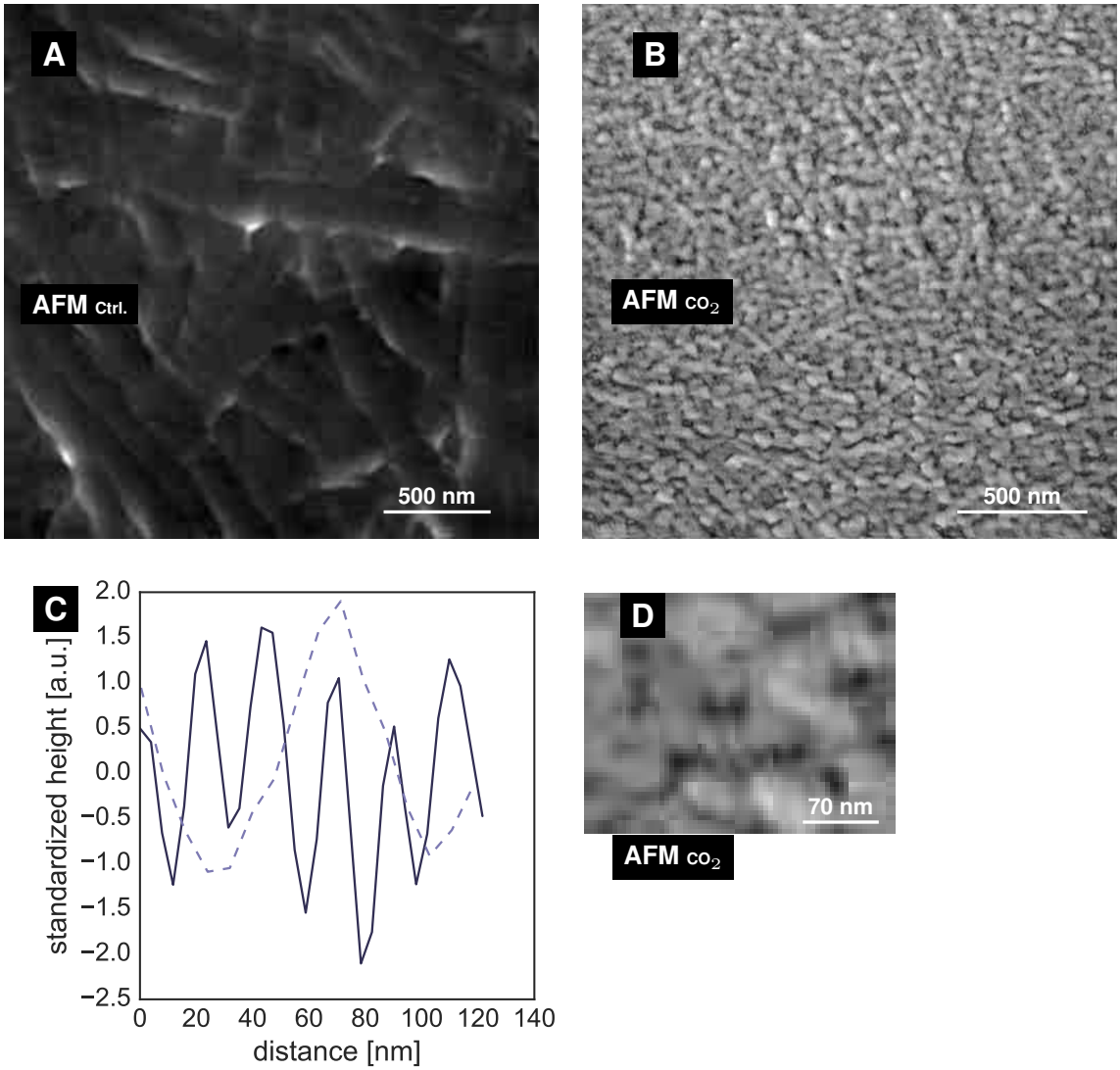

Fig. 5.12: AFM structural analysis of atelocollagen gels. A AFM micrograph of atelocollagen fiber formed by control protocol (right), B,D AFM micrograph of dried atelocollagen gel formed by CO_2 protocol, C AFM phase profiles of fibers formed by CO_2 (solid line) and control (dashed line) protocol.

Tab. 5.2: Quantification fiber diameter and banding length of atelocollagen gels.

sample	imaging method	fiber diameter [nm]	banding length [nm]	concentration [mg.ml^{-1}]	note
CO_2	SEM	9.1±7	-	3	glutaraldehyde fixed, critical point dried, subtracted coating 6 nm on both sites
CO_2	TEM sectioned	8.1±2	-	3	fixed in epoxy, sectioned, osmium tetroxide, lead nitrate contrasting
CO_2	TEM droplet	13.2±2	25.2±5	0.3	fixed in epoxy, sectioned, osmium tetroxide, lead nitrate contrasting
CO_2	AFM	41.9±9 *	23±2	0.03	after self-assembly dehydrated in ethanol to prevent overlapping, air dried, diameter is much bigger probably due low concentration, air drying
CO_2 mean	-	10.1±4	24.2±2	-	* value excluded
Control	TEM sectioned	76±30	67±3	3	fixed in epoxy, sectioned, osmium tetroxide, lead nitrate contrasting
Control	AFM	151±34 **	69±2	3	air dried, diameter is much bigger probably due air drying
Control mean	-	76±30	68±3	3	** value excluded

Tab. 5.3: Quantification of transparency of collagen gels by UV spectroscopy. The samples were prepared according to Table 4.1.

sample	transmittance at 310 nm [%]	transmittance at 550 nm [%]
CO_2 0.5 MPa 37 °C	99.3	99.7
control	79.3	95.5

5.2 Molar Mass Characterization of soluble collagen in native state by Asymetric Flow Field Flow Fractionation-Multi Angle Light Scattering Technique (AF4-MALS)

5.2.1 Results and Discussion

Nearly neutral solvents (pH 6.0 – 7.5) used for characterization of gelatin or denatured collagen by FFF or SEC [6, 30, 73, 79, 90, 91] are not applicable for native soluble collagens, which are generally precipitated at neutral conditions corresponding to its neutral isoelectric point [86]. As soluble collagens generally dissolve in acidic conditions, solvents based on AA (pH 2.4), as used in the present work, are more optimal for the characterization of soluble collagens.

5.2.1.1 Quality of atelocollagen AF4-MALS separation

AF4-MALS separation has been performed for atelocollagen Nutragen molar mass and RMS radius determination. From beginning of experiments there were problems with too fast elution of entire sample (RI detector data are usually not valid 3 min after switching to elution mode according to instrument manufacturer). High Vx, optimized and reproducible (Fig. 5.14B, C errorbars), elution profile (Fig. 5.13A) was developed in order to slow down entire peak according to instrument manufacturer. This resulted in good separation (Fig. 5.13D, Fig. 5.14A) without apparent aggregation or RI baseline deviation (Fig. 5.13B,C). Denatured samples have significantly lower mass recovery (30% and lower Fig. 5.13C, Fig. 5.20A) in comparison to native sample (70% Fig. 5.13B, Fig. 5.20A). Apparently low molar mass spices were excluded during high Vx focus step. Thicker channels could help to slow down the smallest particles , without use of the high Vx [78]. Unfortunately such a channel was not available during the experiments.

A 50 μg injection was found to be more optimal than a 250 μg injection as it has a better linear fit of angular dependency of scattered light (Fig. 5.14A) and sharper molar mass and RMS radius distributions (data not presented). This suggests that the solvent is not optimal and attractive forces are significant (significant A2). Since atelocollagen usually better dissolves at low temperature, we believe temperature (4 °C) could significantly reduce A2. This should allow to use higher injection mass and obtain better sensitivity. Unfortunately, cooled option was not supplied with our system. Another option to improve A2 is to optimize salt concentration.

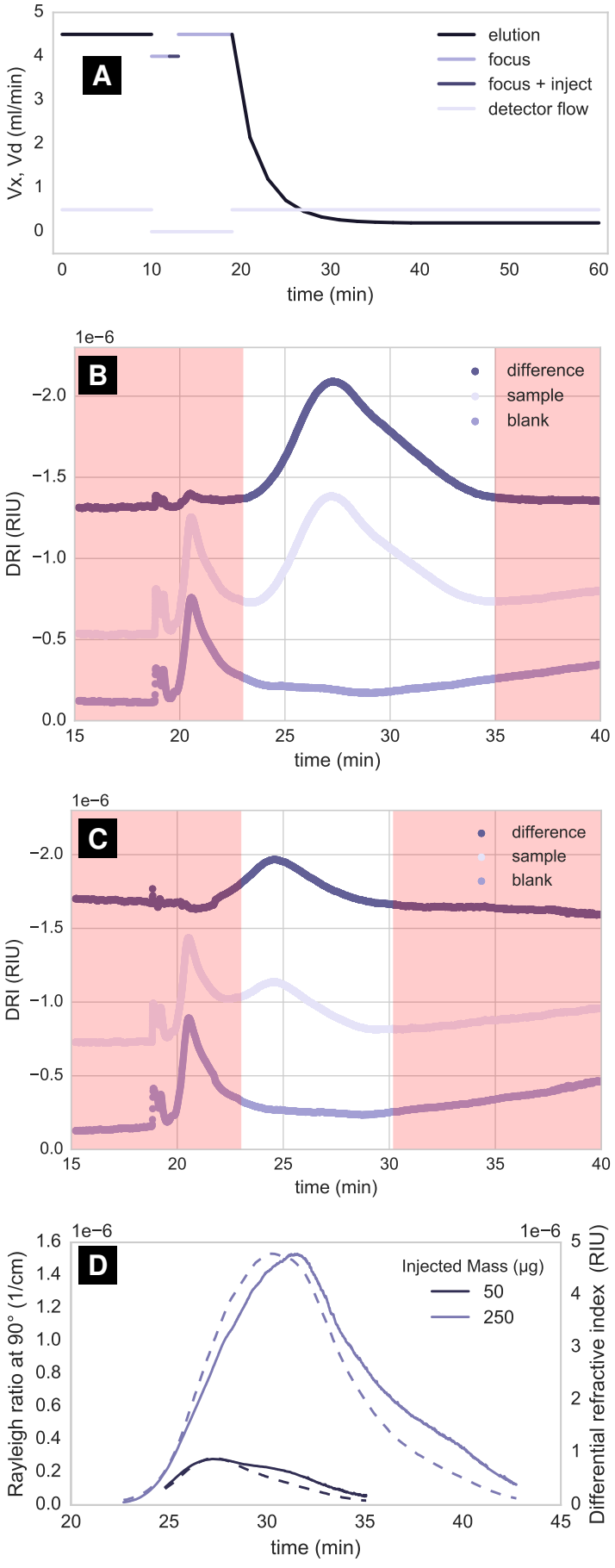

Fig. 5.13: ***A*** *AF4 elution profile used for atelocollagen separation, Raw response of RI detector (blank, sample, difference, 50 µg injection), native sample -* ***B****, 15 min @ 37°C thermally denatured sample -* ***C*** *(note: signals were y-axis shifted to be well visualized),* ***D*** *baseline subtracted response of RI (dashed line) and MALS 90° (solid line) detector.*

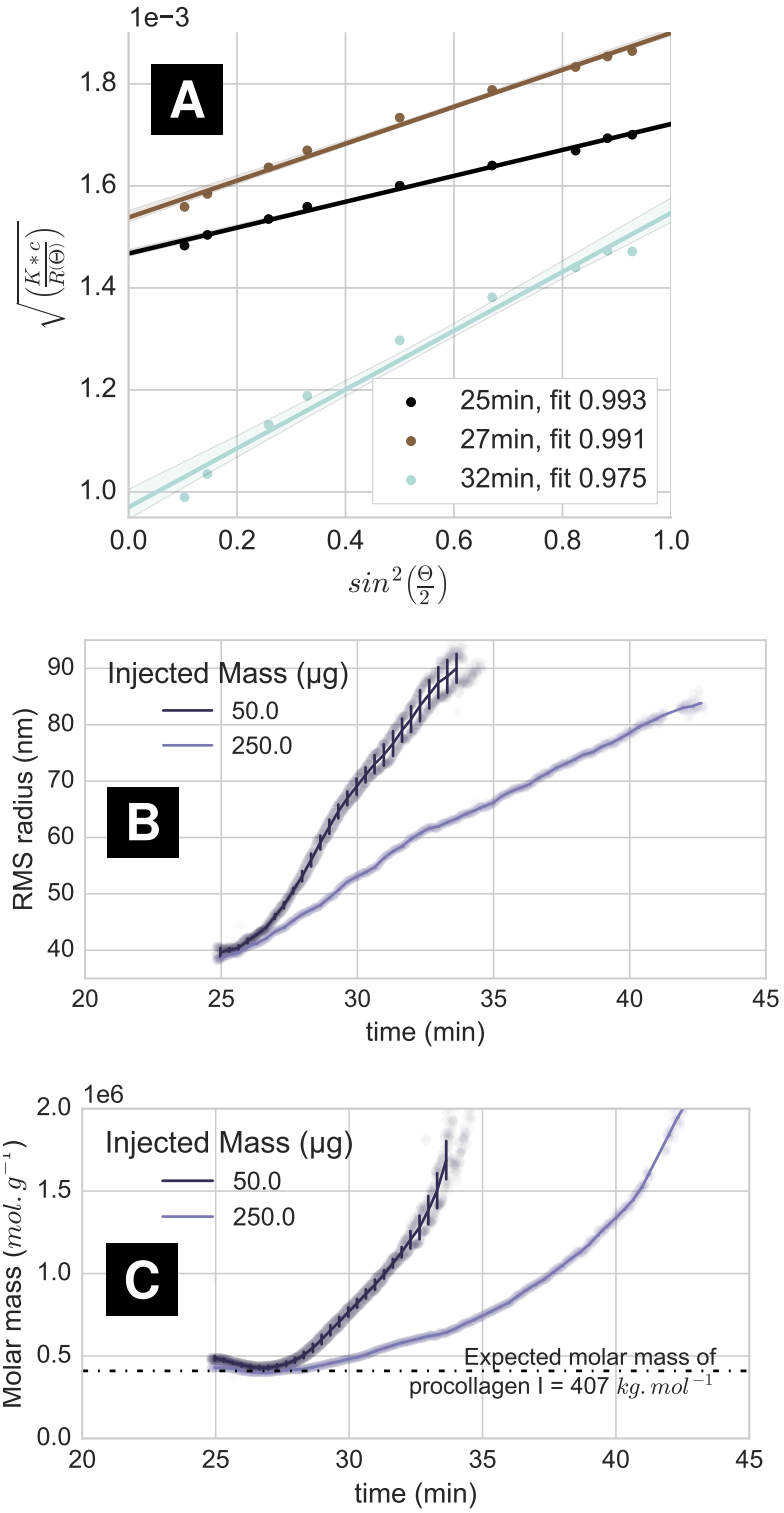

Fig. 5.14: ***A*** *Light scattering angular dependence of 50 µg injection at different times, fit degree demonstrating separation efficiency,* ***B*** *RMS radius calculated and* ***C*** *Molar mass by Berry formalism. Atelocollagen molecules eluted at the time between 25 – 28 min have a molar mass which fits expected the molar mass of procollagen I (407 kg.mol^{-1}).*

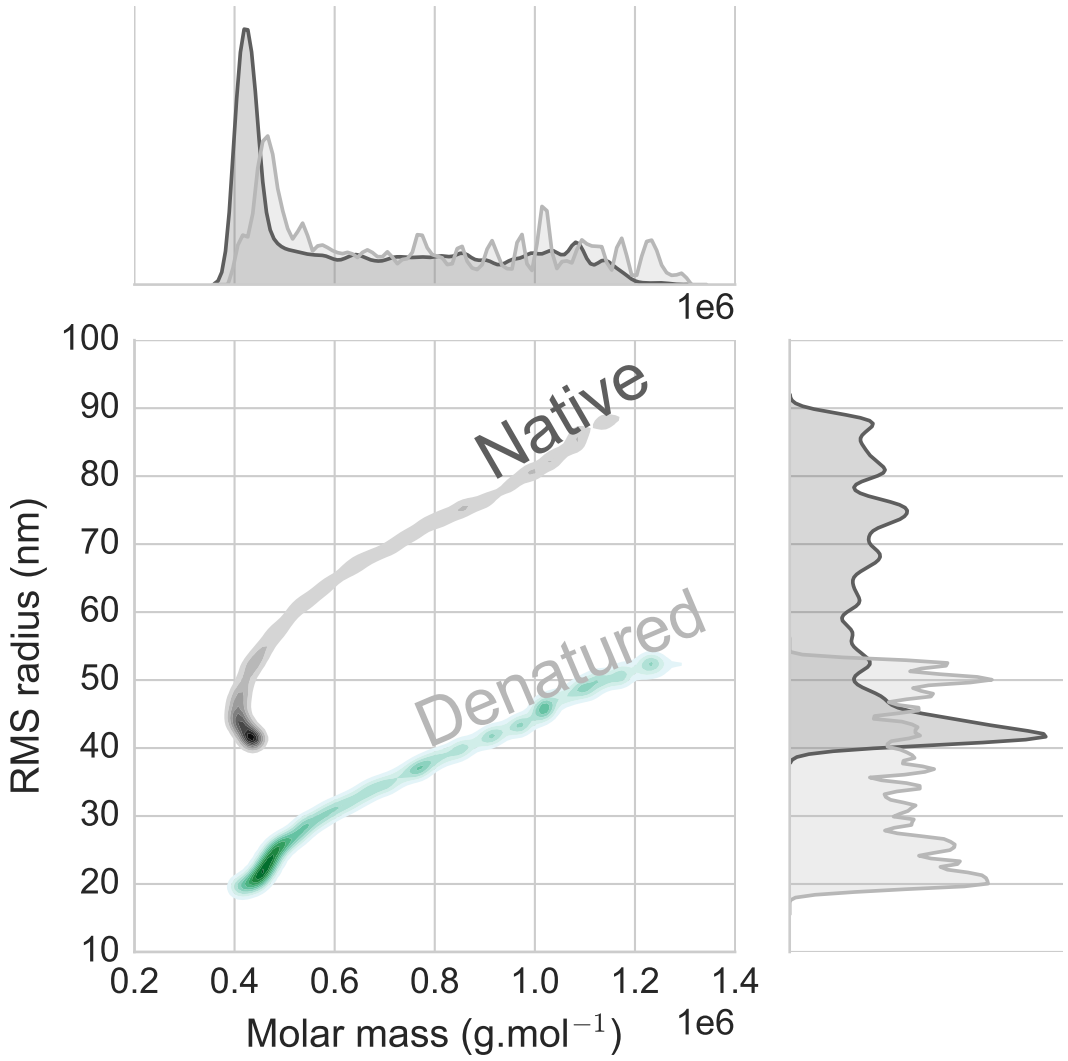

Fig. 5.15: 2D distributions (bottom-left) of native atelocollagen and denatured atelocollagen (37°C, 15 min), 50 µg injection. 1D Distributions are viewed on top (molar mass) and right (RMS radius). Its 2D representation is plotted in center. Whole denatured sample has significantly lower RMS radius and mass recovery (distribution intensities are normalized).

5.2.2 Molar mass and RMS radius distributions

On the plot in Fig. 5.15 the atelocollagen has a distinct molar mass and RMS radius (420 kg.mol^{-1}, 43 nm, respectively), which fits the expected molar mass of procollagen I (407kg.mol^{-1}). Thermally denatured sample has much lower mass recovery than the native sample (30%, respectivelly 70% Fig. 5.22A) and the remaining part collapses into a smaller radius and similar molar mass. The smaller size of collapsed atelocollagen heated for 15 min at 37°C clearly reflects the lower folding (43%) of the helices accessed by CD spectroscopy (Fig. 5.17), indicating damage or partial unfolding of the helices caused by lability at hydroxyproline deficient sites [120, 121].

5.2.2.1 Atelocollagen conformation analysis

Atelocollagen has a distinct molar mass (which fits to the expected molar mass of procollagen I) and RMS radius and unique position on the conformation plot as seen in Fig. 5.16A. By thermal denaturation the whole sample collapses into a smaller radius and similar molar mass, most probably because of molecules' entanglement and breaking alpha chains (Fig. 5.16B). AF4-MALS measurements separated different fractions of atelocollagen labelled as atelocollagen I and atelocollagen U (Unknown) having RMS radius equal to 43 and 54 nm respectively (Fig. 5.16A, Table 5.4).

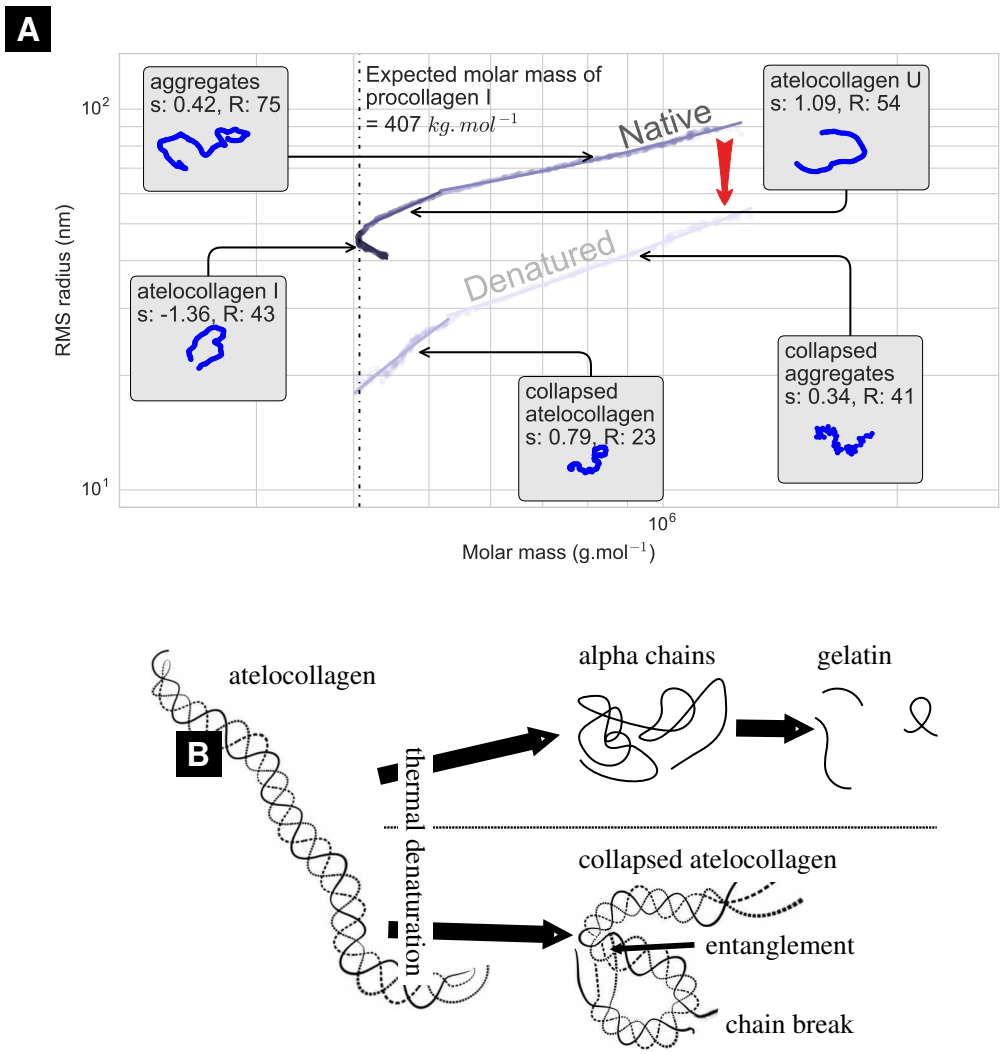

Fig. 5.16: ***A*** *- Conformation plots of native atelocollagen and denatured atelocollagen (37°C, 15 min), 50 µg injection. Distributions are viewed on top and right side marginal views of conformation plots. Whole denatured sample has significantly lower RMS radius. Typical molecular conformations were generated by WLC monte carlo simulation.* ***B*** *– schematic painting of atelocollagen and its denatured forms.*

Heat denaturedfractions labelled as collapsed atelocollagen (25nm, Fig. 5.16A, Table 5.4) have a much smaller RMS radius than atelocollagen I. The smallest size of collapsed atelocollagen heated for 15 min at 37°C clearly reflects the lower folding

(43%) of the helices accessed by CD spectroscopy (Fig. 5.17), indicating damage or partial unfolding of the helices caused by lability at hydroxyproline deficient sites [120, 121].

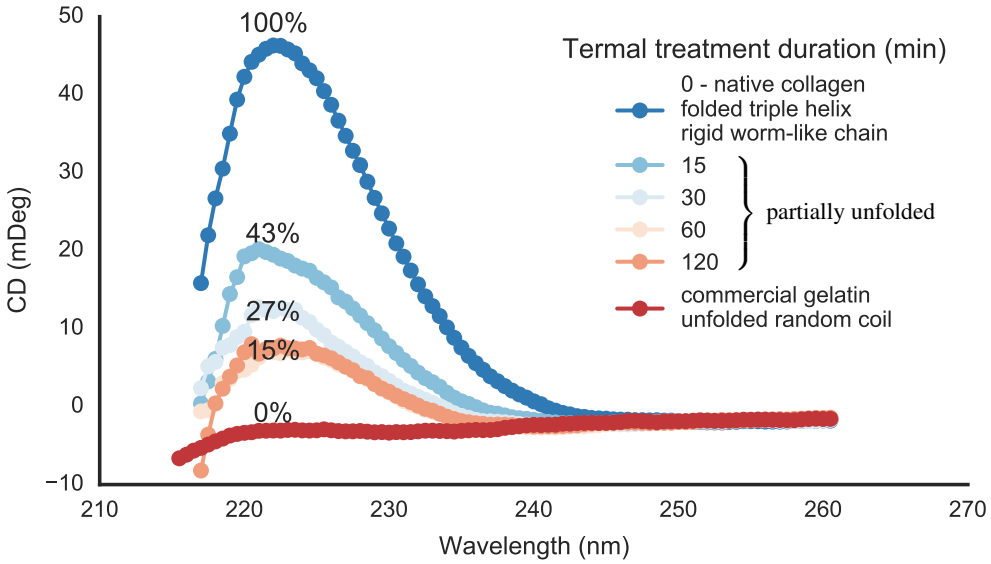

Fig. 5.17: CD spectra of the folded triple helix of native atelocollagen, 37°C thermally denatured atelocollagen at different times (15, 30, 60 and 120 min) and (unfolded random coil) gelatin.

Atelocollagen I (43 nm, 420 kg.mol^{-1}) consists of more rigid (folded) chains of atelocollagen type I. The biggest and the heaviest (54 nm, 453 kg.mol^{-1}) atelocollagen U probably consists of atelocollagen type III, which is about 10 kg.mol^{-1} heavier than atelocolagen type I [122, 123]. This hypothesis is supported by the fact that collagen III consists of three identical collagen III α1 chains equal to 138.564 kg.mol^{-1}) and collagen I is formed by different chains (2x α1 of 138.941 kg.mol^{-1} + 1x α2 of 129.314 kg.mol^{-1}). It seems to be logical that the identical chains of collagen III are forming more regularly, rigidly and larger (in RMS radius) triple helices than the collagen I helix which is assembled from different chains of significantly different molar mass (length). However immunoassays need to be performed to confirm this conclusion. Another possibility is that atelocollagen U is just atelocollagen of type I with covalently attached debris of collagen.

Molar mass measurements also fit previously reported ranges between 342 kg.mol^{-1} - 490 kg.mol^{-1} obtained by MALS in batch (unfractionated) mode [92]. Although present and past work [92] is not fully comparable as it differs in many experimental parameters.

Tab. 5.4: Measured and calculated properties of different fractions of native and denatured samples from ***Fig. 5.16A***

Fraction	**Measured by AF4-MALS**				**WLC monte carlo**				**Analytical results**		
	Conformation plot slope	Mass (%)	Molar mass ($kg.mol^{-1}$)	RMS radius (nm)	Contour length (nm)	Kuhn length (nm)	Square end to end distance (nm)	RMS radius (nm)	Straight rod RMS radius (nm)	Characteristic ratio	Kuhn length fit (nm)
aggregates (dimer)	0.41±0.002	24	849±193	75±8	600	87	163±62	75±16	173	0.42	84
atelocollagen U (Unknown)	1.09±0.010	14	453±30	54±3	300	200	124±61	54±9	87	0.6	185
atelocollagen I	-1.3±0.040	20	420±13	43±2	300	87	98±67	41±8	87	0.47	112
collapsed atelocollagen	0.79±0.020	6	465±30	23±2	300	16	56±28	26±6	87	0.28	7

$Straight\,rod\,RMS\,radius = \frac{1}{N}\sum_{i=1}^{N}(\vec{R}_i - \vec{R}_{cm})^2 = \sqrt{\frac{Contour\,length^2}{12}}$

$Characteristic\,ratio = \frac{Measured\,RMS\,radius}{Straight\,rod\,RMS\,radius}$

Kuhn length fit (nm) = 559*Characteristic ratio + 150, linear fit of WLC: Kuhn length and characteristic ratio

5.2.2.2 Modelling

The CD signal of native collagen at 221.5 nm represents the folded state, whereas no signal (near to zero or slightly negative) at this wavelength determines the unfolded (random coil) gelatin. By collagen heating the maximum of CD spectra at 221.5 nm decreased as a response to thermal treatment (Fig. 5.17). Similarly, RMS radius and Kuhn length obtained by AF4-MALS-WLC (able 1) represents certain levels of molecule folding. Folded native atelocollagen has a Kuhn length of 87 and 200 (Table 5.4, atelocollagen I and U, respectively) and partially unfolded collapsed atelocollagen exhibited significantly lower Kuhn length of 16 nm (CD dropped to 43%). However, a length of 16 nm is still significantly longer than the Kuhn length of gelatin (≈5.0 nm [124]).

The short Kuhn length between 22 – 30 nm (where Kuhn length = 2*persistence length) obtained by optical tweezers [68, 125] has similar values as collapsed atelocollagen, assumed to be due to occurrence of denaturation during procollagen processing or during optical tweezer (laser) experiments. TEM based estimates between 80 - 120 nm [121] and AFM based estimates of 80 nm [67] fit atelocollagen I and U (80 and 120 nm) fraction behaviour. It seems that hydrodynamic methods, which have suggested a Kuhn length between 260 – 360 nm [126, 127], give higher values probably due to insufficient purification of collagen aggregates. AF4-MALS WLC method provides consistent measurement of Kuhn length in comparison with other methods. The difference between works is apparently caused by different experimental conditions (especially fractionation, purity of sample, denaturation, etc.).

Present AF4-MALS results are in excellent agreement with Markov et al. molecular dynamics work [128], which predicted co-existence of multiple conformations (peak broadening of RMS radius of atelocollagen I and atelocollagen U) of rigid amphiphilic molecules in solvents of lower dissolution quality (with significant hydrophobic interactions).

5.2.2.3 Thermally denatured atelocollagen on AF4-MALS

The distributions of native and thermally denatured atelocollagen samples are visualized in Fig. 5.18A, B. Heat denatured atelocollagen has significantly lower RMS radius (Fig. 5.18A), but the mean molar mass has similar values in comparison with untreated samples (Fig. 5.18B, boxplots). Also massive escape of low molar mass debris of atelocollagen through semi permeable membrane was observed (thinner plots). According to conformation plots (Fig. 5.16) the mass of atelocollagen was selectively quantified as mass detected by RI detector of RMS radius between 33 - 55 nm and molar mass between 400 - 550 kg.mol^{-1}. Smaller particles (15 - 33 nm, about half in size) of same molar mass as atelocollagen (400 - 550 kg.mol^{-1}) were marked as denatured collapsed atelocollagen. Particles of molar mass > 550 kg.mol^{-1} were quantified as aggregates and gelatin was quantified as the mass escaping through membrane (i.e. Injected mass – filtered out mass – detected mass). Calculations results are summarized in Table 5.5.

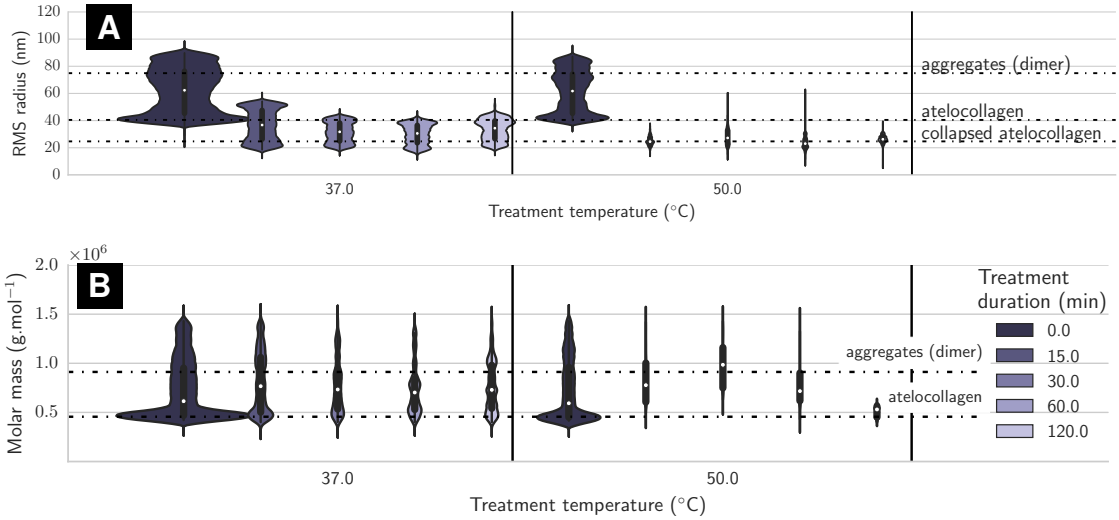

*Fig. 5.18: Distributions (violin plot) of **A** - RMS radius and **B** - molar mass of thermally denatured atelocollagen at 37 and 50°C and treatment duration 0-120 min. Distribution width represents amount of detected mass.*

Tab. 5.5: Untreated and denatured atelocollagen quantitative AF4 analysis

Treatment duration (min)	Treatment temperature (°C)	Atelocollagen mass (μg)	Collaped atelocollagen mass (μg)	Gelatin mass (μg)	Aggregate mass (μg)	Atelocollagen mass (%)	Collapsed Atelocollagen mass (%)	Gelatin mass (%)	Aggregate mass (%)	Filtered out mass (%)
0	37	14	0	24	12	28	0	34	24	14
0	50	16	0	20	14	32	0	25	29	14
15	37	0	3	42	8	0	7	70	16	14
15	50	0	0	49	1	0	0	84	2	14
30	37	0	2	45	5	0	3	77	9	14
30	50	0	0	49	1	0	0	84	2	14
60	37	0	1	46	4	0	3	77	9	14
60	50	0	0	49	1	0	0	84	2	14
120	37	0	2	45	5	0	4	76	10	14
120	50	0	0	49	1	0	1	84	2	14

5.2.2.4 Comparison of thermally denatured atelocollagen with AF4, DLS, CD spectroscopy and electrophoresis

DLS batch measurement (Fig. 5.19) of thermally denatured atelocollagens shows a clear shift of hydrodynamic radius towards smaller radius in comparison to untreated samples. A general comparison of AF4-MALS, batch DLS and batch CD is summarized in Fig. 5.20. In AF4 experiments (Fig. 5.20A), low molar mass debris of denatured atelocollagen were excluded due to its escape through the semi permeable membrane. This caused a sharp drop of mean RMS radius (Fig. 5.20B). DLS - Hydrodynamic radius (Fig. 5.20C) and CD - elipticity (Fig. 5.20D) have not droped as fast due batch operation (low molar mass atelocollagen debris are included).

SDS-PAGE of a atelocollagen sample is visualized in Fig. 5.21A, Fig. 5.22A and marked as standard [35, 69–71, 129]. SDS-PAGE (Fig. 5.22A) and Native-PAGE of thermally denatured atelocollagen (Fig. 5.21B, Fig. 5.22B) showed similar a pattern in the region of (collapsed) atelocollagen and aggregates. But the **Native-PAGE** has only a single intensive band in the region of low molar mass (α_1,α_2,α_3), where the SDS-PAGE shows separated alpha chains (α) and their dimers (β). SDS-PAGE measured molar mass of atelocollagen was equal to 300 kg.mol^{-1}, which is significantly lower than expected molar mass of procollagen I (407 kg.mol^{-1}). However, AF4-MALS provided a more accurate value of 420 kg.mol^{-1} (atelocollagen B, Fig. 5.16B, Table 5.4).

Native-PAGE of native atelocollagen shows a dominant band (Fig. 5.22B, native) identified as atelocollagen. Similar bands in the denatured lane were marked as collapsed atelocollagen of smaller RMS radius and shorter Kuhn length as is suggested by AF4-MALS (Fig. 5.16B, C, Table 5.4).

Quantitative analysis of Native-PAGE (Table 5.6) shows significant sensitivity to the baseline method, which makes the quantification less reliable. Comparison of native-PAGE (Table 5.6) and AF4 (Table 5.5) indicates significant differences.

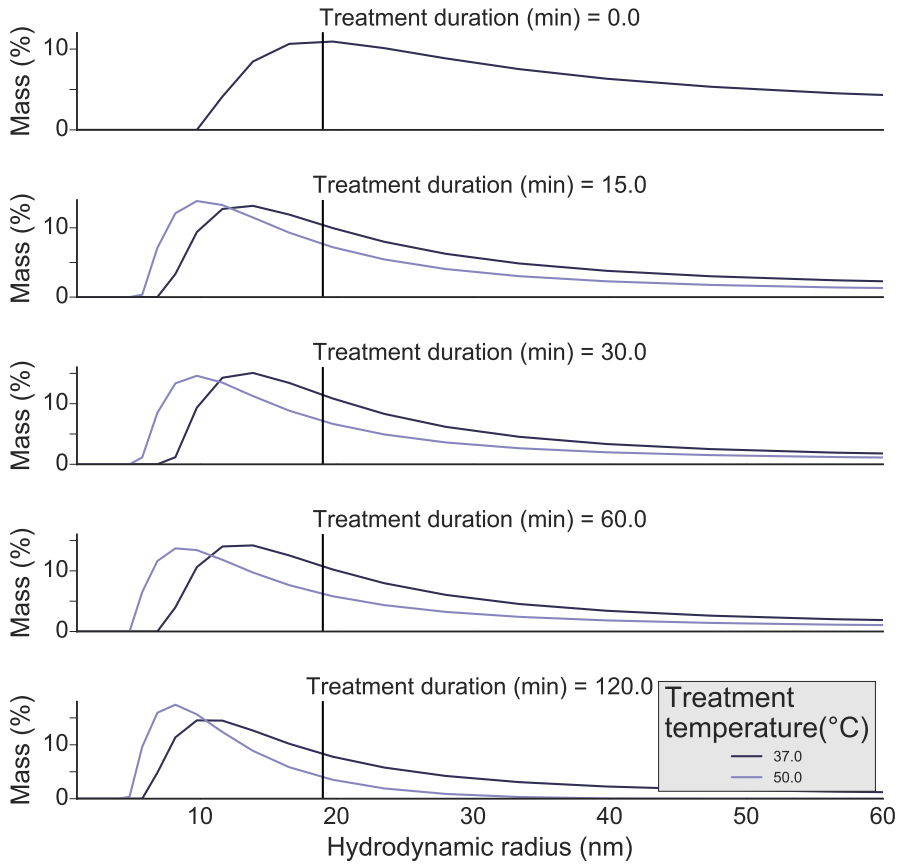

Fig. 5.19: Development of hydrodynamic radius, measured by DLS in batch mode, as a reaction to thermal treatment. The vertical black line indicates peak hydrodynamic radius of untreated atelocollagen.

AF4 and native-PAGE have similar values for native (untreated) and (thermally) denatured samples. However, thermally denatured samples involve more gelatin on AF4.

It can be assumed that the Native-PAGE gives proper measurement of alpha chains and low molar mass spices. Missing low molar mass in AF4 could be explained by multiple phenomenas:

- High Vx increases probability, of alpha chains penetration through membrane,
- Low pH causes swelling of Regenerated Cellulose membrane and increases its permeability (lower attractive forces/lubrication),
- Alpha chains were broken by aggressive flow conditions in the channel (interaction with membrane under low pH),
- Degradation/damage of membrane by low pH causes increase of pore size

More experimental work must be done to evaluate significance of each of this phenomena.

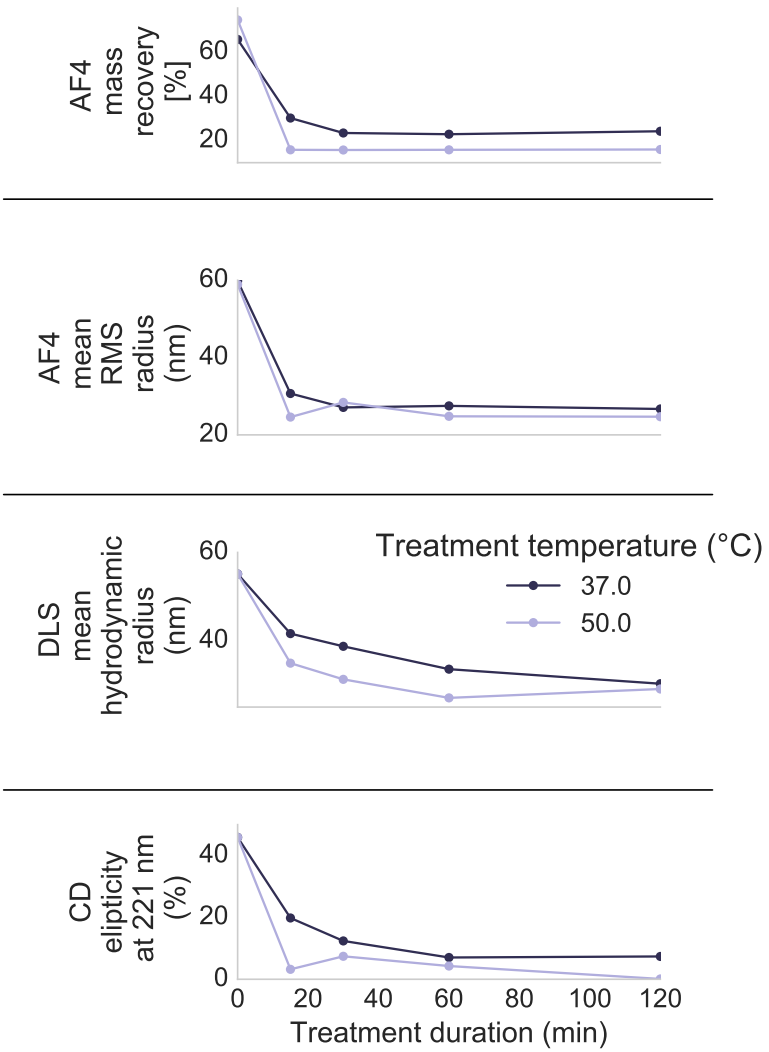

Fig. 5.20: Comparison of thermally denatured samples by different methods: ***A*** *AF4 - Calculated mass and* ***B*** *mean RMS radius,* ***C*** *mean DLS hydrodynamic radius and* ***D*** *mean CD elipticity.*

5.2.2.5 Light scattering formalism selection

Berry, Zimm and Rod formalisms were selected in order to compare their fitting performance of molar mass, RMS radius and rod length (Fig. 5.23, Fig. 5.23). The diagonal plots (Fig. 5.23, position A, E, I) showing number distributions of molar mass, RMS radius and rod length (Fig. 5.23, I). Plots below diagonal (D, G, H) plots two formalisms against each other (f.e. Zimm vs Berry plot D). Ideally proportional relation of formalisms with slope 1.0 is plotted by black dashed line. Their linear fit error is visualized by error plots above diagonal (B, C, F). The 50 μg injection shows atelocollagen peak at position higher (Fig. 5.23 diagonal, about +100 kDa, +8 nm) than the samples of higher injected mass (250 μg). For molar mass measurement the Zimm formalism shows slightly overestimated values against Berry (Fig. 5.23, Fig. 5.23 - D) with negligible effect to the distributions (Fig. 5.23, Fig. 5.23 - A,

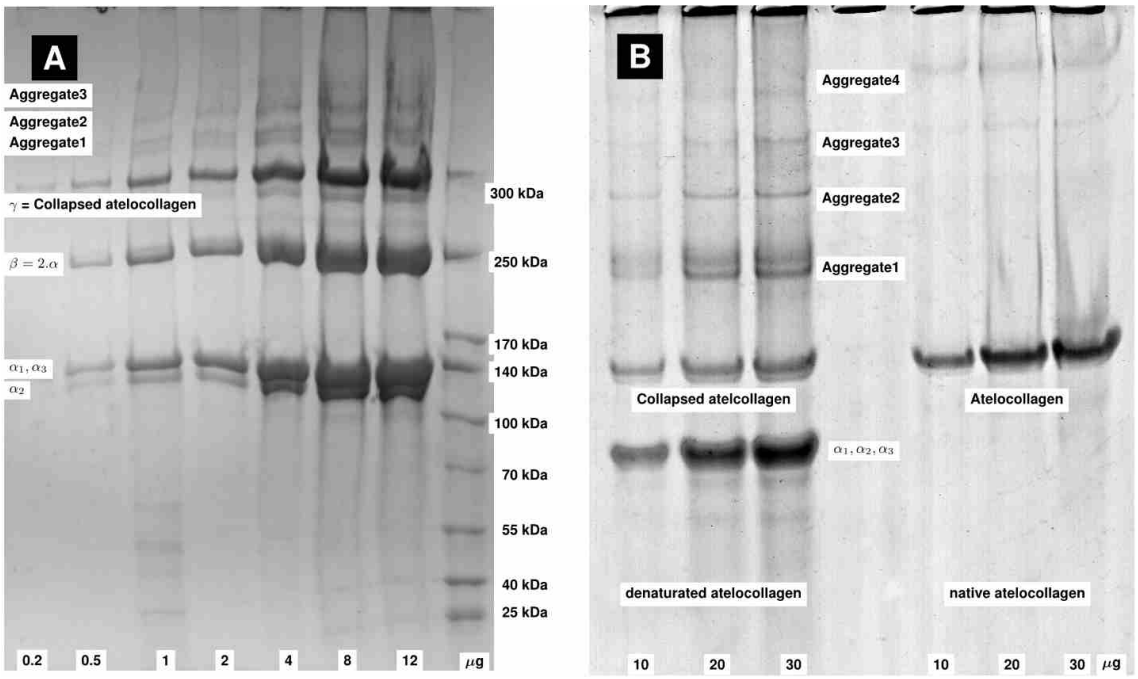

Fig. 5.21: ***A*** *SDS-PAGE of ateocollagen up to 12 μg per lane,* ***B*** *Native-PAGE of denatured atelocollagen (left) and native-atelocollagen (right) at 10, 20,30 μg per lane. The native collagen shown small amount of aggregates (aggregate3,4). Denatured atelocollagen shown more aggregate bands (aggregate1-4), and strong LMW band containing unseparated alpha chains. The aggregate bands seems to correspond in both SDS-PAGE and Native-PAGE.*

Tab. 5.6: Native-PAGE peak area analysis. Background subtraction and area values are in arbitrary units. The denatured samples were heated 15 min at 37°C, 30 μg of sample per line

Sample	Baseline method	Baseline value	Total area	Atelocollagen area	Gelatin area	Aggregate area	Atelocollagen mass (%)	Gelatin mass (%)	Aggregate mass (%)
Native	-	0	668	250	161	257	37	24	38
Native	sample free background	0.07	610	245	136	229	40	22	38
Native	subjective background	0.30	431	230	57	144	53	13	33
Denaturated	-	0	1409	158	599	652	11	42	46
Denaturated	sample free background	0.07	1350	153	573	624	11	42	46
Denaturated	subjective background	0.95	656	93	270	294	14	41	45

E). The molar mass obtained by Rod formalism shows also negligible errors against Berry and Zimm formalism (Fig. 5.23 - G, H). But Rod formalism shows much longer rod length against RMS radius (Fig. 5.23 - G, H) as is different parameter.

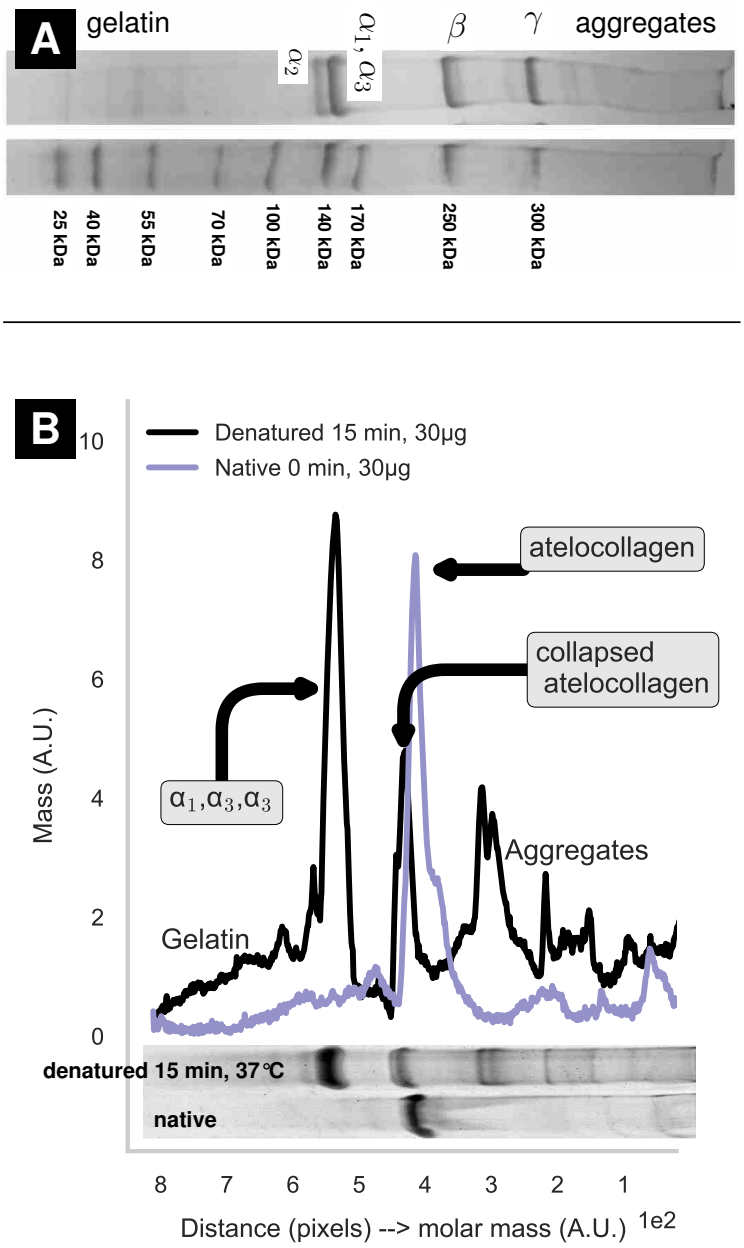

Fig. 5.22: ***A*** *SDS-PAGE of ateocollagen 1 µg per lane and molar mass standard.* β *= dimer of* α *chains,* γ *= collapsed atelocollagen,* ***B*** *Native-PAGE electrophorsis.*

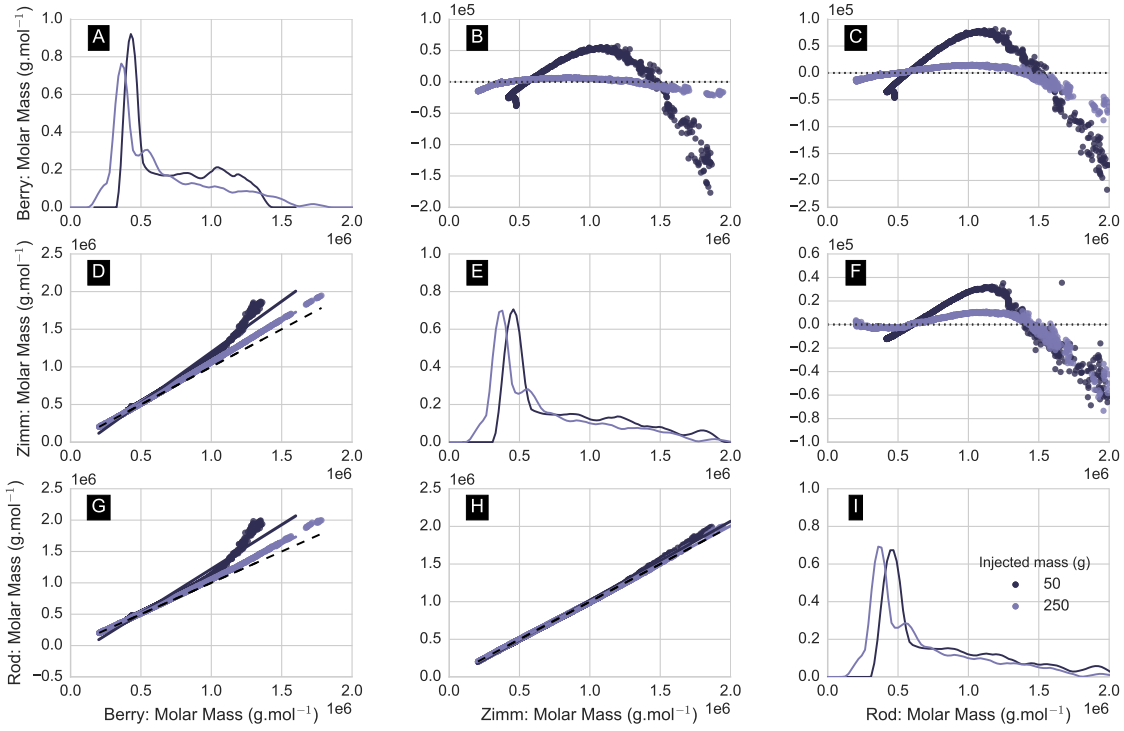

Fig. 5.23: Comparison of Berry, Zimm and Rod formalism used for calculation of molar Mass. Plots above diagonal visualizing error of linear fits. At high molecular masses (> 1.5 M g.mol^{-1}) Zimm and Rod formalism overestimates the molar mass in comparison to Berry formalim.

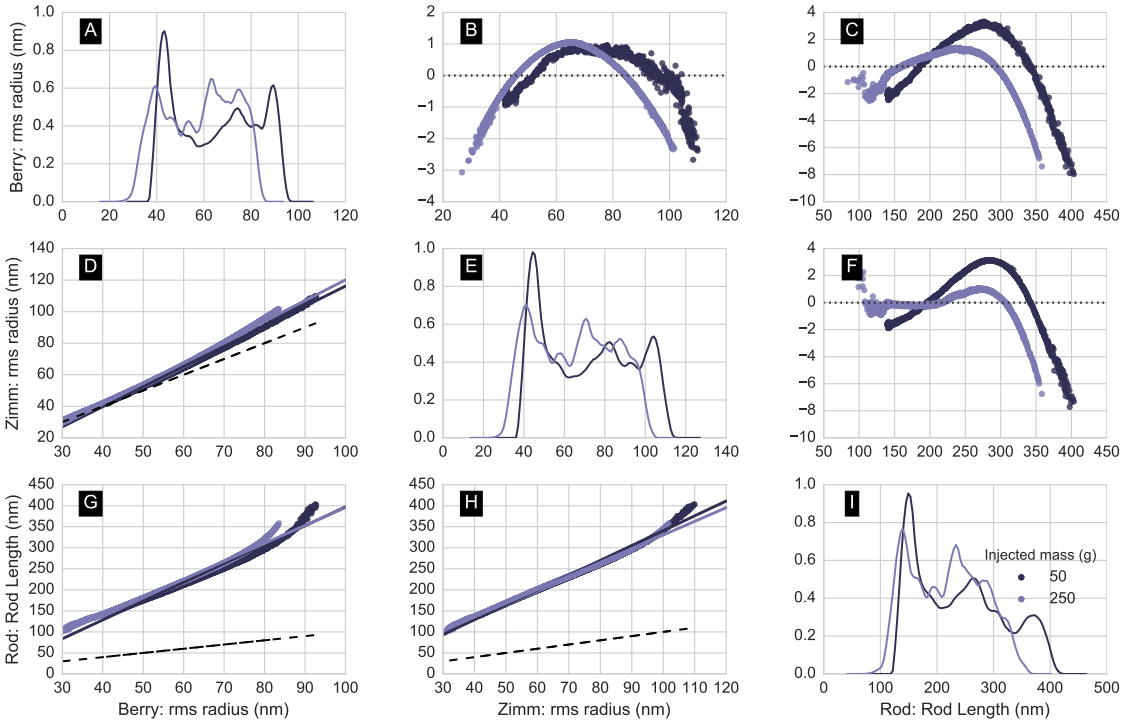

Fig. 5.24: Comparison of Berry, Zimm and Rod formalism used for calculation of RMS radius. For bigger RMS radii (> 80 nm) Zimm formalism overestimates the molecular mass in comparison to Berry formalim. The rod length parametrer of collagen is about 3x higher thean RMS radius, but it still fits linearly to RMS radius values.

6 CONCLUSION

In the presented thesis, first main chapter of experimental part describes utilization of pressurized carbon dioxide/water solutions for atelocollagen dissolving. This technique does not induce any denaturing effect. Transparent gels can be easily formed by removing pressure, due to the CO_2 evaporation from the solutions resulting in the increase of pH. Gels obtained with this method have smaller size of fibrils and larger rheological properties compared to the gels obtained from AA solutions. This dissolution and gelation method is quite versatilewithout the need of any harmful chemicals. Thus, it opens potential applications in various fields including tissue engineering. Medical application, where absence of contaminants, adjustable rheological properties and transparency (e.g., cornea) are required, can be particularly envisioned.

In the second main chapter, the characterization of commercial atelocollagen is provided in native state by AF4-MALS technique in comparison to DLS and CD spectroscopy as well as to SDS-PAGE and Native-PAGE electrophoresis. Obtained molar mass of atelocollagen I (420 $kg.mol^{-1}$) is in excellent agreement with expected molar mass of procollagen I (407 $kg.mol^{-1}$). The native atelocollagen has unique conformation plot, which unambiguously differs from denatured atelocollagen-based gelatin. This allows quantification of atelocollagen by selection of RMS radius between 33 - 55 nm and molar mass between 400 - 550 $kg.mol^{-1}$. The comparative study of thermally denatured samples showed good agreement with DLS and CD spectroscopy, but native-PAGE showed significantly smaller amount of gelatin than AF4-MALS. The presented method could be used for optimization of soluble collagen extraction yields and for its purification or it could be used for detection of denaturation during processing. Since AF4-MALS is GMP/FDA compliant, the method has great potential to become new standard for quality control of medical grade soluble collagens.

6.1 List of Abbreviation and Symbols

AA Acetic Acid

AFM Atomic Force Microscopy

Allogenic Human origin, transplant is received other person donor

Autologous Human origin, transplant is harvested from one part of body and received to other part of same person

CD Circuar dichroism - spectrophotometer which is able to detect secondary structure of chiral molecules

CO_2 Carbon Dioxide

Confluence Percent of surface of flask covered by cells

Decellularized Without cellular content

DI Deionized Water

Decellularized ECM Cell free tissue ECM

DLS Dynamic Light Scattering

ECM Extra Cellular matrix

ES Electrospinning - method for producing nanofibres

FD Freeze-drying - class of strong enzymes secreted by cells

FFF Field Flow Fractionation

Gel Chemically or physically crosslinked polymer network

H_2CO_3 Carbonic Acid

HCL Hydrochloric Acid

SDS-PAGE Sodium Dodecylsulphate Polyacrylamide Gel Electrophoresis

SEM Scanning Electron Microscopy

MALS Multi Angle Light Scattering

MMP Metalloproteinases - class of strong enzymes secreted by cells

NaOH Sodium Hydroxide

Native-PAGE Native Gel Electrophoresis

PBS Phosphate Buffered Solution

PP Polypropylene

Python Python programming language

RI Refractive Index (detector)

R_g Radius of gyration = RMS radius

SEC Size Exclusion Chromatography

TE Tissue Engineering

TEM Transmission Electron Microscopy

RMS Root Mean Square

Tissue Engineered Scaffold Artificial ECM made from natural or synthetic molecules

UV Ultraviolet, range of wavelengths

WLC Worm Like Chain (rigid chain molecule model)

Xenogenic Animal origin, transplant is harvested from animal and implanted to person

6.2 List of Figures

6.3 List of Tables

BIBLIOGRAPHY

[1] E.A. Abou Neel, L. Bozec, J.C. Knowles, O. Syed, V. Mudera, R. Day, and J.K. Hyun. Collagen - emerging collagen based therapies hit the patient. *Advanced Drug Delivery Reviews*, 65(4):429–456, 2013. URL http://www.scopus.com/inward/record.url?eid=2-s2.0-84877026658&partnerID=40&md5=f8a0d8d7fbcb2ddc180e9b4310a635e6. cited By 20.

[2] S. Ricard-Blum. The collagen family. *Cold Spring Harbor perspectives in biology*, 3(1), 2011. doi: 10.1101/cshperspect.a004978. URL https://www.scopus.com/inward/record.uri?eid=2-s2.0-79960647588&partnerID=40&md5=cb71a2186f7469e46eb31996ad20505a.

[3] M.A. Moore, B. Samsell, G. Wallis, S. Triplett, S. Chen, A.L. Jones, and X. Qin. Decellularization of human dermis using non-denaturing anionic detergent and endonuclease: a review. *Cell and Tissue Banking*, 16(2):249–259, 2015. doi: 10.1007/s10561-014-9467-4. URL http://www.scopus.com/inward/record.url?eid=2-s2.0-84928994938&partnerID=40&md5=3f292892b392386d5aaaa296732b75d9.

[4] P.L. Chern, C.L. Baum, and C.J. Arpey. Biologic dressings: Current applications and limitations in dermatologic surgery. *Dermatologic Surgery*, 35(6):891–906, 2009. URL http://www.scopus.com/inward/record.url?eid=2-s2.0-66449101145&partnerID=40&md5=7c3d8f32e4e3b4aa56a21e47e435aa55. cited By (since 1996) 12.

[5] E.A. Abou Neel, L. Bozec, J.C. Knowles, O. Syed, V. Mudera, R. Day, and J.K. Hyun. Collagen - emerging collagen based therapies hit the patient. *Advanced Drug Delivery Reviews*, 2012. URL http://www.scopus.com/inward/record.url?eid=2-s2.0-84866510752&partnerID=40&md5=77fbcfc33b018f29b29b64147510d447. cited By (since 1996) 0; Article in Press.

[6] Z. Deyl, I. Mikšík, and A. Eckhardt. Preparative procedures and purity assessment of collagen proteins. *Journal of Chromatography B: Analytical Technologies in the Biomedical and Life Sciences*, 790(1-2):245–275, 2003. URL http://www.scopus.com/inward/record.url?eid=2-s2.0-0038739337&partnerID=40&md5=819bb79675622add56978e5dfc0fac06. cited By (since 1996)20.

[7] L. Wang, B. Yang, R. Wang, and X. Du. Extraction of pepsin-soluble collagen from grass carp (ctenopharyngodon idella) skin using an artificial neural network. *Food Chemistry*, 111(3):683–686, 2008. URL http://www.scopus.com/inward/record.url?eid=2-s2.0-46049087711&partnerID=40&md5=43177ddaf47ba32bfa62795dabaf64fe. cited By (since 1996)15.

[8] K. Sato, T. Ebihara, E. Adachi, S. Kawashima, S. Hattori, and S. Irie. Possible involvement of aminotelopeptide in self-assembly and thermal stability of collagen i as revealed by its removal with proteases. *Journal of Biological Chemistry*, 275(33):25870–25875, 2000. URL http://www.scopus.com/inward/record.url?eid=2-s2.0-0034682790&partnerID=40&md5=a9c7764f57d506de05cc5dce01623703. cited By (since 1996)63.

[9] G.C. Na, L.J. Butz, and R.J. Carroll. Mechanism of in vitro collagen fibril assembly. kinetic and morphological studies. *Journal of Biological Chemistry*, 261(26):12290–12299, 1986. URL https://www.scopus.com/inward/record.url?eid=2-s2.0-0022970587&partnerID=40&md5=ab5250e1177d2106816487e8f31ca210.

[10] L. Zubal, W. Bonani, D. Maniglio, R. Ceccato, D. Renciuk, A. Hampl, C. Migliaresi, J. Jancar, and L. Vojtova. Soluble collagen dissolution and assembling in pressurized carbon dioxide water solutions. *Express Polymer Letters*, 12(2):159–170, 2018. doi: 10.3144/expresspolymlett.2018.14. URL https://www.scopus.com/inward/record.uri?eid=2-s2.0-85037050404&doi=10.3144%2fexpresspolymlett.2018.14&partnerID=40&md5=0509c966a17936bfe1b51886579783e0. cited By 0.

[11] H.C. Ott, T.S. Matthiesen, S.-K. Goh, L.D. Black, S.M. Kren, T.I. Netoff, and D.A. Taylor. Perfusion-decellularized matrix: Using nature's platform to engineer a bioartificial heart. *Nature Medicine*, 14(2):213–221, 2008. URL http://www.scopus.com/inward/record.url?eid=2-s2.0-38949168818&partnerID=40&md5=c545f396997f5b83f7867c2513519aa6. cited By (since 1996) 447.

[12] C. Vaquette and J.J. Cooper-White. Increasing electrospun scaffold pore size with tailored collectors for improved cell penetration. *Acta Biomaterialia*, 7(6):2544–2557, 2011. URL http://www.scopus.com/inward/record.url?eid=2-s2.0-79955591893&partnerID=40&md5=29fc32bdea28c64706ba34792f79f8b5. cited By (since 1996) 20.

[13] H.M. Powell and S.T. Boyce. Fiber density of electrospun gelatin scaffolds regulates morphogenesis of dermal-epidermal skin substitutes. *Journal of Biomedical Materials Research - Part A*, 84(4):1078–1086, 2008. URL http://www.scopus.com/inward/record.url?eid=2-s2.0-39749171693&partnerID=40&md5=d9771af3447ffcb06f4dcf957f6a2a82. cited By (since 1996) 28.

[14] Z. Tong, E.M. Balzer, M.R. Dallas, W.-C. Hung, K.J. Stebe, and K. Konstantopoulos. Chemotaxis of cell populations through confined spaces at single-cell resolution. *PLoS ONE*, 7(1), 2012. URL http://www.scopus.com/inward/record.url?eid=2-s2.0-84855926245&partnerID=40&md5=da4933b7cc0a9bc8e237d5ed7c3ff89b. cited By (since 1996) 2.

[15] H.M. Powell and S.T. Boyce. Engineered human skin fabricated using electrospun collagen-pcl blends: Morphogenesis and mechanical properties. *Tissue Engineering - Part A*, 15(8):2177–2187, 2009. URL http://www.scopus.com/inward/record.url?eid=2-s2.0-68749098302&partnerID=40&md5=48853faf92244e8ee4a4d28d555a4c13. cited By (since 1996) 33.

[16] H.M. Powell, D.M. Supp, and S.T. Boyce. Influence of electrospun collagen on wound contraction of engineered skin substitutes. *Biomaterials*, 29(7):834–843, 2008. URL http://www.scopus.com/inward/record.url?eid=2-s2.0-37249054208&partnerID=40&md5=a05231abea3873f7884d65743c37a9ca. cited By (since 1996) 59.

[17] K. Wolf and P. Friedl. Extracellular matrix determinants of proteolytic and non-proteolytic cell migration. *Trends in Cell Biology*, 21(12):736–744, 2011. URL http://www.scopus.com/inward/record.url?eid=2-s2.0-81355127254&partnerID=40&md5=815a28ff1dbdb770dd1c55a060a75835. cited By (since 1996) 14.

[18] A.K. Gaharwar, P.J. Schexnailder, B.P. Kline, and G. Schmidt. Assessment of using laponite® cross-linked poly(ethylene oxide) for controlled cell adhesion and mineralization. *Acta Biomaterialia*, 7(2):568–577, 2011. URL http://www.scopus.com/inward/record.url?eid=2-s2.0-78650736275&partnerID=40&md5=9ff4382cfc4a8e6df315c25b02bfcef3. cited By 26.

[19] P.M. Crapo, T.W. Gilbert, and S.F. Badylak. An overview of tissue and whole organ decellularization processes. *Biomaterials*, 32(12):3233–3243, 2011. URL

http://www.scopus.com/inward/record.url?eid=2-s2.0-79951775415&partnerID=40&md5=d6f10fe4438b060919010f511dd0f5c3. cited By (since 1996) 69.

[20] B.N. Brown, R. Londono, S. Tottey, L. Zhang, K.A. Kukla, M.T. Wolf, K.A. Daly, J.E. Reing, and S.F. Badylak. Macrophage phenotype as a predictor of constructive remodeling following the implantation of biologically derived surgical mesh materials. *Acta Biomaterialia*, 8(3):978–987, 2012. URL http://www.scopus.com/inward/record.url?eid=2-s2.0-84856530367&partnerID=40&md5=873f468b018d09e6ca08e999f93093f0. cited By (since 1996) 7.

[21] T.J. Keane, R. Londono, N.J. Turner, and S.F. Badylak. Consequences of ineffective decellularization of biologic scaffolds on the host response. *Biomaterials*, 33(6):1771–1781, 2012. URL http://www.scopus.com/inward/record.url?eid=2-s2.0-83555178369&partnerID=40&md5=b67515750dc0e73ce3b967061dc86a52. cited By (since 1996) 12.

[22] W. Haslik, L.-P. Kamolz, F. Manna, M. Hladik, T. Rath, and M. Frey. Management of full-thickness skin defects in the hand and wrist region: first long-term experiences with the dermal matrix matriderm. *Journal of Plastic, Reconstructive and Aesthetic Surgery*, 63(2):360–364, 2010. URL http://www.scopus.com/inward/record.url?eid=2-s2.0-74849101356&partnerID=40&md5=9cee7ec0be518761be68da220c4234a0. cited By (since 1996) 24.

[23] S.J. Lee, J. Liu, S.H. Oh, S. Soker, A. Atala, and J.J. Yoo. Development of a composite vascular scaffolding system that withstands physiological vascular conditions. *Biomaterials*, 29(19):2891–2898, 2008. URL http://www.scopus.com/inward/record.url?eid=2-s2.0-42249097713&partnerID=40&md5=2e77a97d3014906ba8f88fa929fe35b4. cited By (since 1996) 77.

[24] S. de Valence, J.-C. Tille, D. Mugnai, W. Mrowczynski, R. Gurny, M. Muller, and B.H. Walpoth. Long term performance of polycaprolactone vascular grafts in a rat abdominal aorta replacement model. *Biomaterials*, 33(1):38–47, 2012. URL http://www.scopus.com/inward/record.url?eid=2-s2.0-82855175164&partnerID=40&md5=9f87a783f51566db6951b94883119639. cited By (since 1996) 2.

[25] Y.S. Song, R.L. Lin, G. Montesano, N.G. Durmus, G. Lee, S.-S. Yoo, E. Kayaalp, E. Haggstrom, A. Khademhosseini, and U. Demirci. Engineered 3d tissue models for cell-laden microfluidic channels. *Analytical and Bioanalytical Chemistry*, 395(1):185–193, 2009. URL http://www.scopus.com/inward/record.url?eid=2-s2.0-68949146856&partnerID=40&md5=0777a0211996efc4643aeba3c9c466b7. cited By (since 1996) 22.

[26] E.C. Novosel, C. Kleinhans, and P.J. Kluger. Vascularization is the key challenge in tissue engineering. *Advanced Drug Delivery Reviews*, 63(4):300–311, 2011. URL http://www.scopus.com/inward/record.url?eid=2-s2.0-79957713859&partnerID=40&md5=e1c52d248695f3e213ed2aa04a80f444. cited By (since 1996) 28.

[27] L.D. Muiznieks and F.W. Keeley. Molecular assembly and mechanical properties of the extracellular matrix: A fibrous protein perspective. *Biochimica et Biophysica Acta - Molecular Basis of Disease*, 1832(7):866–875, 2013. URL http://www.scopus.com/inward/record.url?eid=2-s2.0-84877050600&partnerID=40&md5=c74139ec22555908a7d4d55fe22b801e. cited By 4.

[28] R. Parenteau-Bareil, R. Gauvin, and F. Berthod. Collagen-based biomaterials for tissue engineering applications. *Materials*, 3(3):1863–1887, 2010. doi: 10.3390/ma3031863. URL http://www.scopus.com/inward/record.url?eid=2-s2.0-79957625010&partnerID=40&md5=61d83c86b6488e6c5d72b3a782d32c8d. cited By 97.

[29] L. Scipioni, P. Alkemade, V. Sidorkin, P. Chen, D. Maas, and E. Van Veldhoven. The helium ion microscope: Advances in technology and applications. *American Laboratory*, 41(12):26–28, 2009. URL http://www.scopus.com/inward/record.url?eid=2-s2.0-73849123477&partnerID=40&md5=9fff311d94fd509b20bd44412a6b9fc1. cited By 6.

[30] A. KESSLER, H. ROSEN, and S.M. LEVENSON. Chromatographic fractionation of acetic acid-solubilized rat tail tendon collagen. *The Journal of biological chemistry*, 235:989–994, 1960. URL http://www.scopus.com/inward/record.url?eid=2-s2.0-21144446634&partnerID=40&md5=6ae434afef1e8ed5541da7362c9113b9. cited By (since 1996)6.

[31] F. Silver and R. Treslstad. Type i collagen in solution. *The Journal of biological chemistry*, 255:9427–9433, 1980.

[32] S. Zeng, J. Yin, S. Yang, C. Zhang, P. Yang, and W. Wu. Structure and characteristics of acid and pepsin-solubilized collagens from the skin of cobia (rachycentron canadum). *Food Chemistry*, 135(3):1975–1984, 2012. URL http://www.scopus.com/inward/record.url?eid=2-s2.0-84865763437&partnerID=40&md5=0aa30f0d2fac557b387181b43782ddff. cited By (since 1996)4.

[33] R. Duan, J. Zhang, X. Du, X. Yao, and K. Konno. Properties of collagen from skin, scale and bone of carp (cyprinus carpio). *Food Chemistry*, 112(3):702–706, 2009. URL http://www.scopus.com/inward/record.url?eid=2-s2.0-49249088070&partnerID=40&md5=54fb1b92cf198898e126eeb0cfba235c. cited By (since 1996)72.

[34] M. Sadowska, I. Kołodziejska, and C. Niecikowska. Isolation of collagen from the skins of baltic cod (gadus morhua). *Food Chemistry*, 81(2):257–262, 2003. URL http://www.scopus.com/inward/record.url?eid=2-s2.0-0037403159&partnerID=40&md5=0e3faa50a3af684522ac5925243edd0e. cited By (since 1996)105.

[35] B.S. Kim, J.S. Choi, J.D. Kim, H.I. Yoon, Y.C. Choi, and Y.W. Cho. Human collagen isolated from adipose tissue. *Biotechnology Progress*, 28(4):973–980, 2012. URL http://www.scopus.com/inward/record.url?eid=2-s2.0-84864844849&partnerID=40&md5=3a8ba00fa3e97b543dfaf629a4191230. cited By (since 1996)2.

[36] Adhikari B. Dhara S. Pati, F. Isolation and characterization of fish scale collagen of higher thermal stability. *Bioresource technology*, (101):3737–3742, 2009.

[37] ASTM F2212-11. Standard guide for characterization of type i collagen as starting material for surgical implants and substrates for tissue engineered medical products (temps). *ASTM International, West Conshohocken, PA*, pages 1–14, 2011. URL http://www.astm.org/Standards/F2212.htm.

[38] F. Gobeaux, E. Belamie, G. Mosser, P. Davidson, and S. Asnacios. Power law rheology and strain-induced yielding in acidic solutions of type i-collagen. *Soft Matter*, 6(16):3769–3777, 2010. URL http://www.scopus.com/inward/record.url?eid=2-s2.0-77955410164&partnerID=40&md5=a4ddcd043cb27c912177fadeceb00ef2. cited By 10.

[39] Doe. The freezing stage in freeze drying: Fundamental concepts @ONLINE, April 2009. URL http://www.spscientific.com/Freezing-Stage/.

[40] Patel. Process development and scale-up issues in freeze drying @ONLINE, November 2009. URL http://www.spscientific.com/Process-Dev/.

[41] A. Gautieri, S. Vesentini, A. Redaelli, and M.J. Buehler. Hierarchical structure and nanomechanics of collagen microfibrils from the atomistic scale up. *Nano Letters*, 11(2):757–766, 2011. doi: 10.1021/nl103943u. URL http://www.scopus.com/inward/record.url?eid=2-s2.0-79851488199&partnerID=40&md5=d11fd7e2b7d840197bed2940c89951b5. cited By 125.

[42] M.J. Buehler and S.Y. Wong. Entropic elasticity controls nanomechanics of single tropocollagen molecules. *Biophysical Journal*, 93 (1):37–43, 2007. doi: 10.1529/biophysj.106.102616. URL http://www.scopus.com/inward/record.url?eid=2-s2.0-34347403503&partnerID=40&md5=c6c1b2b62ffa0769a0f3df1ee60bc8fb. cited By 82.

[43] Y.-L. Yang and L.J. Kaufman. Rheology and confocal reflectance microscopy as probes of mechanical properties and structure during collagen and collagen/hyaluronan self-assembly. *Biophysical Journal*, 96(4):1566–1585, 2009. URL http://www.scopus.com/inward/record.url?eid=2-s2.0-62649131725&partnerID=40&md5=8faff0250200b68062afa46deedbd597. cited By 57.

[44] D.J.S. Hulmes. *Collagen diversity, synthesis and assembly.* 2008. doi: 10.1007/978-0-387-73906-9_2. URL http://www.scopus.com/inward/record.url?eid=2-s2.0-84886130799&partnerID=40&md5=21032795742c2429c2a2d6de66d48211. cited By 19.

[45] F. Gobeaux, G. Mosser, A. Anglo, P. Panine, P. Davidson, M.-M. Giraud-Guille, and E. Belamie. Fibrillogenesis in dense collagen solutions: A physicochemical study. *Journal of Molecular Biology*, 376(5):1509–1522, 2008. doi: 10.1016/j.jmb.2007.12.047. URL http://www.scopus.com/inward/record.url?eid=2-s2.0-39149121136&partnerID=40&md5=c355358d428f99d68419040a78974e34. cited By 60.

[46] Y.-L. Yang, C. Sun, M.E. Wilhelm, L.J. Fox, J. Zhu, and L.J. Kaufman. Influence of chondroitin sulfate and hyaluronic acid on structure, mechanical properties, and glioma invasion of collagen i gels. *Biomaterials*, 32(31):7932–7940, 2011. doi: 10.1016/j.biomaterials.2011.07.018. URL http://www.scopus.com/inward/record.url?eid=2-s2.0-80051824094&partnerID=40&md5=578a4a915a8e457b3b01f9f68dc18487. cited By 13.

[47] F.H. Silver and R.L. Trelstad. Linear aggregation and the turbidimetric lag phase: Type i collagen fibrillogenesis in vitro. *Journal of Theoretical Biology*, 81(3):515–526, 1979. doi: 10.1016/0022-5193(79)90049-3. URL http://www.scopus.com/inward/record.url?eid=2-s2.0-0018602352&partnerID=40&md5=03369748b467d647e6043994c9456b72. cited By 12.

[48] G.C. WOOD. The formation of fibrils from collagen solutions. 2. a mechanism of collagen-fibril formation. *The Biochemical journal*, 75:598–605, 1960. URL http://www.scopus.com/inward/record.url?eid=2-s2.0-0001358434&partnerID=40&md5=c58f81b05308d8963cc4bf782edb0a18. cited By 66.

[49] M. Yan, B. Li, X. Zhao, and S. Qin. Effect of concentration, ph and ionic strength on the kinetic self-assembly of acid-soluble collagen from walleye pollock (theragra chalcogramma) skin. *Food Hydrocolloids*, 29(1):199–204, 2012. doi: 10.1016/j.foodhyd.2012.02.014. URL https://www.scopus.com/inward/record.uri?eid=2-s2.0-84859346465&doi=10.1016%2fj.foodhyd.2012.02.014&partnerID=40&md5=ecd05f494c212bd7749bf4cd1eb2cbca. cited By 13.

[50] D.L. Christiansen, E.K. Huang, and F.H. Silver. Assembly of type i collagen: Fusion of fibril subunits and the influence of fibril diameter on mechanical properties. *Matrix Biology*, 19(5):409–420, 2000. doi: 10.1016/S0945-053X(00)00089-5. URL http://www.scopus.com/inward/record.url?eid=2-s2.0-0033813556&partnerID=40&md5=24cca12652caa8376f97a5069cdaa720. cited By 152.

[51] A. Tidu, D. Ghoubay-Benallaoua, B. Lynch, B. Haye, C. Illoul, J.-M. Allain, V.M. Borderie, and G. Mosser. Development of human corneal epithelium on organized fibrillated transparent collagen matrices synthesized at high concentration. *Acta Biomaterialia*, 22:50–58, 2015. doi: 10.1016/j.actbio.2015.04.018. URL https://www.scopus.com/inward/record.uri?eid=2-s2.0-84930819157&doi=10.1016%2fj.actbio.2015.04.018&partnerID=40&md5=b4ec593b0dc4fe17b6813f2c53cae0a0. cited By 1.

[52] Z. Duan, R. Sun, C. Zhu, and I.-M. Chou. An improved model for the calculation of co2 solubility in aqueous solutions containing na+, k+, ca2+, mg2+, cl-, and so4 2-. *Marine Chemistry*, 98(2-4):131–139, 2006. URL http://www.scopus.com/inward/record.url?eid=2-s2.0-30144440867&partnerID=40&md5=e85e56dd8d6c88f32b83c6d38e3552f7.

[53] Advanced BioMatrix Inc. Advanced biomatrix website, 2016 may. Available from URL: https://www.advancedbiomatrix.com.

[54] J. Bürck, S. Heissler, U. Geckle, M.F. Ardakani, R. Schneider, A.S. Ulrich, and M. Kazanci. Resemblance of electrospun collagen nanofibers to their native structure. *Langmuir*, 29(5):1562–1572, 2013. URL http://www.scopus.com/inward/record.url?eid=2-s2.0-84873364059&partnerID=40&md5=667a8d003bc614c46106a13c7ce35474. cited By 9.

[55] C. Mu, D. Li, W. Lin, Y. Ding, and G. Zhang. Temperature induced denaturation of collagen in acidic solution. *Biopolymers*, 86(4): 282–287, 2007. doi: 10.1002/bip.20742. URL http://www.scopus.com/inward/record.url?eid=2-s2.0-34447570983&partnerID=40&md5=a592a55fb56f6bfd37bfe88911fbf47c.

[56] E. Leikina, M.V. Mertts, N. Kuznetsova, and S. Leikin. Type i collagen is thermally unstable at body temperature. *Proceedings of the National Academy of Sciences of the United States of America*, 99(3):1314–1318, 2002. doi: 10.1073/pnas.032307099. URL http://www.scopus.com/inward/record.url?eid=2-s2.0-0037022329&partnerID=40&md5=5b7208e75787d7863dbac2e558b0092f.

[57] J. Tanaka, T. Ikoma, and T. Yoshioka. Non-fibrillar collagen molded body and method for producing same, October 2 2013. URL http://google.com/patents/EP2644620A1?cl=pt. EP Patent App. EP20,110,843,692.

[58] J.C. Silva, A.A. Barros, I.M. Aroso, D. Fassini, T.H. Silva, R.L. Reis, and A.R.C. Duarte. Extraction of collagen/gelatin from the marine demosponge chondrosia reniformis (nardo, 1847) using water acidified with carbon dioxide - process optimization. *Industrial and Engineering Chemistry Research*, 55(25): 6922–6930, 2016. doi: 10.1021/acs.iecr.6b00523. URL https://www.scopus.com/inward/record.uri?eid=2-s2.0-84976649630&doi=10.1021%2facs.iecr.6b00523&partnerID=40&md5=a7edbc942ff7022f88570606b5edf4db. cited By 0.

[59] D.O.S.R.R.L. GONÇALVES, D.A.R. Cruz, D.A.L.U.Z.M.J.F. COLARDELLE, L.H. DA SILVA Tiago José QUINTEIROS, A.A.I.M. DE, B.A.A. ANTUNES, and D.A.S.J.C. FERNANDES. Method to obtain collagen/gelatin from marine sponges, October 8 2015. URL https://www.google.com/patents/WO2015151030A1?cl=en. WO Patent App. PCT/IB2015/052,370.

[60] I. S. Chaschin, T. E. Grigoriev, N. P. Bakuleva, S. S. Abramchyk, and L. N. Nikitin. Effect of the clathrate hydrate environment on the structure of collagen xenograft tissue with chitosan coating deposited from solution in the h2o/co2 system at high pressure. *Doklady Chemistry*, 468(2): 195–198, 2016. ISSN 1608-3113. doi: 10.1134/S0012500816060057. URL http://dx.doi.org/10.1134/S0012500816060057.

[61] J.L. Wehmeyer, R.J. Christy, A.L. Andrews, W.N. Bordano, and S. Natesan. Methods of treating amniotic membranes using supercritical fluids and compositions and apparatuses prepared therefrom, September 4 2014. URL https://www.google.com/patents/US20140248328. US Patent App. 13/815,827.

[62] K. Sawada, D. Terada, T. Yamaoka, S. Kitamura, and T. Fujisato. Cell removal with supercritical carbon dioxide for acellular artificial tissue. *Journal of Chemical Technology and Biotechnology*, 83(6):943–949, 2008. doi: 10.1002/jctb.1899. URL http://www.scopus.com/inward/record.url?eid=2-s2.0-44649115904&partnerID=40&md5=10b595c9a260a6262525083ff1a72d0b.

[63] J. Fages, A. Marty, C. Delga, J.-S. Condoret, D. Combes, and P. Frayssinet. Use of supercritical co<inf>2</inf> for bone delipidation. *Biomaterials*, 15(9):650–656, 1994. doi: 10.1016/0142-9612(94)90162-7. URL https://www.scopus.com/inward/record.uri?eid=2-s2.0-0028469065&doi=10.1016%2f0142-9612%2894%2990162-7&partnerID=40&md5=03628154d5725665fb9d4867752f1a96. cited By 47.

[64] E. Sachlos, D.A. Wahl, J.T. Triffitt, and J.T. Czernuszka. The impact of critical point drying with liquid carbon dioxide on collagen-hydroxyapatite composite scaffolds. *Acta Biomaterialia*, 4(5):1322–1331, 2008. doi: 10.1016/j.actbio.2008.03.016. URL http://www.scopus.com/inward/record.url?eid=2-s2.0-48449098778&partnerID=40&md5=bdbce5cd7ec7bd82f6d42e1bef92d77b.

[65] Genecards team. Genecards col1a1 page, 2016–. URL http://www.genecards.org/cgi-bin/carddisp.pl?gene=COL1A1. [Online; accessed 2016-07-22].

[66] Genecards team. Genecards col1a2 page, 2016–. URL http://www.genecards.org/cgi-bin/carddisp.pl?gene=COL1A2. [Online; accessed 2016-07-22].

[67] H.H. Lovelady, S. Shashidhara, and W.G. Matthews. Solvent specific persistence length of molecular type i collagen. *Biopolymers*, 101(4):329–335, 2014. doi: 10.1002/bip.22365. URL https://www.scopus.com/inward/record.uri?eid=2-s2.0-84897365808&partnerID=40&md5=1d6dc15d1c4c8ddbefe82c5024f913cf.

[68] Y.-L. Sun, Z.-P. Luo, A. Fertala, and K.-N. An. Direct quantification of the flexibility of type i collagen monomer. *Biochemical and Biophysical Research Communications*, 295(2):382–386, 2002. doi: 10.1016/S0006-291X(02)00685-X. URL https://www.scopus.com/inward/record.uri?eid=2-s2.0-0036064087&partnerID=40&md5=22a09c79bc2f7d2c03777461bae8feff.

[69] X. Xiong, R. Ghosh, E. Hiller, F. Drepper, B. Knapp, H. Brunner, and S. Rupp. A new procedure for rapid, high yield purification of type i collagen for tissue engineering. *Process Biochemistry*, 44(11):1200–1212, 2009. doi: 10.1016/j.procbio.2009.06.010. URL https://www.scopus.com/inward/record.uri?eid=2-s2.0-70249095291&partnerID=40&md5=5a6faa6afb688f6eac3a1d9c5e144c59.

[70] J. Wu, Z. Li, X. Yuan, P. Wang, Y. Liu, and H. Wang. Extraction and isolation of type i, iii and v collagens and their sds-page analyses. *Transactions of Tianjin University*, 17(2):111–117, 2011. doi: 10.1007/s12209-011-1543-2. URL https://www.scopus.com/inward/record.uri?eid=2-s2.0-79955915759&partnerID=40&md5=ee925dde04b4be06e906b45c6c207302.

[71] P. Chang, S. Kuan, G. Eberlein, D. Burke, and R. Jones. Characterization of bovine collagens using capillary electrophoresis - an alternative to slab gel electrophoresis. *Journal of Pharmaceutical and Biomedical Analysis*, 22(6):957–966, 2000. doi: 10.1016/S0731-7085(00)00246-6. URL https://www.scopus.com/inward/record.uri?eid=2-s2.0-0034021836&partnerID=40&md5=a451f0bc25586014f83962848b54e072.

[72] I. Miksik, P. Sedlakova, K. Mikulikova, and A. Eckhardt. Capillary electromigration methods for the study of collagen. *Journal of Chromatography B: Analytical Technologies in the Biomedical and Life Sciences*, 841(1-2):3–13, 2006. doi: 10.1016/j.jchromb.2006.02.043. URL https://www.scopus.com/inward/record.uri?eid=2-s2.0-33747812140&partnerID=40&md5=af9bd7cd8f26fc811d3c59f349eb6d11.

[73] M. Meyer and B. Morgenstern. Characterization of gelatine and acid soluble collagen by size exclusion chromatography coupled with

multi angle light scattering (sec-mals). *Biomacromolecules*, 4(6):1727–1732, 2003. doi: 10.1021/bm0341531. URL https://www.scopus.com/inward/record.uri?eid=2-s2.0-0345688751&partnerID=40&md5=9fc45e323e492d3a0d370fbed2e156bd.

[74] J. Liu, J.D. Andaya, and S.J. Shire. A critical review of analytical ultracentrifugation and field flow fractionation methods for measuring protein aggregation. *AAPS Journal*, 8(3):E580–E589, 2006. doi: 10.1208/aapsj080367. URL http://www.scopus.com/inward/record.url?eid=2-s2.0-33749452453&partnerID=40&md5=b3a9f340bb5b9b95d8fa3c57e5daaeb2.

[75] L. Yuan and A. Veis. The self assembly of collagen molecules. *Biopolymers*, 12(6):1437–1444, 1973. URL https://www.scopus.com/inward/record.uri?eid=2-s2.0-0015847573&partnerID=40&md5=c2f60978844a81e52cdf358f06ea2bcb.

[76] J.A.M. Ramshaw and J.A. Werkmeister. Electrophoresis and electroblotting of native collagens. *Analytical Biochemistry*, 168(1):82–87, 1988. doi: 10.1016/0003-2697(88)90013-9. URL https://www.scopus.com/inward/record.uri?eid=2-s2.0-0023873172&partnerID=40&md5=45a187c1864f2faad463f3587b6ce696. cited By 13.

[77] S. Ricard-Blum, D.J. Hartmann, and G. Ville. Polyacrylamide gel electrophoresis and immunoblotting of native collagen molecules using the phast system. application to tye xi collagen. *Journal of Chromatography B: Biomedical Sciences and Applications*, 530 (C):432–437, 1990. doi: 10.1016/S0378-4347(00)82346-4. URL https://www.scopus.com/inward/record.uri?eid=2-s2.0-0025029938&partnerID=40&md5=43cbe9547f3900e27784def7cd022320.

[78] S. Podzimek. *Light Scattering, Size Exclusion Chromatography and Asymmetric Flow Field Flow Fractionation: Powerful Tools for the Characterization of Polymers, Proteins and Nanoparticles*. 2011. doi: 10.1002/9780470877975. URL https://www.scopus.com/inward/record.uri?eid=2-s2.0-84891584029&partnerID=40&md5=72637dc1cac72c663ae3c70007c5a195.

[79] S.C. Meredith and F.J. Kézdy. The chromatographic purification of native types i, ii, and iii collagens. *BBA - Protein Structure*, 668(3):357–369, 1981. doi: 10.1016/0005-2795(81)90169-0. URL https://www.scopus.com/inward/record.uri?eid=2-s2.0-0019831476&doi=10.1016%2f0005-2795%2881%2990169-0&partnerID=40&md5=d7df81eb85142d28165aa724887fbddb. cited By 9.

[80] S.K. Ratanathanawongs Williams and D. Lee. Field-flow fractionation of proteins polysaccharides, synthetic polymers, and supramolecular assemblies. *Journal of Separation Science*, 29(12):1720–1732, 2006. doi: 10.1002/jssc.200600151. URL https://www.scopus.com/inward/record.uri?eid=2-s2.0-33748427795&partnerID=40&md5=0100edd27b03674f595d2d503a8256a6.

[81] S. Podzimek, P. Lebedat, and C. Johann. Asymmetric flow field flow fractionation: A powerful method for polymer characterization. *LCGC North America*, 27(1):62–69, 2009. URL https://www.scopus.com/inward/record.uri?eid=2-s2.0-77949658745&partnerID=40&md5=72cc35b8a150922dcfc05856231c42ce.

[82] S.K. Ratanathanawongs Williams and D. Lee. Field-flow fractionation of proteins polysaccharides, synthetic polymers, and supramolecular assemblies. *Journal of Separation Science*, 29(12):1720–1732, 2006. doi: 10.1002/jssc.200600151. URL http://www.scopus.com/inward/record.url?eid=2-s2.0-33748427795&partnerID=40&md5=0100edd27b03674f595d2d503a8256a6.

[83] M.H. Moon, D.Y. Shin, N. Lee, E. Hwang, and I.-H. Cho. Flow field-flow fractionation/multiangle light scattering of sodium hyaluronate from various degradation processes. *Journal of Chromatography B: Analytical Technologies in the Biomedical and Life Sciences*, 864(1-2):15–21, 2008. doi: 10.1016/j.jchromb.2008.01.023. URL https://www.scopus.com/inward/record.uri?eid=2-s2.0-40849130733&doi=10.1016%2fj.jchromb.2008.01.023&partnerID=40&md5=6c6a1cff6e100aebf6b84b9d566d18f6. cited By 14.

[84] J. Janca, I.A. Ananieva, A.Yu. Menshikova, and T.G. Evseeva. Micro-thermal focusing field-flow fractionation. *Journal of Chromatography B: Analytical Technologies in the Biomedical and Life Sciences*, 800(1-2):33–40, 2004. doi: 10.1016/j.jchromb.2003.10.014. URL https://www.scopus.com/inward/record.uri?eid=2-s2.0-0346786420&doi=10.1016%2fj.jchromb.2003.10.014&partnerID=40&md5=630dd24a83407685330352eeb6d439fd. cited By 21.

[85] S. Sitar, A. Kejzar, D. Pahovnik, K. Kogej, M. Tusek-Znidaric, M. Lenassi, and E. Zagar. Size characterization and quantification of exosomes by asymmetrical-flow field-flow fractionation. *Analytical Chemistry*, 87(18):9225–9233, 2015. doi: 10.1021/acs.analchem.5b01636. URL https://www.scopus.com/inward/record.uri?eid=2-s2.

0-84941614986&doi=10.1021%2facs.analchem.5b01636&partnerID=40&md5=9e1015ea7e84889470c4cfec1aef387a. cited By 11.

[86] U. Freudenberg, S.H. Behrens, P.B. Welzel, M. Müller, M. Grimmer, K. Salchert, T. Taeger, K. Schmidt, W. Pompe, and C. Werner. Electrostatic interactions modulate the conformation of collagen i. *Biophysical Journal*, 92(6):2108–2119, 2007. doi: 10.1529/biophysj.106.094284. URL http://www.scopus.com/inward/record.url?eid=2-s2.0-33947679349&partnerID=40&md5=879d502cfce16d71c893383241f78934. cited By 37.

[87] J.H. Highberger. The isoelectric point of collagen. *Journal of the American Chemical Society*, 61(9):2302–2303, 1939. URL https://www.scopus.com/inward/record.uri?eid=2-s2.0-33947441107&partnerID=40&md5=495e6f5859c34267066d680022e0bb30. cited By 24.

[88] B.H. Zimm. The dependence of the scattering of light on angle and concentration in linear polymer solutions. *Journal of Physical and Colloid Chemistry*, 52(1):260–267, 1948. URL https://www.scopus.com/inward/record.uri?eid=2-s2.0-0006876621&partnerID=40&md5=e8e3d82410e60860d6feb8b055a7aed3.

[89] P.J. Wyatt. Light scattering and the absolute characterization of macromolecules. *Analytica Chimica Acta*, 272(1):1–40, 1993. doi: 10.1016/0003-2670(93)80373-S. URL https://www.scopus.com/inward/record.uri?eid=2-s2.0-0027498262&partnerID=40&md5=9f86231f30894eafec55e36a6de09c2b.

[90] K. Rbii, O. Surel, N. Brambati, A.-M. Buchert, and F. Violleau. Study of gelatin renaturation in aqueous solution by afffff-mals: Influence of a thermal pre-treatment applied on gelatin. *Food Hydrocolloids*, 25(3):511–514, 2011. doi: 10.1016/j.foodhyd.2010.08.001. URL https://www.scopus.com/inward/record.uri?eid=2-s2.0-77957769656&partnerID=40&md5=1026f0ce8fbd8a6c03cbc2ba8ecd203e. cited By 7.

[91] K. Rbii, F. Violleau, S. Guedj, and O. Surel. Analysis of aged gelatin by afffff-mals: Identification of high molar mass components and their influence on solubility. *Food Hydrocolloids*, 23 (3):1024–1030, 2009. doi: 10.1016/j.foodhyd.2008.08.004. URL https://www.scopus.com/inward/record.uri?eid=2-s2.0-54249094570&partnerID=40&md5=904df304b9b1b3a94261f8241220cfe5. cited By 7.

[92] H. Boedtker and P. Doty. The native and denatured states of soluble collagen. *Journal of the American Chemical Society*, 78(17):4267–4280, 1956. URL https://www.scopus.com/inward/record.uri?eid=2-s2.0-0000114542&partnerID=40&md5=bf14203dcfe3b8777b4dfcd91aea4370.

[93] Yang Lanti. *Mechanical properties of collagen fibrils and elastic fibers explored by AFM.* dissertation, University of Twente, 2008.

[94] Jess T.J Price N.C. Kelly, S.M. How to study proteins by circular dichroism. *Biochimica et Biophysica Acta*, (1751):119–139, 2005.

[95] S.S. Amruthwar, A.D. Puckett, and A.V. Janorkar. Preparation and characterization of novel elastin-like polypeptide-collagen composites. *Journal of Biomedical Materials Research - Part A*, 101 A(8):2383–2391, 2013. doi: 10.1002/jbm.a.34514. URL http://www.scopus.com/inward/record.url?eid=2-s2.0-84879507477&partnerID=40&md5=53cc45b09c8cf2b8372256791e58cc31. cited By 6.

[96] J.M. Caves, W. Cui, J. Wen, V.A. Kumar, C.A. Haller, and E.L. Chaikof. Elastin-like protein matrix reinforced with collagen microfibers for soft tissue repair. *Biomaterials*, 32(23):5371–5379, 2011. doi: 10.1016/j.biomaterials.2011.04.009. URL http://www.scopus.com/inward/record.url?eid=2-s2.0-79956302282&partnerID=40&md5=acab5006b0adca65d3c0acec291d62e2. cited By 24.

[97] M. Zhang, K. Wu, and G. Li. Interactions of collagen molecules in the presence of n-hydroxysuccinimide activated adipic acid (nhs-aa) as a crosslinking agent. *International Journal of Biological Macromolecules*, 49(4):847–854, 2011. URL http://www.scopus.com/inward/record.url?eid=2-s2.0-80052299542&partnerID=40&md5=25e94123b412d8c191ff8b06768e04b8. cited By 11.

[98] T.-L. Tuan, A. Song, S. Chang, S. Younai, and M.E. Nimni. In vitro fibroplasia: Matrix contraction, cell growth, and collagen production of fibroblasts cultured in fibrin gels. *Experimental Cell Research*, 223(1):127–134, 1996. URL http://www.scopus.com/inward/record.url?eid=2-s2.0-0030039840&partnerID=40&md5=62880931260b32357d2277452ca497c1. cited By 111.

[99] D. Olsen, C. Yang, M. Bodo, R. Chang, S. Leigh, J. Baez, D. Carmichael, M. Perälä, E.-R. Hämäläinen, M. Jarvinen, and J. Polarek. Recombinant collagen and gelatin for drug delivery.

Advanced Drug Delivery Reviews, 55(12):1547–1567, 2003. URL http://www.scopus.com/inward/record.url?eid=2-s2.0-10744222967&partnerID=40&md5=a837a290664892764303f555e9b61bb1. cited By 203.

[100] L. Yang, K.O. van der Werf, P.J. Dijkstra, J. Feijen, and M.L. Bennink. Micromechanical analysis of native and cross-linked collagen type i fibrils supports the existence of microfibrils. *Journal of the Mechanical Behavior of Biomedical Materials*, 6:148–158, 2012. URL http://www.scopus.com/inward/record.url?eid=2-s2.0-83455211478&partnerID=40&md5=2c7253407177a76fd91d038ea6586f2c. cited By 12.

[101] T. Mitra, G. Sailakshmi, A. Gnanamani, and A.B. Mandal. Di-carboxylic acid cross-linking interactions improves thermal stability and mechanical strength of reconstituted type i collagen : Part i. oxalic acid. *Journal of Thermal Analysis and Calorimetry*, 105(1):325–330, 2011. doi: 10.1007/s10973-011-1472-2. URL http://www.scopus.com/inward/record.url?eid=2-s2.0-79959377741&partnerID=40&md5=919d71a8fdd10b7fc19c08d5f96224a6. cited By 8.

[102] C. Burger, B.S. Hsiao, and B. Chu. Preferred orientation in polymer fiber scattering. *Polymer Reviews*, 50(1):91–111, 2010. doi: 10.1080/15583720903503494. URL http://www.scopus.com/inward/record.url?eid=2-s2.0-77649156911&partnerID=40&md5=1a5e4a2bab4b7490a5a6f0816b8bd7dc. cited By 15.

[103] J. Schindelin, I. Arganda-Carreras, E. Frise, V. Kaynig, M. Longair, T. Pietzsch, S. Preibisch, C. Rueden, S. Saalfeld, B. Schmid, J.-Y. Tinevez, D.J. White, V. Hartenstein, K. Eliceiri, P. Tomancak, and A. Cardona. Fiji: An open-source platform for biological-image analysis. *Nature Methods*, 9(7):676–682, 2012. doi: 10.1038/nmeth.2019. URL http://www.scopus.com/inward/record.url?eid=2-s2.0-84862520770&partnerID=40&md5=7928b064f04b447b75219fcacf27bb58.

[104] S. Van Der Walt, S.C. Colbert, and G. Varoquaux. The numpy array: A structure for efficient numerical computation. *Computing in Science and Engineering*, 13(2):22–30, 2011. doi: 10.1109/MCSE.2011.37. URL https://www.scopus.com/inward/record.uri?eid=2-s2.0-79952595565&partnerID=40&md5=0fb519474b03838f01585b9dfce0dddb.

[105] Eric Jones, Travis Oliphant, Pearu Peterson, et al. SciPy: Open source scientific tools for Python, 2001–. URL http://www.scipy.org/. [Online; accessed 2016-06-13].

[106] J. D. Hunter. Matplotlib: A 2d graphics environment. *Computing In Science & Engineering*, 9(3):90–95, 2007.

[107] Murray Rosenblatt. Remarks on some nonparametric estimates of a density function. *Ann. Math. Statist.*, 27(3):832–837, 09 1956. doi: 10.1214/aoms/1177728190. URL http://dx.doi.org/10.1214/aoms/1177728190.

[108] D.W. Scott. On optimal and data-based histograms. *Biometrika*, 66(3):605–610, 1979. URL https://www.scopus.com/inward/record.uri?eid=2-s2.0-0018734781&partnerID=40&md5=74c55c2cffa6a1327baa285a042c05b8.

[109] Michael Waskom, Olga Botvinnik, drewokane, Paul Hobson, Yaroslav Halchenko, Saulius Lukauskas, Jordi Warmenhoven, John B. Cole, Stephan Hoyer, Jake Vanderplas, gkunter, Santi Villalba, Eric Quintero, Marcel Martin, Alistair Miles, Kyle Meyer, Tom Augspurger, Tal Yarkoni, Pete Bachant, Constantine Evans, Clark Fitzgerald, Tamas Nagy, Erik Ziegler, Tobias Megies, Daniel Wehner, Samuel St-Jean, Luis Pedro Coelho, Gregory Hitz, Antony Lee, and Luc Rocher. seaborn: v0.7.0 (january 2016), January 2016. URL http://dx.doi.org/10.5281/zenodo.45133.

[110] rhymeswithlion. Worm like chain monte carlo, 2016 dec. Available from URL: https://github.com/rhymeswithlion/wlcmc.

[111] RA Pethrick. Polymer physics. edited by michael rubinstein and ralph h colby oxford university press, oxford, 2003. isbn 019852059x. pp 440. *Polymer International*, 53(9):1394–1395, 2004. ISSN 1097-0126. doi: 10.1002/pi.1472. URL http://dx.doi.org/10.1002/pi.1472.

[112] N. Khorshid, Md.M. Hossain, and M.M. Farid. Precipitation of food protein using high pressure carbon dioxide. *Journal of Food Engineering*, 79(4):1214–1220, 2007. doi: 10.1016/j.jfoodeng.2006.04.037. URL https://www.scopus.com/inward/record.url?eid=2-s2.0-33750935077&partnerID=40&md5=4aa563dcaf9d9df5175bd41897674aad.

[113] A.K. Tashima, M. Ottens, L.A.M. Van Der Wielen, D.E. Cintra, J.R. Pauli, P. De Alcantara Pessoa Filho, and E.A. Miranda. Precipitation of porcine insulin with carbon dioxide. *Biotechnology and Bioengineering*, 103(5):909–919, 2009. doi: 10.1002/bit.22319. URL http://www.scopus.com/inward/record.url?eid=2-s2.0-67650819012&partnerID=40&md5=e151da93bf62a21e8148611475b75588.

[114] M.L. Floren, S. Spilimbergo, A. Motta, and C. Migliaresi. Carbon dioxide induced silk protein gelation for biomedical applications. *Biomacromolecules*, 13(7):2060–2072, 2012. doi: 10.1021/bm300450a. URL http://www.scopus.com/inward/record.url?eid=2-s2.0-84868282979&partnerID=40&md5=b2495bf1f8ac1708b41c0a9de22eefed.

[115] E. Sachlos and Czermuzska J.T. Makking tissue engineering scaffolds work. review of the application of solid freeform fabrication technology to the production of tissue engineering scaffolds. *Europen Cells and Materials*, (5):29–40, 2003.

[116] R. Usha and T. Ramasami. The effects of urea and n-propanol on collagen denaturation: Using dsc, circular dicroism and viscosity. *Thermochimica Acta*, 409(2):201–206, 2004. doi: 10.1016/S0040-6031(03)00335-6. URL https://www.scopus.com/inward/record.uri?eid=2-s2.0-1042302160&doi=10.1016%2fS0040-6031%2803%2900335-6&partnerID=40&md5=d701d70c0501bc874f81a6bdf283bd1e. cited By 88.

[117] G. Forgacs, S.A. Newman, B. Hinner, C.W. Maier, and E. Sackmann. Assembly of collagen matrices as a phase transition revealed by structural and rheologic studies. *Biophysical Journal*, 84(2 I):1272–1280, 2003. URL https://www.scopus.com/inward/record.url?eid=2-s2.0-0037306373&partnerID=40&md5=7baf392ca2864e3dc319f5f83257a0ab.

[118] R.D.B. Fraser, T.P. MacRae, A. Miller, and E. Suzuki. Molecular conformation and packing in collagen fibrils. *Journal of Molecular Biology*, 167(2):497–521, 1983. doi: 10.1016/S0022-2836(83)80347-7. URL https://www.scopus.com/inward/record.url?eid=2-s2.0-0020545965&partnerID=40&md5=42c171e65d80b93907f6c7e6070455eb.

[119] A.J. Bray. Theory of phase-ordering kinetics. *Advances in Physics*, 43(3):357–459, 1994. doi: 10.1080/00018739400101505. URL https://www.scopus.com/inward/record.url?eid=2-s2.0-0346505865&partnerID=40&md5=06112c5c78905225ec3b22ddac77a047.

[120] C.A. Miles and A.J. Bailey. Thermally labile domains in the collagen molecule. *Micron*, 32(3):325–332, 2001. doi: 10.1016/S0968-4328(00)00034-2. URL https://www.scopus.com/inward/record.uri?eid=2-s2.0-0035219275&partnerID=40&md5=28e9861f0d099d0a138973a251dcad3e.

[121] H. Hofmann, T. Voss, K. Kühn, and J. Engel. Localization of flexible sites in thread-like molecules from electron micrographs. comparison of interstitial, basement membrane and intima collagens. *Journal of Molecular Biology*, 172(3):325–343, 1984. doi: 10.1016/S0022-2836(84)80029-7. URL https://www.scopus.com/inward/record.uri?eid=2-s2.0-0021770213&partnerID=40&md5=31ea24117b0c80faa081793082badc27.

[122] W. Cheng, R. Yan-Hua, N. Fang-Gang, and Z. Guo-An. The content and ratio of type i and iii collagen in skin differ with age and injury. *African Journal of Biotechnology*, 10(13):2524–2529, 2011. URL https://www.scopus.com/inward/record.uri?eid=2-s2.0-79953661664&partnerID=40&md5=5d982ce4a61546130f95375d29e7e3d0. cited By 25.

[123] Genecards team. Genecards col3a1 page, 2016–. URL http://www.genecards.org/cgi-bin/carddisp.pl?gene=COL3A1. [Online; accessed 2016-11-04].

[124] Biswaranjan Mohanty and H.B. Bohidar. Microscopic structure of gelatin coacervates. *International Journal of Biological Macromolecules*, 36(1–2):39 – 46, 2005. ISSN 0141-8130. doi: http://dx.doi.org/10.1016/j.ijbiomac.2005.03.012. URL http://www.sciencedirect.com/science/article/pii/S0141813005000577.

[125] Y.-L. Sun, Z.-P. Luo, and K.-N. An. Stretching short biopolymers using optical tweezers. *Biochemical and Biophysical Research Communications*, 286(4):826–830, 2001. doi: 10.1006/bbrc.2001.5426. URL https://www.scopus.com/inward/record.uri?eid=2-s2.0-0034807221&partnerID=40&md5=f08666113406b3854892d9aa536b4b34.

[126] H. Utiyama, K. Sakato, K. Ikehara, T. Setsuiye, and M. Kurata. Flexibility of tropocollagen from sedimentation and viscosity. *Biopolymers*, 12(1):53–64, 1973. doi: 10.1002/bip.1973.360120106. URL https://www.scopus.com/inward/record.uri?eid=2-s2.0-0015535046&partnerID=40&md5=e576c3224cc562190f0bda2aa4dad1d0.

[127] F.H.M. Nestler, S. Hvidt, J.D. Ferry, and A. Veis. Flexibility of collagen determined from dilute solution viscoelastic measurements. *Biopolymers*, 22(7):1747–1758, 1983. doi: 10.1002/bip.360220710. URL https://www.scopus.com/inward/record.uri?eid=2-s2.0-0020790435&partnerID=40&md5=3d5a692cf0b344db9428fd0eaa82c2f1.

[128] V.A. Markov, V.V. Vasilevskaya, P.G. Khalatur, G. Ten Brinke, and A.R. Khokhlov. Conformational properties of rigid-chain amphiphilic macromolecules: The phase diagram. *Polymer Science - Series A*, 50(6):621–629, 2008. doi: 10.1134/S0965545X08060059. URL https://www.scopus.com/inward/record.uri?eid=2-s2.0-46749133229&partnerID=40&md5=57990b879e6f89ae34c896b6ae2c2d9c.

[129] K. Hofman, N. Tucker, J. Stanger, M. Staiger, S. Marshall, and B. Hall. Effects of the molecular format of collagen on characteristics of electrospun fibres. *Journal of Materials Science*, 47(3):1148–1155, 2012. URL http://www.scopus.com/inward/record.url?eid=2-s2.0-84855519170&partnerID=40&md5=652dafd6b48a07db8d51c5e00963849f. cited By 5.

7 ANNEXES

7.1 List of Publications

1. **Soluble collagen dissolution and assembling in pressurized carbon dioxide water solutions**
   Zubal, L.; Bonani, W.; Maniglio, D.; Ceccato, R.; Renciuk, D.; Hampl, A.; Migliaresi, C.; Jancar, J.; Vojtova, L. *Express Polymer Letters, 2018, 12 (2), pp. 159-170., DOI: 10.3144/expresspolymlett.2018.14. IF = 2,983.*
2. **Accurate micro-computed tomography imaging of pore spaces in collagen-based scaffold**
   Žídek, J.; Vojtová, L.; Abdel-Mohsen, A.; Chmelík, J.; Zikmund, T.; Brtníková, J.; Jakubíček, R.; **Zubal, L.**; Jan, J.; Kaiser, J. *Journal of Materials Science: Materials in Medicine, 2016, 27(6) p. 1-18. ISSN: 0957-4530. IF = 2,59.*

7.2 Participated Conferences and Workshops

1. *Separace a charakterizace atelokolagenu*
   Zubal L., Mohsen A., Vojtová L., Matoušková P., Konečná Z. VI. Mezinárodní conference Bioimplantologie 2014 Brno: Společnost pro Bioimplantologii, 2014, p. 34-34.
2. *Nový způsob zpracování atelokolagenu a přípravy kolagenových gelů*
   Zubal L., Bonnani W., Maniglio D., Vojtová L., Jančář J., Migliaresi C. VI. Mezinárodní conference Bioimplantologie 2015 Brno: Společnost pro Bioimplantologii, 2015.
3. *New atellocollagen procesing method and preparation of collagen gels*
   Zubal L.., Bonnani W., Migliaresi C, Vojtová L. PhD Retreat 2015 Valtice: CEITEC, 2015, p. 129. ISBN: 978-80-210-7825-3
4. *Stereoscopic analysis of collagen scaffolds in real 3D volume*
   Žídek, J.; Vojtová, L.; Zikmund, T.; Abdel-Lattif, A.; Jakubíček, R.; Chmelík, J.; Kaiser, J.; Brtníková, J.; **Zubal, L.**; Jan, J. Polymery 2014, sborník abstraktů. Praha: Ústav Makromolekulární chemie, 2014. s. 98-99. ISBN: 978-80-85009-81- 1.
5. *3D zobrazení skafoldů a buněk pomocí mikroCT*
   Vojtová, L.; Žídek, J.; **Zubal, L.**; Zikmund, T.; Prosecká, E.; Rampichová, M.; Chmelík, J.; Jakubíček, R.; Walek, P.; Jan, J.; Kaiser, J. VI. Mezinárodní conference Bioimplantologie 2014 Brno: Společnost pro Bioimplantologii, 2014. p. 36-36.

6. *Studium morfologie biopolymerních skafoldů pomocí rentgenové počítačové mikrotomografie*

   Vojtová, L.; Žídek, J.; **Zubal, L.**; Brtníková, J.; Abdel-Lattif, A.; Zikmund, T.; Prosecká, E.; Rampichová, M.; Chmelík, J.; Jakubíček, R.; Jan, J.; Kaiser, J. In Programová brožura konference: VIII. česko- slovenská konference Polymery. 1. Praha: ÚMCH AVČR, 2014. s. 23-25. ISBN: 978-80-85009-81-1.

7. *3D Imaging of Biopolymeric Scaffolds Using X-Ray Computed Micro- Tomography and Stereoscopy*

   Vojtová, L.; Žídek, J.; **Zubal, L.**; Brtníková, J.; Abdel-Lattif, A.; Zikmund, T.; Chmelík, J.; Jakubíček, R.; Jan, J.; Kaiser, J. CEITEC anual conference "Frontiers in Materials and Life Sciences". first. Brno, Czech Republic: Masaryk University, 2014. s. 243-243. ISBN: 978-80-210-7159- 9.

CURRICULUM VITAE

PERSONAL Lukáš Zubal

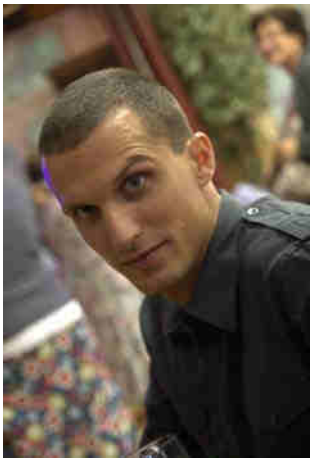

Matůlkova 1806/15, Brno, 60200, Česká republika

+420 777 256 288

Lukas.zubal@gmail.com

Sex Male | Date of birth 16/04/1984 | Nationality Czech

EDUCATION

2013-2018 **PhD. study**

- CEITEC – Central European Institute of Technology, Advanced Materials
- **Soluble collagen processing in pressurized CO_2.**
- **Characterization of soluble collagen by Field Flow Fractionation - Multi Angle Light Scattering (new method).**
- Lab workflow automation – Export data from multiple instruments -> load data into python -> process/combine/select important information from multiple instruments using Pandas -> (statistical) visualization using Seaborn
- GUI application for microCT project development – python and matlab based on Camelot (QT, SQL), Mayavi (3D visualizations).
- Collagen sample characterization by SEM, TEM, AFM, microCT, rheology, CD spectrophotometry, SDS-PAGE, Native-PAGE.
- 2 times at University of Trento, Italy

2007-2009 **Master study**

- Faculty of Electrical Engineering and Communication Brno University of Technology, Department of biomedical engineering, thesis: Acquisition contrast in projection and reconstruction imaging
- Healthcare technics
- Signal processing
- Communication with physician

2003- 2007 **Bachelor study**

Faculty of Electrical Engineering and Communication Brno University of Technology, communication technic

- Analog and digital technics
- Programming
- Wireless communication

1999-2003 **High Scholl**

Electrical high school Mohelnice

- Electronics and automatization

WORK EXPERIENCE

2017-now

Junior SW developer

Mautilus s.r.o

- SmartTV development
  - Work on customer VOD (Video on Demand) front end app (Netflix like)
  - Member of young agile team
  - **React, Redux, ES2016, Flow, Mocha, PIXI, CANVAS,** company SDK
- Development of distributed test platform
  - My own test framework for Roku platform, mocha for JavaScript
  - **Node.js server - ES2016 promises**
    - Running tests parallel on multiple TVs
    - First version in python
  - React client for loading and running test packages

Sector IT, Media, smartTV

2014-2015

Erasmus +

2 times at University of Trento, Italy

- **CO_2 soluble collagen processing developed here**
- **First experience with multi angle light scattering**
- **Partially successful extraction of atelocolagen in high pressure CO_2 cooled reactor**

Sector Collagen processing

2012-2014

Optical microCT development

Home project – small optical computed tomography scanner

- Concept, choice of parts
- Machine assembly, changes, improvements
- Hardware driven by python (**openCV, HDF5**, sockets, swig, pyLaback)
- Reconstruction and visualization in **python** (**Traits, Vitables, VTK, Mayavi**) and **matlab**

Sector Imaging systems

2011-2013

Material engineering leader

National Cell and Tissue Centre a.s. www.natic.cz

- Concept, development and preparation of scaffolds for Tissue Engineering
- Machine operator - nanospider, Tap biosystems select, SEM, TEM
- Scientific and patent literature search
- Clean room operation, cell culture
- Business plan preparation

Sector Healthcare – Tissue Engineering

2010

SW developer

Beta Control s.r.o.

- Part time
- **Python, SQL** programming

Sector IT, electronics

2009

SW developer

S-pro comp s.r.o.

- Part time
- PHP, SQL, HTML, JavaScript, XML programming

Sector IT

2007-2008

Wireless cow stomach probe development

Cow breeding institute, Pohořelice

- Part time
- PCB and electronics development

Sector electronics and measurement

PERSONAL SKILLS

Mother tongue: Czech

Other languages

	UNDERSTANDING		SPEAKING		WRITING
	Listening	Reading	Spoken interaction	Spoken production	
English	B1	B1	B1	B1	B1
German	A1	A1	A1	A1	A1

Levels: A1/2: Basic user - B1/2: Independent user - C1/2 Proficient user Common European Framework of Reference for Languages

Organisational / managerial skills

- Concept work, new ideas

Communication skills

- Communication in multifield environment - electronics, IT, mechanics, medicine, microbiology, chemistry

Other skills

- Basic cell culture

Computer skills

- Advanced work on PC
- Good with Microsoft Office™, Latex
- **Python**
  - Database – Pandas, SQLAlchemy (ORM)
  - Plotting/Visualization – matplotlib, seaborn, VTK, Mayavi
  - GUI – Camelot, traits
  - Signal processing – Scipy, OpenCV, ITK
- matlab (general signal processing),
- basic C++ and Java skills
- Signal, image, volume processing – fourier, convolution, clustering

Driving license

B